AN INVESTIGATION INTO THE ROLE OF PROTEIN-LIGAND INTERACTIONS ON OBLIGATE AND TRANSIENT PROTEIN-PROTEIN INTERACTIONS

A Dissertation

by

ROBERT JASON QUINLAN

Submitted to the Office of Graduate Studies of
Texas A&M University
in partial fulfillment of the requirements for the degree of

DOCTOR OF PHILOSOPHY

December 2004

Major Subject: Biochemistry

AN INVESTIGATION INTO THE ROLE OF PROTEIN-LIGAND INTERACTIONS ON OBLIGATE AND TRANSIENT PROTEIN-PROTEIN INTERACTIONS

A Dissertation

by

ROBERT JASON QUINLAN

Submitted to Texas A&M University
in partial fulfillment of the requirements
for the degree of

DOCTOR OF PHILOSOPHY

Approved as to style and content by:

Gregory D. Reinhart (Chair of Committee)	James C. Hu (Member)
Arthur E. Johnson (Member)	Paul S. Cremer (Member)
Gregory D. Reinhart (Head of Department)	

December 2004

Major Subject: Biochemistry

ABSTRACT

An Investigation into the Role of Protein-Ligand Interactions on Obligate and Transient Protein-Protein Interactions. (December 2004)

Robert Jason Quinlan, B.Sc. (Hons.), Laurentian University

Chair of Advisory Committee: Dr. Gregory D. Reinhart

Protein-ligand and protein-protein interactions are critical to cellular function. Most cellular metabolic and signal tranduction pathways are influenced by these interactions. Consequently, molecular level understanding of these associations is an important area of biochemical research. We have examined the thermodynamics of several protein-protein associations and the protein-ligand interactions that mediate them.

Using Fluorescence Correlation Spectroscopy, we have examined the putative interaction between pig heart malate dehydrogenase (MDH) and citrate synthase (CTS). We demonstrate a specific, low-affinity interaction between these enzymes. The association is highly polyethylene glycol (PEG)-dependent, and at high concentrations of NaCl or PEG, non-specific aggregates are formed. We demonstrate that oxaloacetate, the intermediate common to both CTS and MDH, induces the association at concentrations below the K_m of CTS, suggesting that the open conformation of CTS is involved in the association.

Using several biophysical techniques, we have examined the subunit associations of *B. stearothermophilus* phosphofructokinase (PFK). We demonstrate that the inhibitor bound conformation of the enzyme has reduced subunit affinity. The kinetics and

thermodynamics of the phosphoenolpyrvuate (PEP)-induced dissociation of PFK have been quantified. Binding substrate, fructose-6-phosphate (F6P), stabilizes the enzyme to inhibitor-induced dissociation by 132-fold. These data suggest that subunit associations may play a role in the allosteric inhibition of PFK by PEP.

The thermodynamics of the protein-ligand associations and allosteric inhibition of *E. coli* phosphofructokinase have been examined using intrinsic fluorescence and hydrostatic pressure. Both ligand-binding affinity and PEP inhibition are diminished by pressure, whereas substrate-binding affinity for inhibitor-bound enzyme is pressure-insensitive. Larger entropic than enthalpic changes with pressure lead to the overall reduction in free energies.

Using a fluorescence-based assay, we have developed a series of baroresistant buffer mixtures. By combining a buffer with acid dissociation of negative volume with a buffer of positive volume, a pressure-resistant mixture is produced. Alteration of the molar ratio of the two component buffers yields mixtures that are pressure-insensitive at pH values around neutrality.

This dissertation is dedicated to the memory of my "Unca Moe", a kindred scientist and an academic at heart. Our discussions will be missed, as will you. The word "consequently" appears 32 times in these pages - I thought of you each time that I wrote it.

ACKNOWLEDGEMENTS

Writing this dissertation and the years of lab work that went into it would not have been possible without the generous help of countless people. To them I owe a debt of gratitude that I won't be able to express, but will nonetheless attempt.

First and foremost, to "da boss" Greg Reinhart, "thank you, thank you, thank you". I'm sure that on countless occasions I've caused you immeasurable stress, grief and no small amount of teasing and joking around. For all those times, I apologize. You gave me the opportunity to play in a lab with the coolest toys on earth, the best of labmates, and a minimum of oversight. From the first days in the lab when I'd venture into your office with a question and venture back out - often more confused than when I entered - you have always been great at *pointing out* a direction, rather than *giving* me a direction. You have been a generous boss, and some of my fondest lab memories will be of dinners in high places! Thank you.

Secondly to my committee: Jim Hu, Art Johnson and Paul Cremer, I can't thank you enough. I feel that each of you has contributed significantly, and uniquely, to my continuing development as a scientist. After each committee meeting, after my prelims and now after my defense I have asked myself "why didn't *I* think of that?" in response to many of your questions or comments. In hindsight, I think that was the point. Each of you has helped to point out a different way for me to think about my data or my experiments. I hope someday that I'll be able to return the favor and help students to bring their science to the "next level", as you all have helped me.

To my labmates - I couldn't love "y'all" more. All my current and former lab members: Mauricio Lasagna, Aron Fenton, Michelle Lovingshimer, Jen Kimmel, Ally Ortigosa, Jason Johnson, Monique Parichartttanakul, Libby Badgett, Cuijuan Tie, Lin Fan, Ann Menefee, Andrew Bigley and Scarlett Blair have made every day great. May we drink together in hotel bars for years to come!

To my friends here in the department - what can I say? I had a great time with you during recruiting weekend so many years ago, and the party hasn't ended. You are the reason it was easy for me to come to A&M, and the reason that it will be hard for me to leave. You are the best and brightest group of people I've ever met and I've been truly blessed to be a part of our little group of "usual suspects".

To my "sweetie", Karen. During the past few months you have been a rock for me. When I have been a tired, cranky monster after hours and sometimes days in front of a computer screen, you have put up with my crankiness and been there with all the hugs a man could want. I love you so very much.

Finally to my family. You have always been my safety net. I've always felt that whatever happened here, you would be there for me, and you have been - letting me vent the frustrations, cheering the successes and sharing my ups and downs. It's been a long road, and I've been a long way from home but with you behind me I never doubted that I'd be here in the end. I love you all, and thank you.

NOMENCLATURE

Å	Angstroms (10^{-10}m)
A^-	General base
ADP	Adenosine 5′-diphosphate
AMP	Adenosine 5′-monophosphate
APD	Avalanche photodiode
ATP	Adenosine 5′-triphosphate
B. stearothermophilus	*Bacillus stearothermophilus*
BsPFK	*Bacillus stearothermophilus* phosphofructokinase
1,1-CDA	1,1-cyclohexane diacetic acid
CHES	2-[N-cyclohexylamino]-ethanesulfonic acid
cMDH	Cytosolic malate dehydrogenase
CTS	Citrate synthase
CW	Constant wave
DNA	Deoxyribonucleic acid
DMSO	Dimethylsulfoxide
E	Glutamate, enzyme
E. coli	*Escherichia coli*
EcPFK	*Escherichia coli* phosphofructokinase
EDTA	Ethylenediaminetetraacetic acid
EPPS	N-[2-hydroxyenthyl]piperazine-N′–[3-propanesulfonic acid]

FBP	Fructose 1,6-bisphosphate
FCS	Fluorescence correlation spectroscopy
F6P	Fructose 6-phosphate
F-2,6-BP	Fructose 2,6-bisphosphate
FRET	Förster resonance energy transfer
H^+	Proton
HA	General acid
HEPES	N-[2-hydroxyethyl]piperazine-N′-[2-ethanesulfonic acid]
HPTS	Hydroxypyran-1,2,3-trisulfonic acid
IPTG	Isopropyl-thiogalactoside
IR	Infrared
K	Lysine
K_a	Acid dissociation constant or general association constant
K_d	Dissociation constant
K_m	Michaelis-Menten constant
kbar	kilobar
KCl	Potassium Chloride
$KHPO_4$	Potassium phosphate (monobasic)
kHz	Kilohertz
KNF	Koshland, Nemethy and Filmer
K_2PO_4	Potassium phosphate (dibasic)
KSCN	Potassium thiocynate

M	Molar
MDH	Malate dehydrogenase
MES	2-[N-Morpholino]ethanesulfonic acid
MHz	Megahertz
MgADP	Magnesium adenosine 5′-diphosphate
MgATP	Magnesium adenosine 5′-triphosphate
$MgCl_2$	Magnesium chloride
mg	Milligram
mL	Milliliters
mM	Millimolar
mMDH	Mitochondrial malate dehydrogenase
MOPS	3-[N-Morpholino]propanesulfonic acid
MPE	Multiphoton excitation
MW	Milliwatt
MWC	Monod, Wyman and Changeux
NA	Numerical aperture
Na_2CO_3	Sodium carbonate (dibasic)
NaCl	Sodium chloride
$NaHCO_3$	Sodium carbonate (monobasic)
NADH	Nicotinamide adenine dinucleotide (reduced form)
NAD^+	Nicotinamide adenine dinucleotide (oxidized form)
Nb:YVO_4	Neobium: yttrium vanadate laser

NH_4Cl	Ammonium chloride
nm	Nanometers
OAA	Oxaloacetate (oxalacetic acid)
P	Polarization
PAGE	Polyacrylamide gel electrophoresis
PCH	Photon counting histogram
PEG	Polyethylene glycol (8000)
PEP	Phospho(enol)pyruvate
PIPES	2-[N-morpholino]ethanesulfonic acid
pK_a	$-\log(K_a)$
PMT	Photomultiplier tube
PFK	Phosphofructokinase
Q	Coupling constant, quantum yield
r	Anisotropy
R	Gas constant
SDS	Sodium dodecyl sulfate
SNAFL-1	5&6-carboxy-seminaphthofluorescein-1
T	Temperature
Ti: Sapph	Titanium: Sapphire pulsed laser
Tris	Tris[hydroxymethyl]aminomethane
Trp	Tryptophan
UV	Ultraviolet

UV-Vis	Ultraviolet-visible absorbance spectroscopy
V	Volt
W	Tryptophan, watt
Y	Phenylalanine, phosphoenolpyruvate
ΔG^0	Standard state free energy
ΔG_{ay}	Free energy of coupling
ΔH^0	Standard state enthalpy
ΔP	Change in pressure
ΔpH	Change in pH
ΔS^0	Standard state entropy
ΔV^0	Standard state reaction volume
μL	Microliters
μM	Micromolar
μg	Microgram
2-PE	Two photon excitation

TABLE OF CONTENTS

CHAPTER Page

Page

LIST OF FIGURES

LIST OF TABLES

CHAPTER I

INTRODUCTION

Protein-protein and protein-ligand interactions are fundamental processes underlying many aspects of cellular function. Consequently, development of tools and models for association is pivotal to fields of biochemical inquiry including proteomics and biophysics. The research outlined herein has examined protein subunit associations as a model of high-affinity protein-protein interactions at single molecule resolution. Similarly, weak or transient protein-protein interactions have been interrogated using putatively interacting metabolic enzymes. The effects of ligand binding on each of the respective protein-protein interactions were elucidated.

Protein-ligand interactions

A ligand can be broadly defined as anything to which a protein binds, either for purposes of catalysis, regulation, transport or structure. Classic examples of these ligands include nucleic acids and nucleotides, metabolic substrates, enzyme cofactors, and other proteins. Each of these ligands performs a specific role with regard to protein function. Enzymes bind the substrates on which they perform the catalytic function for

---

This dissertation follows the style and format of Analytical Biochemistry.

which they have evolved, and often bind metabolic intermediates or regulator molecules to attenuate that function. Many enzymes requisite bind ligand cofactors or prosthetic groups including porphyrins, metal ions or reductive organic molecules in order to carry out their catalytic function. DNA binding interactions serve to regulate gene expression, and small molecule binding to DNA-bound protein factors is often a cellular signal of metabolic or environmental conditions, inducing dissociation from or association with the DNA. Proteins are also responsible for mediation of transport of biologically essential material, either within the cell or between tissues of the body; a function that requires that these materials be bound and later released. Examples of biological ligand transport include the transport of lipids by albumin, transport of oxygen by hemoglobin and transport of glucose across the plasma membrane of the cell by the glucose transporter. Ligand binding therefore plays a critical role in cellular and physiological function.

The role of small molecule ligand-binding in the regulation of enzyme activity is most significant to the research described herein. Ligand-binding interactions frequently moderate protein-protein interactions, facilitating associations or altering specificity. Alternatively, ligand-binding interactions may directly alter enzyme catalysis. In most metabolic pathways one or more enzymatic reactions are regulatory points for both the reaction itself and for subsequent or previous reactions in the pathway [1]. A well-studied example of this type of feedback regulation occurs in the glycolytic pathway, which is regulated at each irreversible reaction in most organisms. These reactions

include glucose phosphorylation by hexokinase, fructose 6-phosphate phosphorylation by phosphofructokinase and the pyruvate kinase catalyzed phosphoenolpyruvate-dependent phosphoryl transfer of ADP to ATP [1]. In each case an effector molecule, itself either a product or reactant in the glycolytic pathway or a molecule synthesized specifically as a regulator, is bound by the enzyme and regulates catalytic function. The metabolic utility of ligand binding of this type is its feedback to the cellular concentrations of critical metabolic intermediates. Understanding both the mechanism and nature of regulatory ligand-binding is a fundamental aim in Biochemistry, as is the determination of the molecular-level detail of mediation of enzymatic catalysis by ligand binding. The interrelated regulation of multiple metabolic pathways to enable the proper integration of energy utilization, macromolecule synthesis and degradation and homeostasis allows the adequate response of living organisms to environmental conditions. Consequently, regulatory ligand-binding is of the utmost importance both biologically and as a fundamental question at issue in biochemistry.

Protein-protein interactions

The interaction of proteins with other proteins and/or with another copy of itself is a fundamental method of regulation and mediation of protein function [2,3]. At some level, either directly or indirectly, protein associations can be linked to all aspects of

cellular function. These interactions may play a direct role in the cellular processes, or may indirectly alter cellular function by regulating or changing the specificity of protein and enzyme activity.

Protein-protein interactions may be broadly classified as being either obligate or transient. An obligate protein association is one in which the proteins are only observed bound to the other proteins in the macromolecular assembly. These interactions are considered permanent and the interaction interfaces are optimized [3,4]. A transient association is one in which the protein interaction is weak or persists only for a short duration. Transient interactions occur for purposes of function or regulation, and then dissociation occurs. These interactions involve proteins that must be independently stable, and are optimized to allow association and dissociation according to cellular conditions or signaling events [3]. Fundamental questions that arise in the study of transient interactions are: (1) how transient are they? (2) What causes the association? (3) What does the interaction accomplish? As the duration of the interaction is related to the strength of the interaction the first question addresses the affinity of the interaction. The second and third questions address issues of function, specifically the cellular conditions under which an association occurs and the functional significance of the interaction.

Obligate associations

Many enzymes and proteins function as components of obligate oligomeric complexes. The key characteristic delineating obligate oligomers is a strong protein-protein affinity or slow dissociation rate that allows the interaction to persist for extended durations. While many classic examples of obligate multisubunit enzymes, including core RNA polymerase of many bacteria, tryptophan synthase and hemoglobin consist of relatively few subunits, multisubunit enzymes also comprise many of the most complicated biological assemblies known. The signal recognition particle, ribosome, proteasome and bacterial flagellar motor are examples [2]. Most homotypic, oligomeric enzymes have similar function in each subunit, and quaternary associations are frequently, but not always, necessary for protein function in these enzymes [3-5]. Examples of obligate homotypic oligomers include prokaryotic phosphofructokinase, malate dehydrogenase and citrate synthase. Conversely, heterotypic oligomers may contain different enzymatic functionalities within each of the constituent subunits or may be composed of subunits that exclusively provide either regulatory or catalytic function. Examples of oligomeric complexes containing subunits with different enzymatic functions include eukaryotic fatty acid synthase [1,6], and pyruvate dehydrogenase [1,7]. Heterooligomers in which regulatory and catalytic functions are carried out by different subunits include ATCase [8]. The characteristic trait of obligate

oligomers is high subunit affinity, whether the interfaces are composed of differing subunits or multiple copies of the same subunit.

Transient associations

Transient protein-protein associations are characterized by low affinity and hence persist for short durations. These interactions are often induced by chemical stimuli and dissociation occurs according to cellular conditions. The potential benefit of this type of interaction is the time-dependent regulation of protein-mediated processes, including regulation of cellular functions. Similarly, steady-state conditions are also maintained in metabolic pathways by transient alterations in enzyme activity mediated by protein-protein interactions. The enzymes that control the cell cycle exemplify transient protein-protein interactions that mediate time-dependent regulatory proteins. Interactions between cyclins and cyclin-dependent kinases allow cell cycle progression and checkpoint regulation [9]. Signal transduction pathways including Ca^{2+} and cAMP signaling pathways rely extensively on protein-protein associations [1,2]. Proteins also interact transiently in order to mediate catalytic function. All covalent modifications of proteins including phosphorylation, dephosphorylation, glycosylation, methylation, acetylation and proteolysis are the result of transient protein-protein interactions. Transient protein interactions between *E. coli* RNA polymerase and σ-factors regulate

the binding of the polymerase core enzyme to DNA promoter elements and the initial catalysis of RNA synthesis [1]. Transient interactions can therefore have significant impact on the regulation of cellular function and on the modulation of catalytic function.

The existence of transient protein-protein interactions between many of the enzymes of intermediary metabolism has been debated for several decades. The "metabolon hypothesis" proposes that enzymes within a metabolic pathway, the citric acid cycle for instance, are noncovalently associated in large assemblies and are localized specifically within organelles or in the cytoplasm [10-13]. In addition to regulation of substrate specificity, catalysis and time-dependent cellular function, the metabolon hypothesis postulates that transient protein interactions allow substrate channeling [10,14-18]. Substrate channeling is a phenomenon whereby a common intermediate is conveyed between two adjacent active sites without release to bulk solution. The putative advantages of such a transfer arise from the micro-compartmentalization of the metabolite from bulk solution by the enzyme complex. In a channeling scheme, local concentrations and enzyme bound substrates, rather than bulk phase substrate concentrations control enzyme reaction rates. Intermediates are isolated from exposure to non-productive enzyme activity and may avoid the unfavorable energetics of desolvation prior to binding. Labile intermediates are sequestered from solvent hydrolysis, or are preserved in a stabilizing microenvironment. Membrane-soluble intermediates are prevented from cellular escape by free diffusion and toxic intermediates

are prevented from causing cellular damage. Also important to the metabolon hypothesis, channeling reduces the solvation requirements of the cell [12]. Based on the premise that the intracellular environment is largely unlike solution conditions *in vitro*, containing high concentrations of protein, polycations, metabolites, nucleic acids and carbohydrates, the metabolon hypothesis proposes that the hydration capacity of the cell is scarce. In an environment in which complete solvation of proteins is difficult, interactions occur between proteins that are not observed *in vitro* [11,12]. Due to the inherently weak affinity of transient interactions, empirical evidence for these associations is often difficult to obtain. Despite this fact, a growing number of interaction partners have been identified and their associations confirmed *in vitro* [10,15,18-25].

A putative transient interaction between the sequential citric acid cycle enzymes malate dehydrogenase (MDH) and citrate synthase (CTS) has been demonstrated under conditions of enzyme precipitation [26-34]. A fusion of the two enzymes shows increased rate of conversion of malate to citrate [28]. The interacting pair shares a common intermediate, oxaloacetate (OAA), which is reported to undergo channeling between the active sites of the two enzymes during the protein-protein association [28-31]. A molecular modeling simulation of the docking interaction illustrates the presence of an electrostatic cleft between the two active sites, which is reported to facilitate OAA channeling [32], however the evidence for OAA channeling and for an MDH-CTS

interaction is indirect and has been questioned [11]. The putative heterotypic association between MDH and CTS is used to study the union of transiently or weakly interacting proteins in solution, as discussed in chapter IV. Ligation of these enzymes by their common intermediate is anticipated to increase the dimerization affinity and thus the effects of ligand-binding on the protein-protein association are also examined.

Malate dehydrogenase

Pig heart (*Sus scrofa*) malate dehydrogenase (EC number 1.1.1.37) has two distinct isoforms, each with independent intracellular localization – mitochondrial (mMDH) and cytoplasmic (cMDH) [35-38]. Both variants are homodimers, with monomer molecular weights of 36 kDa for cMDH and 34 kDa for mMDH (figure 1-1). mMDH is encoded by mitochondrial genes and is localized to the mitochondrial matrix. cMDH is localized to the cytoplasm and is found associated with the cytoplasmic face of the outer mitochondrial membrane [35]. Malate dehydrogenase catalyzes the oxidation of malate by NAD^+ to give oxaloacetate and NADH, the final step in the citric acid cycle.

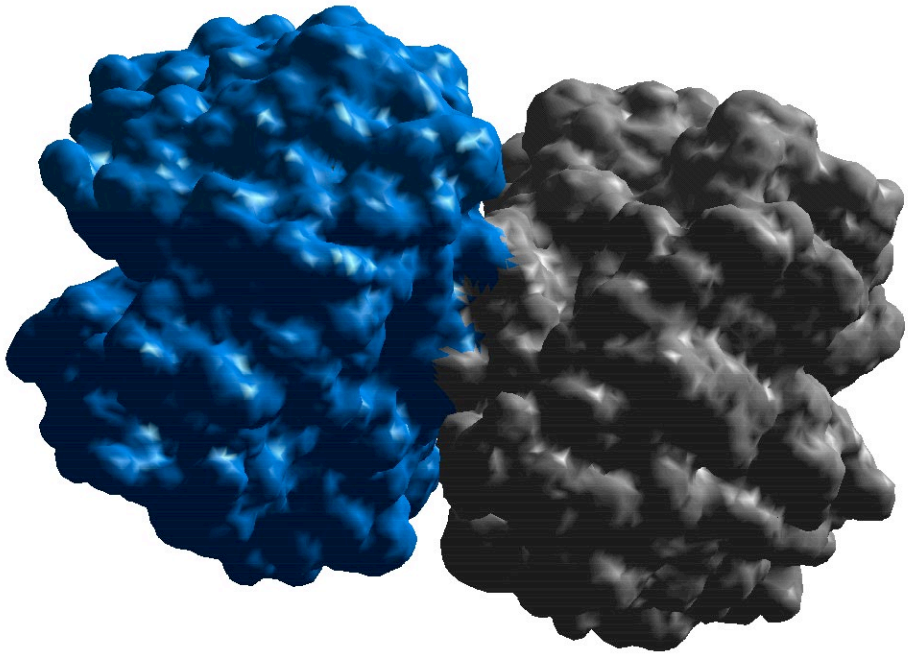

Figure 1-1: The crystal structure of malate dehydrogenase.
The crystal structure of a mMDH dimer is shown, with individual subunits colored blue and grey [37].

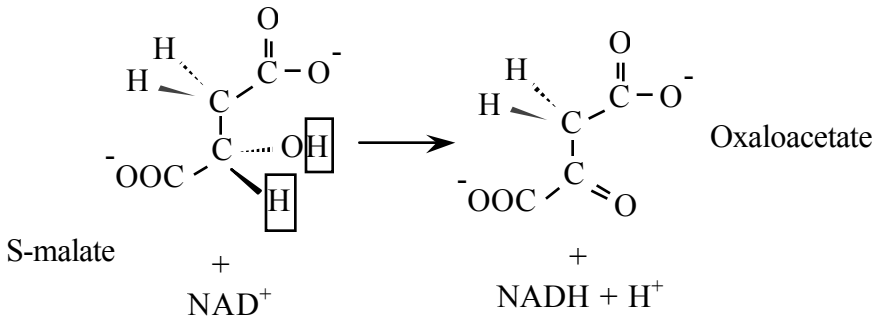

Figure 1-2: The mechanism of malate dehydrogenase.
MDH catalyzes the NAD^+-dependent oxidation of S-malate to oxaloacetate. A hydride ion is transferred from the C3-OH of malate to the *re* face of NAD^+ in a reaction similar to those observed for lactate dehydrogenase and alcohol dehydrogenase [1].

The MDH reaction mechanism involves hydride ion transfer to NAD^+ from the C3- hydroxyl of malate (figure 1-2). Under standard state conditions this reaction is highly endergonic (+29.7 kJ/mol) and coupling to the exergonic citrate synthase catalyzed condensation of oxaloacetate with acetyl-CoA (-31.5 kJ/mol) allows the reaction to proceed in the forward direction *in vivo* [1]. The K_m of the enzyme for NAD^+ is 0.14 mM and the K_m for the product OAA is 0.03mM [39]. The localization of the two isoforms allows MDH to play a role in the transport of reducing equivalents into the mitochondria, functioning in the malate-aspartate shuttle. The MDH-catalyzed reaction also plays an accessory role in the urea cycle as an intermediate reaction in the reconversion of fumarate to aspartate [1]. Interestingly, the two isoforms of pig heart MDH differ in their spectroscopic characteristics, as mMDH contains no tryptophan residues [40,41,42]. This property is exploited to assay the purity of the individual isoforms.

Citrate synthase

Pig heart citrate synthase (EC number 4.1.3.7) is a homodimer with subunit molecular weight of 47 kDa [1]. The enzyme catalyzes the first reaction of the citric acid cycle: condensation of oxaloacetate with acetyl-CoA to give citrate and coenzyme A [1, 42]. The enzyme follows an ordered, sequential mechanism in which oxaloacetate

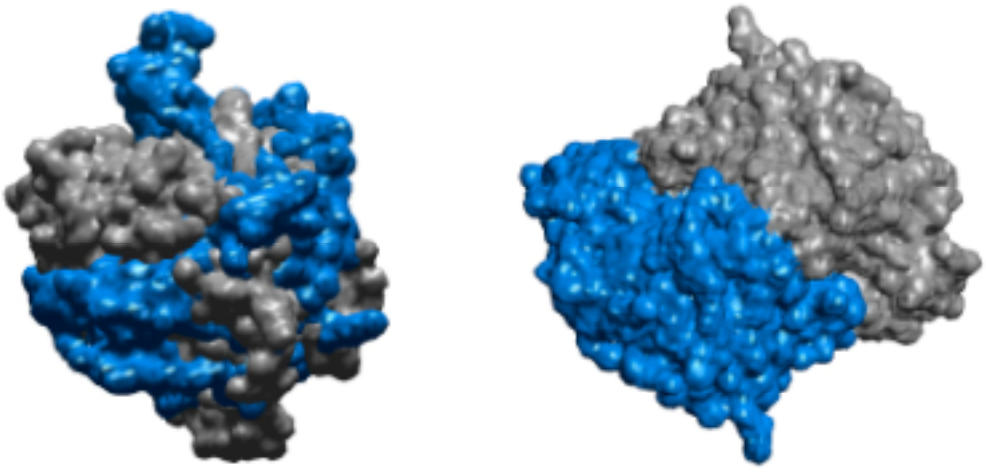

Figure 1-3: The crystal structure of citrate synthase.
Panel A shows the crystal structure of CTS in the closed conformation. Panel B shows the crystal structure in the open conformation. Individual subunits are shown in blue and grey. Oxaloacetate binding induces the conformational change, which creates the binding site for acetyl-CoA [44].

binding induces a large conformational change and generates the acetyl-CoA binding site [44,45]. The two subunits are initially in an "open" conformation, and upon OAA binding the small domain in each subunit undergoes an 18° rotation, which corresponds to movements in relative interatomic distances of up to 15 Å (figure 1-3) [44]. The reaction mechanism of CTS involves 3 steps (figure 1-4). First, the methyl group of acetyl-CoA is deprotonated to form an acetyl-CoA enol in the rate-limiting step of the reaction. The nucleophilic enol acetyl-CoA then attacks the electrophilic carbonyl of oxaloacetate to form citryl-CoA. Citryl-CoA is then hydrolyzed to form citrate and CoA in a strongly exergonic step that drives the overall reaction and provides the free energy necessary to pull the MDH catalyzed reaction as discussed previously [1,43]. Citrate synthase is subject to product inhibition by citrate and like many of the other enzymes of the citric acid cycle is regulated by product availability [1]. The K_m values of the enzyme for substrates are 5 μM and 0.22 mM for acetyl CoA in the closed and open conformations respectively, and 5.9 μM for oxaloacetate [43].

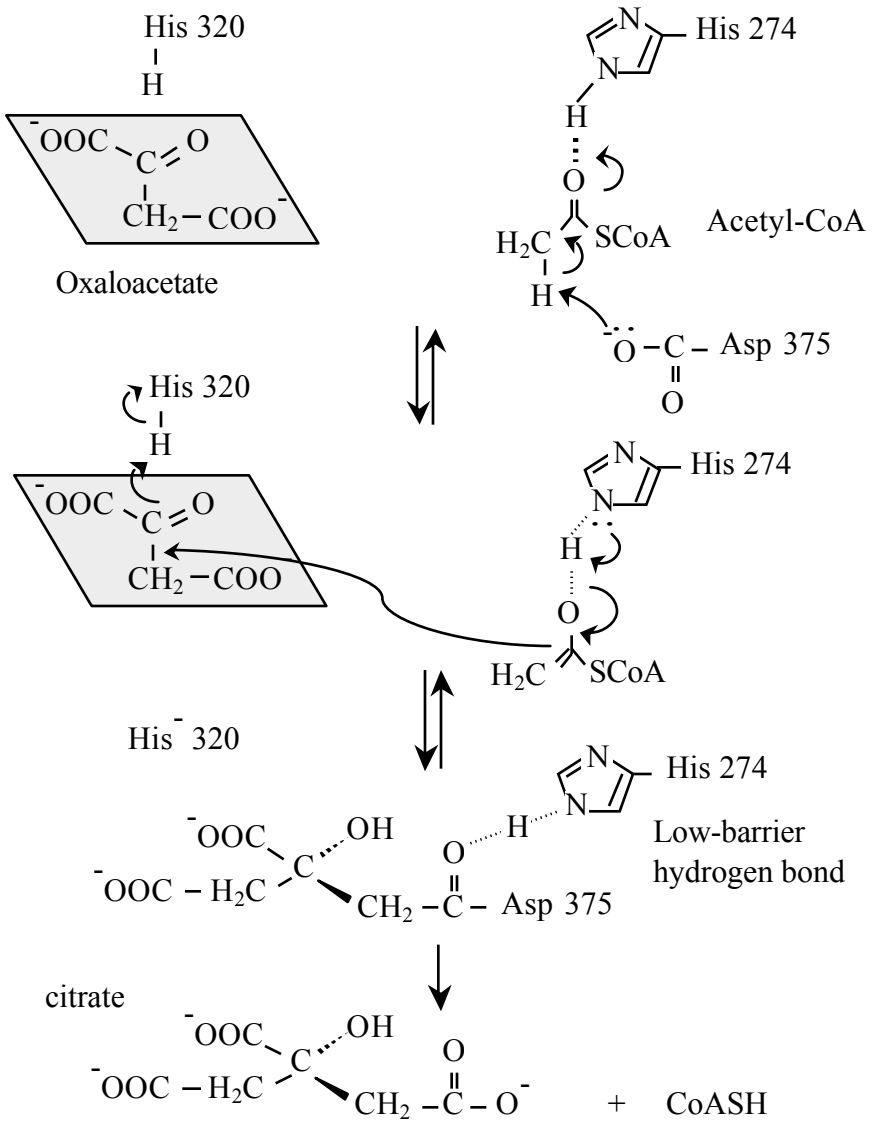

Figure 1-4: The mechanism of citrate synthase activity.
Oxaloacetate binding causes a conformational change in CTS, from "open" to "closed" forms and generates the acetyl-CoA binding site. Asp 375 acts as a general base, and His 274 acts as a general acid to generate the acetyl-coA enol, which is stabilized by a low energy hydrogen bond to the His 274 anion. The nucleophilic enol attacks the *si* face of oxaloacetate, and in a concerted acid-base reaction, His 274 reabstracts the donated proton and His 320 donates a proton to the oxaloacetyl anion to generate citryl-CoA. Finally, citryl-CoA is hydrolyzed to generate citrate and coenzyme A [1].

Characteristics of protein-protein interfaces

Protein-protein interfaces have characteristics that differentiate them from non-interacting surfaces, and characteristics that differentiate between specific interaction surfaces. These characteristics play a role in molecular recognition, and contribute to the overall free energy of binding. The traits common to interfaces include a high degree of hydrophobicity, planarity and complementarity to the interaction partner. The traits that distinguish between interaction surfaces include hydrophobicity, planarity, degree of hydrogen bonding and buried accessible surface area (ASA) [46]. These traits represent general characteristics and interfaces vary widely in the types of characteristics they possess; individual interfaces may or may not demonstrate any of the common characteristics of interfaces in general. The broad distribution of characteristics has made sequence or structure-based prediction of interfaces difficult [46,47]. While protein associations can be functionally delineated into obligate and transient interactions; the interface characteristics of the two types of interactions can likewise be classified. The ASA for typical protein-protein interfaces of known structure is approximately 1600 $Å^2$, and this size varies widely, from 1100 $Å^2$ to 4500 $Å^2$ [47]. Obligate interaction interfaces tend to have a larger interaction surface, whereas transient interactions are often smaller. Within an interface between two soluble protomers, the relative composition of aliphatic amino acid residues is often high relative to the percent

composition of hydrophobic amino acids that exist on all other protein surfaces. In high-affinity obligate interactions, the extent of hydrophobicity is higher than that observed for transient interactions. This phenomenon is attributed to the thermodynamic instability that arises from solvent exposure of hydrophobic residues when interaction partners are not associated [46]. The numbers of both hydrogen bonds and electrostatic interactions that exist in protein-protein interfaces are highly variable between interactions, but tends to be higher in obligate or high-affinity interactions than in transient interactions. The degree of planarity again varies between obligate and transient interactions. High-affinity interfaces are frequently non-planar, whereas lower-affinity interfaces have a higher degree of planarity, allowing rapid molecular recognition [46].

Evolution of interaction interfaces

Much like species, individual proteins and protein-protein interaction interfaces themselves have evolved by imparting selective advantage to a particular function. There are several selective advantages ascribed to multisubunit enzymes and protein interactions. There is an energetic advantage to translation of multiple copies of a smaller subunit over a single, large polypeptide. Producing a single copy of a protein with multiple interaction partners is advantageous to the presence of the gene encoding the subunit in multiple copies in the genome. Translation errors are introduced at a relatively

constant rate; therefore smaller proteins or subunits are less likely to contain errors than larger proteins. Finally, homotypic oligomers with a selective advantage or deleterious effect are more rapidly selected for or against than are monomers because the associated phenotype is evident in higher copy [2, 48].

The rates of protein evolution, quantified by the number of amino acid mutations incorporated with time, vary widely in nature. Enzymes that catalyze the most critical functions have the highest degree of sequence conservation with ancient ancestry [1]. These slowly evolving proteins are frequently those associated with gene regulation or DNA maintenance, and a classic example is the histone family of proteins. The most rapidly evolving proteins are those with non-essential functions, including fibrinogens. In a protein, the rates of evolution of specific protein domains similarly depend on the importance and specificity of the function associated with the domain. Active site residues evolve most slowly based on the absolute requirement for 3-dimensional orientation of the catalytic and associating amino acids relative to the bound substrate and adjacent residues. Any amino acid perturbation in the active site can severely hamper substrate binding or chemical catalysis [49]. Conversely, the residues that compose the outer surface of a protein evolve most rapidly [49]. In many cases, these residues can be altered significantly with minimal effects on protein structure, stability and function. Interface surfaces evolve at an intermediate rate, as protein-protein binding can affect stability or functionality of the protein. Changes in the amino acid

composition at an interface can lead to reduction or enhancement of the affinity of the interface, disrupting charge or hydrophobic interactions or by adding steric hindrance to the protein-protein contact [46,49].

Methods for the quantification of protein-protein interactions

Quantification of protein-protein interactions is fundamental to our understanding of cellular function. If protein-protein interactions underlie all cellular function at some level, then understanding the degree and thermodynamic influences of these interactions is critical. There are several techniques, both genetic and biophysical, used to demonstrate and to quantify macromolecular interactions. A brief summary of common examples of both genetic and biophysical techniques for the quantification of protein-protein interactions follows. The fluorescence techniques that are used extensively in chapters II-V are presented in additional detail.

Genetic methods

Genetic methods that demonstrate protein-protein interactions exploit the power of genetically pliable organisms to identify novel interactions and to confirm putative interactions. Genetic methods are simple, rapid and powerful tools for the identification

of associations. The disadvantages to these techniques are that they can be used in organisms other than yeast or prokaryotes only rarely, and that they are very seldom quantitative. Genetic methods can therefore be used to demonstrate an interaction but the affinity of the interaction can only be assessed qualitatively, if at all. The methods that are based most closely on classical genetic approaches are suppressor screens and screens for synthetic lethality [50]. In both of these techniques, a mutant phenotype is used as the basis to screen for additional mutations that produce an augmented or suppressed phenotype. Extragenic suppressors or synthetically lethal mutations are frequently, but not conclusively, evidence for a protein-protein interaction between the two gene products. Genetic methods to demonstrate protein-protein interactions also include a number of library-based techniques. The classic examples of these methods are the yeast two-hybrid scheme [51,52], and more recent one-hybrid variations including the λ-repressor scheme [52]. These methods involve screens or selections of a library of protein fusions between proteins of interest and the DNA-binding domain of a transcription factor. An interaction between the fusion products of two proteins results in transcriptional activation or repression of a reporter or selection gene. Phage display, while not strictly a genetic method, exploits the genetic pliability of filamentous phage to express a library of recombinant protein along with the coat protein of the phage. The population of phage displaying an interacting peptide is specifically increased by successive rounds of "panning" the phage; allowing interaction with an immobilized

protein of interest. Between each round of panning, the phage titer is increased and the process repeated. The process is essentially an *in vitro* selection, and ultimately the interacting gene product is identified [51].

Physical separation techniques

A number of techniques exist in which an interaction is demonstrated by physical separation of the interaction partners from non-interacting proteins. The advantage to methods of this kind is that they can explicitly demonstrate an interaction, and many of these techniques are quantitative under suitable conditions. The weakness inherent to any assay in which bound and unbound species are separated is that the association is no longer under conditions of equilibrium. The rates of association, and more particularly dissociation, must be carefully considered in the determination of equilibrium constants and affinities using these techniques. Examples of this type of method include immunological techniques, electrophoretic mobility shift assay, and affinity or size exclusion chromatography. Co-immunoprecipitation (Co-IP) immunodepletion and immunoblot can be classified together as immunological techniques. The underlying principle of each of these techniques involves the use of specific antibodies to one of the two interaction partners in a heteroassociation followed by physical separation from non-interacting biomolecules. The presence of the opposite member of the interacting

pair is then probed using a second specific antibody [2]. Electrophoretic Mobility Shift Assay (EMSA) or gel-shift assay exploits the difference in electrophoretic mobility between a free and bound protein form. These assays have been most commonly used to quantify protein-nucleic acid interactions, and are often visualized using radiolabeled nucleotides, however protein associations have also been demonstrated [53]. Quantitative size exclusion chromatography uses a cross-linked matrix to separate proteins based on their size. This technique takes advantage of the increased hydrodynamic radius of the associated species, and separates free protein from bound using a calibrated chromatography column [1,2]. Affinity chromatography exploits the interaction between two proteins to impede the elution of an interacting species on a chromatography column containing a matrix-immobilized interaction partner.

Steady-state fluorescence

Steady-state fluorescence methodologies including anisotropy and fluorescence intensity are commonly used biophysical techniques in the quantification of macromolecular assemblies [54-59]. The intrinsic fluorescence of native or engineered aromatic residues in a protein, particularly tryptophan, reports on the chemical environment in which those residues reside. Changes in protein conformation are often accompanied by alteration of the fluorescence properties of tryptophan residues as the

microenvironment of the residue is altered [54,59,60]. Thus the intensity of the emission is often a particularly useful monitor of both protein-protein and protein-ligand association. Anisotropy is a technique in which rotational correlation time is exploited to determine the Stoke's radius of the molecules in solution. A protein undergoing association increases in hydrodynamic radius and thus anisotropy is particularly sensitive to protein-protein interactions [54-57].

An extrinsic fluorophore with greater intensity, more suitable excitation or emission wavelengths, higher environmental sensitivity or longer fluorescent lifetime may be used to chemically modify a protein in order to enhance the fluorescence properties of the protein. A wide variety of these extrinsic fluorophores are available, and various chemical reactive groups may be conjugated to each, enabling the modification of the protein at amino acid residues containing thiol or amine groups. Use of extrinsically labeled proteins with such fluorescence probes as fluorescein, rhodamine and their chemical derivatives to examine macromolecular associations in the literature is extensive [40,42,54,55].

Principles of fluorescence

Fluorescence involves two fundamental and independent processes: excitation and emission. Excitation of a fluorescent molecule involves absorption of a photon of

sufficient energy to promote an electron from the ground state, S_0, to an excited state molecular orbital, denoted S_1, S_2, S_3, etc. (figure 1-5) [54, 61,62]. The excitation process occurs in 10^{-15}sec, and relative to the rate of molecular motion is instantaneous. The rapid excitation process ensures that the nuclei of the fluorophore are spatially fixed during excitation, a phenomenon is known as the Franck-Condon principal [54]. Each quantized energy level is subdivided into vibrational energy levels. The electron is promoted to a singlet, excited state and rapidly (10^{-12} sec) relaxes to the lowest energy excited state, a process known as internal conversion [63,64]. The promoted electron remains in the excited state for ~10^{-9}sec, a duration referred to as the fluorescence lifetime [54,60-67]. The relatively long duration of the fluorescence lifetime allows dynamic processes of the fluorophore on this timescale to be evaluated. Under conditions of sufficient photon flux, multiphoton excitation can occur [54]. The total energy of a single photon of excitation radiation of a given wavelength is equivalent to that of two photons of light with double the wavelength. Consequently, if two photons of light interact simultaneously with the fluorophore during the 10^{-15}s timescale of excitation then promotion to the excited state can occur [68,69]. The second major process is fluorescence emission. Emission involves return of the excited state electron to the ground state with concomitant release of a photon of corresponding wavelength. Fluorescence emission is a unimolecular reaction, and its time evolution is characterized by the following exponential decay:

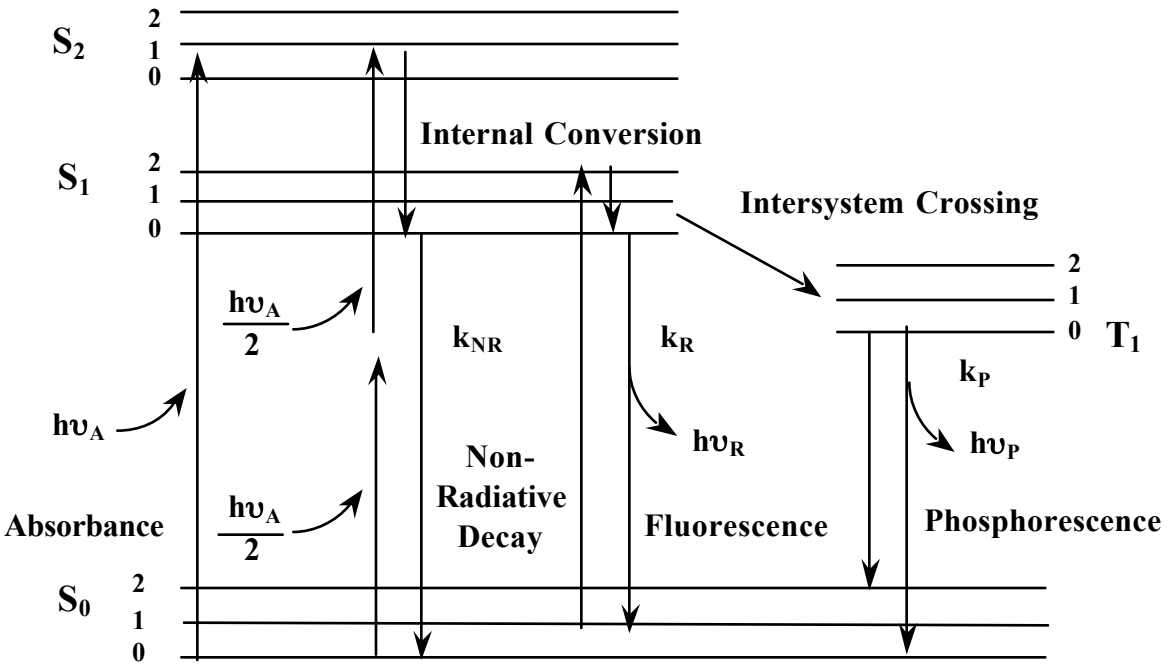

Figure 1-5: Jablonski diagram.
The Jablonski diagram depicts the two fundamental processes of fluorescence – excitation and emission. Excitation occurs when a photon of sufficient energy is absorbed, promoting a ground state (S_0) electron to a higher energy orbital (S_1, S_2, etc). In the excited state, the electron rapidly relaxes to the lowest energy excited state (S_1) before returning to the ground state either by non-radiative decay or with accompanying release of a photon of fluorescence emission. Occasionally, the excited state electron will cross to the triplet state (T_1). Return to ground state from the triplet excited state is a long-duration process, and if it is accompanied by photon release it is referred to as phosphorescence. Two-photon excitation occurs when two long wavelength photons, each with half the energy of $h\upsilon_A$, simultaneously interact with the fluorophore [54,61,62].

$$I(t) = I_0 e^{t/\tau} \qquad [1\text{-}1]$$

where I(t) refers to the intensity at time t, I_0 is the initial emission intensity and τ is the fluorescence lifetime [54].

The rate of emission of the photon is given by the equation:

$$k_R = \frac{1}{\tau_R + \sum \tau_{NR}} \qquad [1\text{-}2]$$

where k_R refers to the rate of photon emission, τ_R refers to the excited state lifetime of the fluorophore, and τ_{NR} refers to the lifetime of each non-radiative decay process. The extent of emission is characterized by the quantum yield, Q, a parameter that relates the yield of emission photons to the number of absorbed photons. The quantum yield, Q, is given by the rate of photon release relative to the rates of all decays to the ground state:

$$Q = \frac{k_R}{k_R + \sum k_{NR}} = \frac{\tau_{NR}}{\tau_R + \sum \tau_{NR}} \qquad [1\text{-}3]$$

where k_{NR} and τ_{NR} refer to the rate and the lifetime of the non-radiative decay process, respectively. Mechanisms of non-radiative decay include solvent relaxation, collisional quenching and resonance energy transfer.

Excited state electrons infrequently undergo intersystem crossing to the triplet state. In this conversion, the electron flips spin state and becomes unpaired. Decay of the unpaired electron from the triplet excited state to the ground state is not formally permitted and consequently the electron must flip spins prior to decay, leading to much longer triplet state lifetimes than fluorescence lifetimes. Triplet state lifetimes typically range from milliseconds to seconds or longer in duration. Photon emission that results from decay of the triplet state is referred to as phosphorescence [54].

Fluorescence intensity

Steady-state fluorescence intensity is a measure of the total fluorescence emission emanating from the fluorophore under excitation. The total emission is given by the sum of emission intensities at all emission wavelengths for all fluorescent emitters in solution. For a single fluorescent species, the area under the time-dependent decay of the excited state gives the total intensity:

$$I_{tot} = \int_{t=0}^{t=\infty} I_0 e^{-t/\tau} dt \qquad [1\text{-}4]$$

where I_0 is the initial intensity, t is time and τ is the fluorescence lifetime [54]. Measurement of the emission spectrum of the fluorescent sample and integration of the

spectral curve experimentally determine total emission intensity. When polarizers are used, the lab axis is generally accepted as the vertical orientation. Under vertically polarized excitation light, the total emission is given by the following equation:

$$I_{tot} = I_{\parallel} + 2I_{\perp} \qquad [1\text{-}5]$$

where $I_{||}$ refers to the measured emission intensity when excitation and emission polarizers are positioned in a parallel orientation and $I_{\perp}$ refers to the intensity when the polarizers are oriented perpendicular to one another. Alternatively, polarization artifacts are eliminated by measurement of emission intensity with the excitation polarizer oriented vertically, and the emission polarizer oriented at the magic angle, 54.7° [54].

Anisotropy

Anisotropy and polarization measurements exploit the random rotational motion of particles in solution during the excited state lifetime of a fluorophore to gain information regarding the hydrodynamic radius and hence the size of the fluorescent molecule. Using plane-polarized excitation light in the vertically oriented lab axis, only those fluorophores with excitation dipoles aligned with the orientation of that excitation

are excited, according to selection rules [54, 70]. The selection rules are given by the equation:

$$I_{\parallel}(\theta) = k < \cos^2 \theta > \qquad [1\text{-}6]$$

where θ is the angle between the vertical lab axis and the excitation transition moment of the fluorophore. Those fluorophores undergo rotation during the excited state lifetime, and the emission is depolarized by an amount corresponding to the degree of rotation. The extent of depolarization relative to total emission yields the anisotropy:

$$r = \frac{I_{\parallel} - I_{\perp}}{I_{\parallel} + 2I_{\perp}} \qquad [1\text{-}7]$$

where anisotropy is denoted by r, and the total intensity is given by $I_{||} + 2\ I_{\perp}$ (equation 1-5) [54,56].

The experimental design for a typical anisotropy experiment is demonstrated in figure 1-6. The excitation polarizer restricts the excitation to only those fluorophores with excitation dipole moments aligned within $\cos^2\theta$ of the polarized excitation light. The solution is hence anisotropic with respect to excited state fluorophores. The

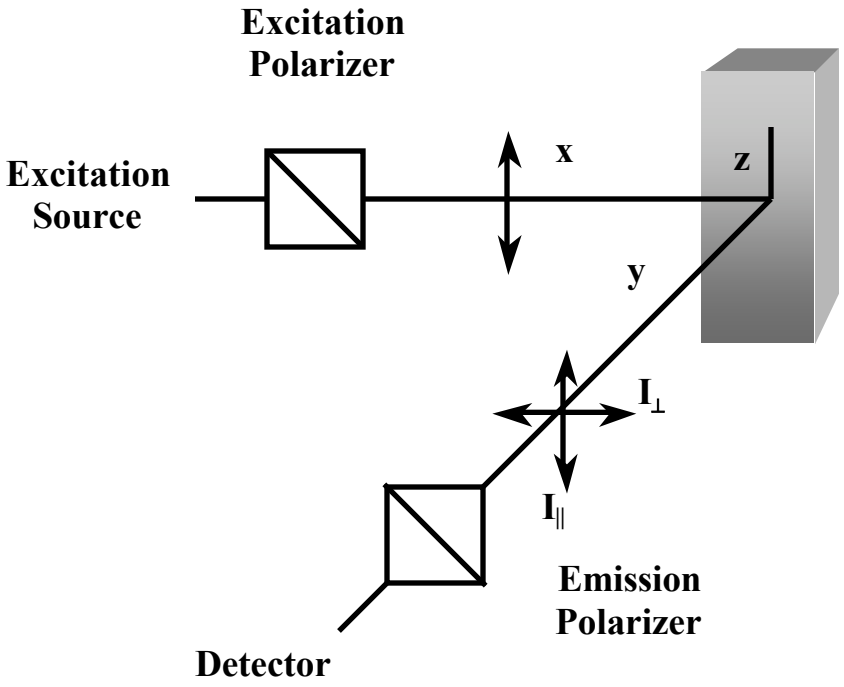

Figure 1-6: Anisotropy experimental design.
Monochromatic excitation light passes through an excitation polarizer, which allows only vertically polarized light to reach the sample. Those fluorophores in solution with excitation dipoles aligned with the vertically polarized excitation light are excited, according to the selection rules. Fluorescence emission passes through a second polarizer that is oriented vertically and horizontally in succession, and the emission intensity is measured in each orientation [54].

excitation of a fluorophore involves absorption of a photon of incident light, accompanied by excitation of an electron between its ground state orbital and an excited state. The excitation dipole moment of a fluorophore is a function of the physical geometry of the movement between the ground and excited state of the electron. In the absence of motion, the excited state electron returns to the ground state with the concomitant emission of a photon depolarized to some degree. This depolarization, referred to as the intrinsic anisotropy (r_0), is a degree of depolarization that relates to the angle between the excitation and emission dipole moments of the fluorophore [54,70]. Emission arises from the electronic transition from the lowest energy excited state to the ground state, and relaxation to the lowest excited state occurs prior to emission. Emission from this dipole is rarely collinear with the excitation dipole, and consequently this electronic rearrangement causes a degree of depolarization. The intrinsic anisotropy is thus a function of the physical geometry between the excitation dipole and the emission dipole [56]. During the excited state lifetime, typically several nanoseconds, random rotation of each molecule occurs. This molecular motion enhances the depolarization of the emission, and the measured anisotropy is therefore related to both the physical geometry of the fluorophore and the degree of rotation of the fluorophore. The anisotropy of a spherical fluorophore with single exponential emission decay is predicted by the Perrin equation: excitation of a fluorophore involves absorption of a photon of incident light, accompanied by excitation of an electron between its ground

state orbital and an excited state. The excitation dipole moment of a fluorophore is a function of the physical geometry of the movement between the ground and excited state of the electron. In the absence of motion, the excited state electron returns to the ground state with the concomitant emission of a photon depolarized to some degree. This depolarization, referred to as the intrinsic anisotropy (r_0), is a degree of depolarization that relates to the angle between the excitation and emission dipole moments of the fluorophore [54,70]. Emission arises from the electronic transition from the lowest energy excited state to the ground state, and relaxation to the lowest excited state occurs prior to emission. Emission from this dipole is rarely collinear with the excitation dipole, and consequently this electronic rearrangement causes a degree of depolarization. The intrinsic anisotropy is thus a function of the physical geometry between the excitation dipole and the emission dipole [56]. During the excited state lifetime, typically several nanoseconds, random rotation of each molecule occurs. This molecular motion enhances the depolarization of the emission, and the measured anisotropy is therefore related to both the physical geometry of the fluorophore and the degree of rotation of the fluorophore. The anisotropy of a spherical fluorophore with single exponential emission decay is predicted by the Perrin equation:

$$r = \frac{r_0}{1 + (\tau/\theta)} \qquad [1\text{-}8]$$

where the parameter θ is the rotational correlation time [71]. The rotational correlation time for a single, exponential fluorescence decay is given by:

$$r = r_0 e^{-t/\theta} \qquad [1\text{-}9]$$

The rotational correlation time is also dependent on the solution conditions under investigation:

$$\theta = \frac{\eta V}{RT} \qquad [1\text{-}10]$$

where η refers to solution viscosity, V is the partial specific volume of the rotating species, R is the gas constant and T is temperature [54]. Larger fluorescent particles rotate more slowly and the degree of depolarization is reduced, hence the anisotropy is direct method for the quantification of macromolecular interactions.

Polarization is an alternative method to anisotropy in the examination of rotational correlation. Polarization and anisotropy measurements contain the same information content, but differ in the analysis of the data. Polarization is given by the equation:

$$P = \frac{I_{\parallel} - I_{\perp}}{I_{\parallel} + I_{\perp}} \qquad [1\text{-}11]$$

where P refers to the polarization, and $I_{||}$ and $I_{\perp}$ are intensity measurements as described for anisotropy.

These two measurements can be interconverted using the following equations:

$$r = \frac{2P}{3 - P} \qquad [1\text{-}12]$$

$$P = \frac{3r}{2 + r} \qquad [1\text{-}13]$$

As the two forms of measurement can be easily interconverted, there is no experimental advantage to using one over the other. The benefit of anisotropy is the additive nature of anisotropy values in a multicomponent solution of fluorophores [70].

Förster Resonance Energy Transfer

From the excited state, the return to the ground state can be accomplished by radiative emission or by non-radiative decay (equation 1-2). One mechanism of non-radiative decay that can be utilized in quantification of protein interactions is Förster Resonance Energy Transfer (FRET). FRET is non-emissive energy transfer between a fluorophore, referred to as the donor, with an emission spectrum that overlaps the

absorbance of a second, proximally oriented chromophore, called the acceptor. In this interaction, the excited state energy of the donor species is gained by the acceptor chromophore with concomitant return of the donor to the ground state. The process does not involve emission of a photon by the donor followed by absorption of the photon by the acceptor; rather the process is a dipole-dipole interaction between the two species. The acceptor molecule is often a fluorophore itself, but this is not necessarily the case. The conditions for resonance energy transfer are spectral overlap, close proximity and relative dipole-dipole orientation. The rate of energy transfer, k_T, is given by:

$$k_T(r) = \frac{Q_D \kappa^2}{\tau_D r^6}\left[\frac{9000(\ln 10)}{128\pi^5 N n^4}\right]\int_0^x F_D(\lambda)\varepsilon_A(\lambda)\lambda^4 d\lambda \qquad [1\text{-}14]$$

where Q_D is the quantum yield of the donor in the absence of acceptor, κ^2 is an orientation factor relating the emission and excitation dipoles of the donor and acceptor, τ_D is the lifetime of the donor in the absence of acceptor, r is the donor-acceptor distance, N is Avogadro's number, n is the refractive index of the solution, $F_D(\lambda)$ is the normalized fluorescence intensity of the donor over the wavelength region examined, and $\varepsilon_A(\lambda)$ is the extinction coefficient of the acceptor over the same wavelength region. The integral term of the equation is referred to as the overlap integral and describes the extent to which the donor emission and acceptor absorbance spectra overlay. The orientation factor κ^2 is

typically taken as 2/3, which corresponds to the average value assuming randomization of both excitation and emission dipoles by rotational diffusion. The rate of energy transfer is inversely proportional to the 6th power of the distance between donor and acceptor, and this strong distance dependence imposes a limiting distance of <100 Å on energy transfer; though this limit depends on both the donor-acceptor pair and experimental conditions. For a specific donor-acceptor pair a term called the Förster distance can be defined:

$$k_T = \frac{1}{\tau_D}\left[\frac{R_0}{r}\right]^6 \qquad [1\text{-}15]$$

where τ_D is the decay time of the donor in the absence of the acceptor, and R_0 is the Förster distance [54,72]. At a donor-acceptor distance equivalent to the Förster distance, the transfer efficiency is 50%; therefore the donor emission intensity is half of the total emission in the absence of acceptor. The Förster distance encompasses all constant terms for a given donor-acceptor pair, including the overlap integral, orientation factor and refractive index.

The strong distance-dependence of FRET can be exploited to examine macromolecular interactions. If two biomolecules are modified with extrinsic fluorophores: a donor and an acceptor respectively, an association between those biomolecules may closely align the donor and acceptor. Conversely, two non-interacting fluorophores or extrinsically labeled proteins in solution will show minimal FRET.

Experimentally, FRET is monitored by measurement of either the fluorescence lifetime of the donor; or the fluorescence intensity of either donor or acceptor, if the acceptor itself is fluorescent. Energy transfer is useful only if the rate of transfer is comparable to or faster than the rate of the fluorescence decay of the donor. The FRET efficiency is the ratio of photons transferred to the acceptor to the total number of photons absorbed by the donor. This efficiency is expressed in terms of the rate of transfer relative to the sum of all rates of return to the ground state:

$$E = \frac{k_T}{(1/\tau_D) + k_T} \qquad [1\text{-}16]$$

From this equation, it is clear that if the rate of decay is high, then minimal transfer will be observed during the excited state lifetime of the donor; hence the efficiency of transfer will be low. Conversely, FRET is maximal when the rate of transfer is high relative to the other decay rates. The FRET efficiency is experimentally determined by measurement of the emission or lifetime of the donor in the absence and in the presence of the acceptor:

$$E = 1 - \frac{\tau_{DA}}{\tau_D} = 1 - \frac{F_{DA}}{F_D} \qquad [1\text{-}17]$$

where τ_D and τ_{DA} refer to the fluorescence lifetime of the donor in the absence and presence of the acceptor, and F_D and F_{DA} refer to the fluorescence intensities of the donor under the same two conditions.

While experimentally the FRET donor and acceptor typically consist of two different fluorophores with overlapping emission and excitation spectra, this need not necessarily be the case. Homotransfer, which refers to a situation in which two copies of the same fluorophore act as both donor and acceptor, is periodically observed. These cases are characterized by an increase in the stoichiometry of fluorophore that does not lead to a corresponding increase in the fluorescence intensity of the molecule, and typically occur for fluorophores with a small Stoke's shift [54]. Furthermore, homotransfer is strongly depolarizing, and consequently the observed anisotropy of the fluorophore is much lower than would be predicted. The excited state electron can undergo resonance transfer to an adjacent fluorophore, particularly when excited at lower wavelengths. The excited state electron can occupy the higher vibrational energy states of the excited state, and transfer can occur to a lower energy excited state of a proximal fluorophore. Exciting the fluorescent sample at higher wavelengths can minimize homotransfer, utilizing the so-called "red-edge effect" [73].

Fluorescence Correlation Spectroscopy

Fluorescence Correlation Spectroscopy (FCS) is a technique that interrogates fluctuations in fluorescence intensity to determine diffusion and temporally variable characteristics [74,75]. This technique involves focusing a coherent laser excitation source using a microscope objective lens onto a sample of randomly oriented, randomly diffusing fluorophores. The lens produces a microscopic volume within which fluorescence excitation occurs. The excitation volume shaped by the objective lens is on the order of femtoliters under typical experimental conditions. Small numbers of fluorescent particles diffusing randomly from a larger volume through the small volume of excitation produce fluctuations in intensity around the average fluorescence intensity, and these fluctuations correspond to changes in the number of particles within the volume. The intensity arising from a small volume of laser excitation is given by the equation:

$$F(t) = \kappa Q \int W(r)c(r,t)d\Omega \qquad [1\text{-}18]$$

where κ is a constant, Q is the product of absorptivity, quantum yield and experimental collection efficiency and c(r,t) refers to the number density of fluorescent particles at

position r and time t, Ω is a volume element and the function is integrated through 3-dimensional space. W(r) is a function describing the emission:

$$W(r) = I(r)S(r)T(r) \qquad [1\text{-}19]$$

where I(r) is the spatial intensity profile of the excitation beam, S(r) defines the extent of the sample and T(r) refers to the volume of excitation [76]. In most cases, the laser beam has a gaussian intensity profile, thus a 2-D gaussian model is often used to describe the focal point of the microscope. In 2-photon excitation experiments, the x and y-axis follow a Lorentzian intensity contour; therefore the excitation volume is described by a Gaussian-Lorentzian profile. Fluctuations in particle concentration from the average concentration at position, r, and time, t, are given by the following equation:

$$\delta C(r,t) = C(r,t) - \langle C \rangle \qquad [1\text{-}20]$$

where the term <C> denotes the average concentration. Substitution of equation [1-20] into equation [1-19] gives us the average fluorescence intensity and the fluctuation in intensity at time, t.

$$\langle F \rangle = \kappa Q \langle C \rangle \int W(r) d\Omega \qquad [1\text{-}21]$$

$$\delta F(t) = \kappa Q \int \delta C(r,t) W(r) d\Omega \qquad [1\text{-}22]$$

Thus it is evident from equation [1-22] that fluctuations in intensity arise primarily from fluctuations in concentration of fluorescent particles.

The time-resolved fluctuations that arise from particle diffusion through the focal point of the lens are interrogated using autocorrelation analysis. Autocorrelation is a statistical method that determines the degree of non-randomness in a temporally derived data set. The normalized autocorrelation function is given by the following equation, where i = j.

$$G(t) = \frac{\sum_{m=1}^{m} < F_i(t) F_j(t-\tau) > - < F(t) >^2}{< F_i(t) >< F_j(t) >} \qquad [1\text{-}23]$$

$$G(t) = \frac{\sum_{m=1}^{m} < \delta F_i(t) \delta F_j(t-\tau) >}{< F_i(t) >< F_j(t) >} \qquad [1\text{-}24]$$

where $F_i(t)$ refers to the measured fluorescence intensity of species i at time t. $F(t\text{-}\tau)$ refers to the fluorescence intensity at a time delay, τ, later, <F(t)> refers to the average fluorescence intensity and $\partial F(t)$ refers to the fluctuation in fluorescence from the average at time t. The fluctuations in intensity are non-random and correlate precisely with the

fluctuations in concentration of fluorophore within the focal volume, as described by equation [1-22]. The normalized fluorescence autocorrelation function is derived by substitution of equations [1-21] and [1-22] into [1-24]:

$$G(\tau) = \frac{\iint W(r)W(r')f(r,r',\tau)d\Omega d\Omega'}{\left[< C > \int W(r)d\Omega\right]^2} \qquad [1\text{-}25]$$

$$f(r,r',\tau) = < \delta C(r,r',t+\tau)\delta C(r',t) > \qquad [1\text{-}26]$$

$$f(r,r',\tau) = < \delta C(r,\tau)\delta C(r',0) > \qquad [1\text{-}27]$$

The equation f(r, r′,τ) defines the correlation between concentration fluctuations at position r with concentration fluctuations at position r′ a time, τ, earlier. Correlation of fluctuations in fluorescence intensity results directly from fluctuations in particle number of fluorescent species arising from changes in position with time caused by Brownian diffusive motion [76]. Fluctuations in the number of particles observed in a small volume relate to the duration of persistence of a fluorophore within the excitation volume. The persistence time of a fluorophore within the volume is a function of the size of the volume and the diffusion properties of the fluorophore. For an excitation volume with precisely defined geometry, autocorrelation analysis yields a time-dependent decay from which apparent diffusion coefficient and particle number can be derived. The autocorrelation analysis is fit to an exponential decay, relating the time

dependent decay of the fluctuation to the time dependent diffusion characteristics of the fluorescent particle:

$$G(t) = \frac{G(0)}{1 + (\tau/\tau_D)} \qquad [1\text{-}28]$$

where τ_D is the diffusional correlation time. The diffusional correlation time is related to the both the excitation volume and the diffusion constant of the fluorophore:

$$\tau_D = \frac{s^2}{4D} \qquad [1\text{-}29]$$

where D is the diffusion coefficient and s is the $1/e^2$ radius of the focused laser beam. Differences in diffusion coefficient relate closely to differences in particle size and can be utilized to differentiate oligomeric forms. The diffusion coefficient is related to hydrodynamic radius, as well as solution conditions by the Stokes-Einstein equation:

$$D = \frac{k_B T}{6\pi\eta R} \qquad [1\text{-}30]$$

where k_B refers to the Boltzman constant, T is temperature, η is the solution viscosity and R is the radius, assuming a spherical molecule [77]. The autocorrelation function at τ

= 0 reduces to the variance normalized to the average number of particles within the excitation volume. For a Gaussian distribution of particles in solution, the variance and the mean are equivalent and the amplitude of the autocorrelation function is correspondingly inversely proportional to the particle number [78].

$$G(0) = \frac{< N^2 >}{< N >^2} = \frac{1}{< N >} \qquad [1\text{-}31]$$

The amplitude of the autocorrelation function yields the particle number, which can then be utilized to determine concentration if the focal volume is known precisely. Both the particle number and the diffusion coefficient yield data relating to associations, since an association between two particles will decrease the total particle number and increase the size of each individual particle. The small excitation volume and the free diffusion of particles between that volume and the dilute solution that surrounds it combine to give this technique resolution that approaches a single molecule level.

The FCS technique is most proficient when the concentration of fluorophore is low, or when the focal volume is small such that the average number of particles in the volume at any time approaches one [77]. To experimentally minimize the focal volume, two techniques are utilized: confocal optics or multi-photon excitation. In the confocal optical arrangement a lens and a pinhole are placed in the emission path (figure 1-7). The emission lens and the pinhole define the z-axis or focal plane by filtering all off-plane

emission. In this method, excitation occurs throughout the laser path, but only emission arising from the focal plane is detected. This restricts the observation volume in the z-axis, but reduces the emission intensity. In the second method, multiphoton excitation is utilized to minimize the focal volume. In this case, an infrared pulsed-laser is used as excitation source. The mode-locked, Ti: Sapph pulse laser has a pulse width of $\sim 10^{-13}$ sec, at a frequency of 80 MHz and output power of 1.2 W, hence the maximal pulse intensity is approximately 100 kW. The temporally compressed photons emitted by the pulsed-laser are incident on the objective lens, which compresses those photons spatially. The photon flux at the focal point of the microscope exceeds 10^{31} $sec^{-1}cm^{-2}$ [79]. With the vast photon flux at the focal point, two high wavelength photons can simultaneously interact with the fluorophore inducing excitation of an electron to the excited state. One photon of low wavelength high-energy excitation is energetically equivalent to two photons of double the wavelength. Under these excitation conditions, because a single photon of infrared excitation has insufficient energy to induce excitation, the excitation follows a quadratic with respect to excitation power. Photon flux sufficient to induce excitation occurs only at the focal point of the objective lens. The benefits of multiphoton excitation are its relative ease of use compared with confocal

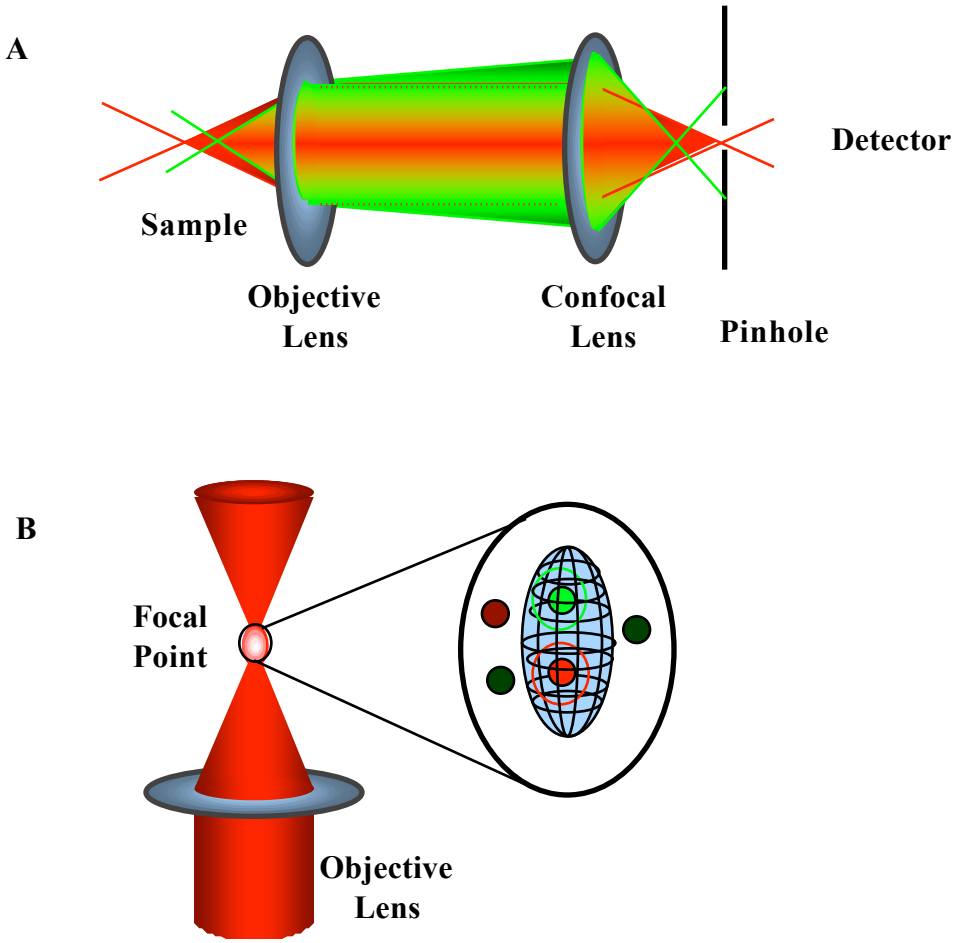

Figure 1-7: Optic diagrams of confocal and multi-photon FCS.
Panel A: confocal optic diagram. Fluorescence emission arising at the focal plane is shown in red, emission from off-plane fluorophores is shown in green. Off-plane emission is filtered by the confocal pinhole.Panel B: multiphoton optic diagram. The IR-excitation laser is focused by the objective, and sufficient photon flux to achieve two-photon excitation occurs only within the focal volume.

optics, the non-invasive nature of IR irradiation and hence depth of sample field that can be interrogated, and broad two photon absorbance spectra of most fluorophores [78]. The two-photon absorbance spectrum, or cross section, of most fluorophores is much broader than the corresponding single photon absorbance spectrum. Consequently, multi-photon, multi-channel FCS is accomplished with a single laser excitation source [79]. With a confocal optical arrangement, multi-channel FCS requires laser excitation of multiple fluorophores using the overlaid emission beams of multiple lasers.

FCS utilizes the fluctuation in fluorescence intensity caused by the time-dependent changes in the number density of fluorescent particles within a small, defined volume of examination. From the autocorrelation analysis of these temporal fluctuations in intensity, particle numbers (varies with $1/G(0)$) and diffusion co-efficient (τ_D) are derived. Both of these parameters are effective in the examination of association reactions as diffusion is closely linked to molecular size, and particle number is reduced in a bimolecular association. The strength of this technique over conventional fluorescence methodologies is its detection of single molecule emission, and hence experimental fluorophore concentrations are small. Examination of high affinity association equilibria can therefore be accomplished. Drawbacks with the technique arise from its dependence on detectable fluctuations and consequently the dynamic range of fluorophore concentrations is limited. As fluorophore concentration increases, the corresponding amplitude of fluctuations in intensity decreases. Furthermore, diffusion

coefficient scales with the cubic root of molecular weight, and inherent noise in the analysis prevents discrimination of differences in diffusion coefficient less than 2. Consequently, differences in size of less than 8-fold may not be effectively resolved by this technique. Correlation amplitude varies inversely with concentration, thus can be used to monitor association regardless of the observed diffusion characteristics.

Fluorescence Cross-correlation Spectroscopy

Multi-channel Fluorescence Cross-correlation allows differentiation of multiple species with spectrally distinct fluorescence characteristics [80]. Utilizing fluorophores with emission of two different wavelengths, and separating emission using a dichroic into 2 or more detector channels (figure 1-8) allows simultaneous correlation of each species in solution. Cross-correlation analysis extends the autocorrelation function to accurately quantify doubly labeled fluorescent species yielding emission in multiple wavelength regimes, both red ($\lambda > 625$ nm) and green ($\lambda \cong 525 - 575$ nm). Cross-correlation analysis interrogates the concomitant fluctuations between red and green spectral channels caused by direct interaction of these two fluorophores (or fluorophore-linked biomolecules) in solution. The cross-correlation function is given by equation 1-23, where $i \neq j$. Cross-correlation of multichannel FCS data directly addresses molecular interaction, and the concentration of the interacting species can be derived from the cross-correlation

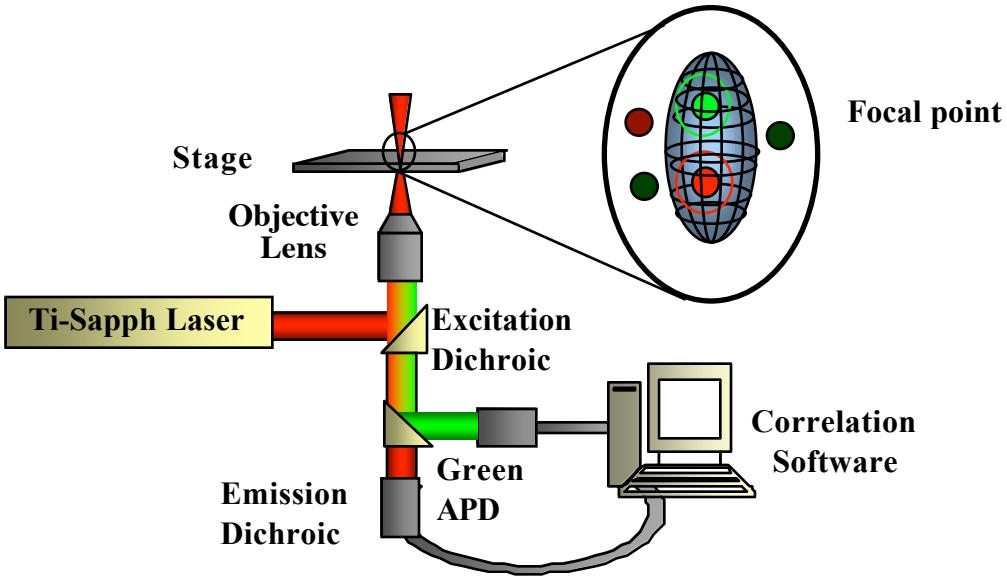

Figure 1-8: Fluorescence Correlation Spectroscopy experimental arrangement. Infrared emission from a Titanium: Sapphire pulsed laser is directed through the objective lens of an inverted microscope and is focused onto the sample. Excitation occurs only at the focus of the lens, shown inset. Fluorescence emission is collected in the epi-fluorescence direction, through the objective lens and is separated onto red and green channel avalanche photodiode detectors by a dichroic mirror.

amplitude [81,82]. The overlapping beams of two laser sources are used to stimulate 1-photon FCS exciation, or altermatively a Titanium:Sapphire pulsed laser emitting in the near-IR is used to stimulate 2-photon excitation of the fluorophores. The broad 2-photon absorbance spectra of most fluorophores enable simultaneous excitation of both fluorophores with a single excitation wavelength. Cross-correlation analyzes the concomitant red and green fluctuations arising from emission of a double-labeled molecular species. The amplitude of the cross-correlation function is directly proportional to particle number, and the decay yields the diffusion coefficient of the double-labeled species. In an examination of biomolecular association, the double-labeled species arises from association between fluorophores or fluorophore-linked protein molecules; thus cross-correlation is a direct measurement of the extent of the association reaction under experimental conditions. An advantage of this technique over autocorrelation is the relatively small background arising from single labeled molecules, and elimination of complications with analysis arising from intersystem crossing. Unfortunately, due to spectral overlap between green and red emission and the inability to completely filter red-edge emission of green fluorophores from detection in the red channel, spectral contamination of cross-correlation will occur. This phenomenon is referred to as detector cross talk. Another limitation of this technique is the dependence of the amplitude of the cross-correlation on the amplitude of the individual autocorrelation amplitudes, each of which is inversely related to total fluorophore

concentration. Consequently, at high fluorophore concentrations, the cross-correlation amplitude is small regardless of the degree of molecular association.

Photon Counting Histogram

The Photon Counting Histogram (PCH) is utilized to analyze fluorescence fluctuation data based on the intensity of individual fluctuations rather than their time-dependence [82]. A histogram of photon counts is plotted against the number of times that count number occurs, and yields two parameters: the particle number (N) and the molecular brightness (ε). A bimolecular association between two fluorophores or labeled biomolecules is predicted to reduce the particle number and increase the brightness of the associated pair. This analytical technique has an advantage over cross-correlation in determination of association in its use of a single fluorophore rather than multiple fluorophores. As with correlation analysis, PCH analysis becomes less sensitive as particle number increases. The relative fluctuation intensity decreases with fluorophore concentration, and consequently, the histogram is most accurate at low concentrations.

Enzyme regulation

Significance of enzyme regulation

Enzyme regulation occurs in all living organisms and is of critical importance in biology. In most metabolic pathways, at least one step is tightly controlled, allowing metabolic flux to be attenuated with environmental and cellular conditions [1]. Conflicting pathways are coordinately regulated, preventing the simultaneous synthesis and breakdown of a metabolic intermediate, a so-called "futile cycle". Conversely, related pathways are jointly activated or inhibited by the same regulatory molecules. Enzyme regulation thus allows the metabolic conditions of the cell to adequately reflect the environmental conditions and maximizes the efficient use of metabolites.

Types of enzyme regulation

Enzyme regulation takes two broad forms: covalent and non-covalent regulation. Each of these types has specifically evolved to perform functions as necessary, and for purposes herein we limit our discussion to non-covalent modification of the enzymes involved. Non-covalent regulation is characterized by small molecule binding, and is in turn classified into two broad types: dead-end and allosteric; differentiated by the

position on the enzyme at which the regulatory molecule binds. Dead-end inhibition refers to ligand binding at the active site, and allosteric regulation refers to ligand binding elsewhere on the enzyme. There are three types of dead-end inhibition: competitive, uncompetitive and noncompetitive. These methods of regulation differ in the enzyme form to which each binds. Competitive inhibitors are typically substrate analogs and compete with substrate for binding to the enzyme. These inhibitors alter the apparent K_m of the enzyme for substrate. Uncompetitive inhibitors bind to the enzyme-substrate complex, and subsequently reduce the catalytic rate of the enzyme, V_{max}, and decrease K_m. Uncompetitive inhibitors are characterized by parallel double reciprocal plots in the presence of inhibitor. For multisubstrate enzymes, an uncompetitive inhibitor will often be competitive with respect to one substrate, and uncompetitive for the other. Noncompetitive inhibitors bind to both free enzyme and the Michaelis complex, and consequently alter both K_m and V_{max}. The second type of non-covalent regulation involves binding a regulatory molecule at a specific ligand-binding site distant on the enzyme from the active site and is known as allosteric regulation [1,83,84,85].

Allosteric regulation

Allosteric regulation is distinguished by attenuation of catalysis through binding an allosteric ligand to a binding site distant on the enzyme from the active site, called an

allosteric site. This type of regulation can be classified into two types: V-type allosteric regulation, under which ligand binding induces a change in V_{max}, and K-type allosteric regulation, under which ligand binding alters K_m. The characteristic of allosteric regulation that differentiates this form from all other types of regulation is binding of the inhibitor or activator to the enzyme at a unique regulatory site. The consequence of this distal binding site is that for K-type effectors, the inhibitor does not completely ablate substrate binding, and therefore inhibition cannot be complete. Saturation can occur at both active site and allosteric site simultaneously and catalysis can still occur. This gives rise to a replot of substrate affinity vs. inhibitor concentration that approaches maximal and minimal values. In the case of dead-end inhibition, at infinite concentration of inhibitor, inhibition is complete and consequently no saturation is observed at high concentrations of inhibitor in a similar replot [86, 87].

In addition to the K and V-type effects, allosteric regulation can be delineated into homotropic and heterotropic regulation, based on the nature of the ligand that causes the effect. Homotropic interactions, which lead to a phenomenon known as cooperativity, are enhancements or restriction of binding a substrate or ligand caused by binding the same substrate or ligand at another binding site. A well-characterized example of this type of interaction is the binding of oxygen by hemoglobin. Hemoglobin is a homotetramer containing an oxygen-binding heme prosthetic group in each subunit. Each heme can independently bind a molecule of oxygen; the tetramer can therefore bind

4 oxygen molecules in total. The first oxygen binding association has low affinity, and this first association increases the affinity of subsequent binding events leading to the characteristic sigmoidal saturation profile. The induced binding is the defining characteristic of homotropic cooperativity [1].

Binding of a ligand or substrate molecule to a single or homogeneous binding site is described by the following general reaction:

$$E + S \underset{}{\overset{K_a}{\rightleftharpoons}} E\text{-}S$$

where K_a represents the association constant for the creation of the enzyme-substrate complex, ES. The dissociation constant, K_d, is given by the equilibrium expression for the reverse reaction.

$$K_d = \frac{[E][S]}{[ES]} \qquad [1\text{-}32]$$

The binding equilibrium is also described in terms of fractional saturation:

$$\theta = \frac{[S]}{K_d + [S]} \qquad [1\text{-}33]$$

where the fractional saturation, θ, is defined as the fraction of enzyme bound relative to the total enzyme concentration. The equations described apply to a single, homogeneous binding site or binding affinity and the functional dependence of saturation with concentration of substrate is hyperbolic. While this type of binding is commonly observed, it applies only to enzyme binding in which only a single binding site is present, or independent binding events at multiple sites. In the case where multiple, non-independent binding sites are present the general equation is modified as follows:

$$E + nS \underset{}{\overset{K_a}{\rightleftharpoons}} E\text{-}nS$$

In this case, n is the substrate binding stoichiometry, and n is an integer greater than one. The dissociation constant is given by the following equation:

$$K_d = \frac{[E][S]^n}{[E - nS]} \qquad [1\text{-}34]$$

where the substrate concentration is raised to an exponent equivalent to the stoichiometry of binding. The fractional saturation is given by the Hill equation [88]:

$$\theta = \frac{[S]^{n_H}}{K_d + [S]^{n_H}} \qquad [1\text{-}35]$$

where n_H is referred to as the Hill constant. For K-type allosteric effects, with $n_H > 1$ this equation represents positive cooperativity in substrate binding. This is the functional dependence observed for oxygen binding by hemoglobin. For $n_H < 1$, negative cooperativity is observed; binding a ligand makes successive binding events more difficult. An important consequence of the binding reaction shown is that the stoichiometry, n, cannot exceed the number of ligand binding site on the enzyme. Accordingly, the Hill constant also cannot exceed the number of binding sites. Furthermore, for cooperativity to exist, successive ligand binding events must be interdependent. For multiple binding sites in which binding is independent, homogeneous affinity for all sites and hyperbolic saturation are observed.

For positive cooperativity to exist in the hemoglobin tetramer, oxygen binding must induce a structural or energetic alteration within the protein leading to increased oxygen affinity in the adjacent subunits. The mechanism by which information is conveyed through the protein between binding sites, however, is largely unknown. Predictions concerning the mechanism of the observed allosteric cooperativity have arisen from structural descriptions of deoxyhemoglobin and hemoglobin in oxygen bound conformations [89]. Based on these structures, a two-state model of allosteric regulation has been proposed, wherein an allosteric enzyme or protein can exist in one of two preexisting conformations, dubbed the R and T state [90]. The R-state, or relaxed conformation, is the high affinity protein conformation. The T-state, or taut

conformation, has low oxygen affinity and corresponds to the deoxyhemoglobin structure. The two conformations are in equilibrium with each other and ligation of the enzyme by oxygen causes the poise of the equilibrium to shift toward the R-state. Issues concerning the mechanism by which the two conformations interconvert have led to adaptations of this model. The Monod, Wyman and Changeux (MWC) or concerted model predicts that all subunits in a multimeric allosteric enzyme convert from T to R conformations in a concerted manner upon ligand binding to a single subunit [91]. This model predicts that a complete conversion of all subunits in the tetramer from T to R conformations will occur regardless of the subunit to which oxygen binds. The Koshland, Nemethy and Filmer (KNF) or sequential model proposes that each subunit converts from T to R sequentially as successive allosteric ligands bind to each subunit [92]. In this model, a conformational change occurs only within the subunit to which the oxygen binds. Intersubunit interactions propagate changes in binding affinity throughout the protein.

Heterotropic interactions comprise the second type of allosteric interaction. Heterotropic interactions refer to enhancements or reductions in substrate binding or ligand caused by binding a different ligand at a separate binding site. Unlike homotropic cooperativity, binding two distinct ligands is required for an effect to be observed. Consider the case of a K-type allosteric effect, wherein binding an allosteric effector alters substrate binding. In the absence of effector, substrate binding follows a typical

hyperbolic saturation profile whereas in the presence of inhibitor, the curve is shifted to higher substrate concentrations, and in the presence of activator the curve is shifted to lower substrate concentrations. The MWC model predicts that binding an allosteric effector influences the pre-existing equilibrium between R and T states, and the defining characteristic of the effector is the state to which that effector can bind [91]. An activator, therefore, binds only to the R-state and shifts the equilibrium toward the R-state. The inhibitor binds to the T-state and shifts the equilibrium toward the T-state. The KNF model predicts that an allosteric effector binds to a subunit and influences the R – T transition within that subunit, and intersubunit interactions may extend that influence to neighboring subunits within the enzyme [92].

In the past few years, the inadequacies of the various two-state models have been demonstrated for hemoglobin [93], for phosphofructokinase [94,95] and for other enzymes [96,97]. The weakness of most applications of a two-state model for allosteric regulation is the failure to consider the implication that both an allosteric ligand and substrate may bind the enzyme concurrently, leading to ternary complex formation. Consequently, a model-independent quantitative analysis based on linked-function thermodynamics is proposed to best describe the allosteric response [96,98-101]. In this scheme, the energetics of binding of substrate, allosteric ligand and both concurrently are considered. The concurrent binding of two ligands: either a heterotropic interaction in which an allosteric ligand and a substrate molecule bind, or a homotropic interaction in

which two similar ligands bind to separate binding sites within an enzyme is described by the following general reaction:

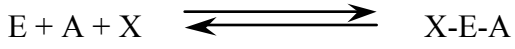

where A represents the substrate, X the allosteric ligand and X-E-A represents the ternary complex. For each of the binding events, a unique equilibrium constant and associated binding free energy can thus be derived:

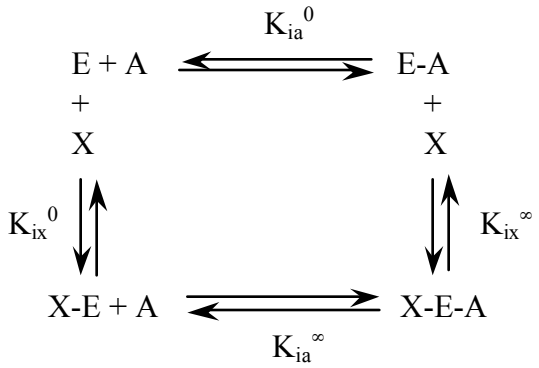

where each K_{ia} and K_{ix} refers to the respective thermodynamic dissociation constant for the ligand demonstrated. The superscript, 0, denotes the binding constant for the ligand in the absence of other ligands, and the superscript, ∞, denotes the binding constant for the ligand to the enzyme with the second ligand previously bound. The dissociation constants have an associated free energy, as follows:

$$\Delta G_a = RT \ln K_{ia}^0 \qquad [1\text{-}36]$$

$$\Delta G_x = RT \ln K_{ix}^0 \qquad [1\text{-}37]$$

$$\Delta G_{a/x} = RT \ln K_{ia}^\infty \qquad [1\text{-}38]$$

$$\Delta G_{x/a} = RT \ln K_{ix}^\infty \qquad [1\text{-}39]$$

In this thermodynamic linkage analysis, formation of the ternary complex from free enzyme, ligand and substrate is independent of pathway, and consequently:

$$K_{ia}^\infty K_{ix}^0 = K_{ia}^0 K_{ix}^\infty \qquad [1\text{-}40]$$

Rearrangement of the terms of equation 1-40 demonstrates the fractional extent to which bound effector has altered the substrate binding affinity.

$$\frac{K_{ia}^0}{K_{ia}^\infty} = \frac{K_{ix}^0}{K_{ix}^\infty} \qquad [1\text{-}41]$$

The degree to which effector alters binding constants, given by the ratio of these two binding constants, is dubbed the coupling constant, Q. Equation 1-41 demonstrates the principal of reciprocity; the extent to which a bound effector influences the binding affinity for the substrate is equivalent to the extent that bound substrate alters the

binding of effector. The coupling constant quantifies both the magnitude and direction of the allosteric effect and derives directly from the free energy of coupling: the energetic influence that one ligand has on the other.

$$Q_{ax} = \frac{K_{ia}^{0}}{K_{ia}^{\infty}} = \frac{e^{\Delta G_a/RT}}{e^{\Delta G_{a/x}/RT}} \qquad [1\text{-}42]$$

$$Q_{ax} = e^{\Delta G_a/RT - \Delta G_{a/x}/RT} \qquad [1\text{-}43]$$

$$\Delta G_a - \Delta G_{a/x} = -RT \ln Q_{ax} = \Delta G_{ax} \qquad [1\text{-}44]$$

Since ΔG_a - $\Delta G_{a/x}$ quantifies the difference between the free energy of substrate binding in the absence of ligand and binding to the ligand-bound enzyme; ΔG_{ax} quantifies the effect that the bound ligand has on substrate binding. For an allosteric inhibitor, K_{ia}^{∞} and K_{ix}^{∞} will exceed K_{ia}^{0} and K_{ix}^{0} and the resultant coupling parameter Q_{ax} will be less than one. For an allosteric activator, the binding constants will decrease; thus K_{ia}^{∞} and K_{ix}^{∞} will be smaller than K_{ia}^{0} and K_{iy}^{0} leading to a Q value greater than one.

The coupling constant, Q_{ax}, can also be shown to be the equilibrium constant for the following disproportionation equilibrium [99,102]:

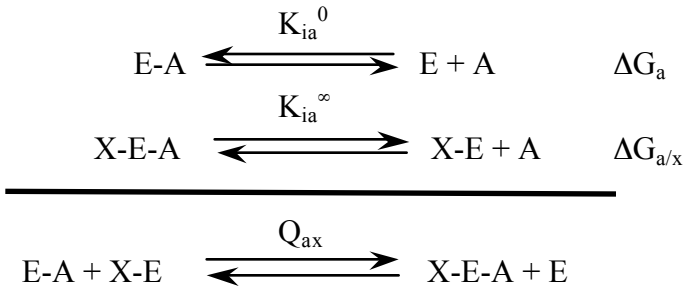

$$Q_{ax} = \frac{K_{ia}^{0}}{K_{ia}^{\infty}} \qquad \Delta G_{ax} = \Delta G_a - \Delta G_{a/x} \qquad [1\text{-}45]$$

As such, the thermodynamic parameters associated with allosteric regulation can be determined:

$$\Delta G_{ax} = -RT \ln Q_{ax} \qquad [1\text{-}46]$$

$$\Delta G_{ax} = \Delta H - T\Delta S \qquad [1\text{-}47]$$

For inhibition, Q_{ax} is less than one, and consequently ΔG_{ax} is positive. Intuitively, as an inhibitor binds the allosteric site, the binding of substrate to the active site is reduced and its free energy becomes less negative. The loss of binding free energy arises from binding the inhibitor and Q_{ax} quantifies this change. For activation, Q_{ay} is less than one and the associated free energy of coupling is negative. Intuitively, as an activator binds to the allosteric site, substrate binding becomes tighter and the associated free energy of binding

becomes more negative. In this case, the coupling constant and the associated negative free energy of coupling quantify the increasing binding energy that arises from binding the activator [102].

In the absence of simple two-state models of allosteric behavior, the precise mechanism by which binding energy is transferred between binding sites is largely unknown. Some structural or energetic element or elements must be altered when a regulatory molecule is bound at an allosteric site leading to an effect on binding or catalysis at the distant active site. Current efforts are underway to map the residues that impart coupling energy within each of the heterotropic, or active site to allosteric site, interactions of phosphofructokinase [103-105] and in the homotropic interactions between oxygen binding sites in hemoglobin [106]. It is of note that most allosteric enzymes are multisubunit enzymes, either composed of separate catalytic and regulatory subunits or composed of multiple subunits containing both active and allosteric sites. The question thus arises as to the role of intersubunit interactions in the allosteric response.

The thermodynamic driving forces underlying the allosteric response as quantified by the disproportionation equilibrium and the coupling parameter Q are determined by van't Hoff analysis of this equilibrium. Van't Hoff analysis allows the free energy of a reaction to be parsed into its component enthalpic and entropic terms (equation 1-47). For inhibition, the positive free energy of coupling can arise from either

positive enthalpy or from negative entropy of coupling. Interestingly, the thermodynamic forces driving inhibition differ between enzymes, and even between homologous enzymes from different sources [107,108]. Historically, the study of allosteric regulation has involved demonstration of an allosteric effect on substrate binding. More recently, the effects of various physicochemical perturbants on the disproportionation equilibrium that defines the allosteric response have been examined. Alteration of temperature, pH, amino acid residues and application of hydrostatic pressure are effective methods to examine the thermodynamics of allostery [109,110].

Hydrostatic pressure as a biological perturbant

Hydrostatic pressure is an effective perturbant in the study of protein-protein and protein-ligand interactions, allowing binding equilibria to be altered in the direction of smallest overall volume. Protein folding, protein association, protein-ligand interactions, protein dynamics and protein regulation have all been examined under pressure. Most importantly to the research described herein, pressure is an effective tool in the examination of ligand binding and allosteric regulation [111]. Unlike the more commonly utilized perturbants including pH and temperature, hydrostatic pressure is a particularly useful tool as it enables examination of a biochemical phenomenon without changing the chemistry of the system under study. Variation in temperature alters the energy of the

system and modification of either the solution pH or the amino acids involved in binding and catalysis changes the chemical nature of the system. Pressure enables the perturbation of equilibria without these alterations. The ensuing change in equilibrium constant with pressure gives the standard volume change:

$$\Delta V = -RT\ln\left[\frac{\Delta K}{\Delta P}\right] \qquad [1\text{-}48]$$

where ΔV is the standard volume change for a reaction, ΔK is the change in equilibrium constant and ΔP is the change in pressure. Experimentally, the volume change can be determined in one of two ways: maintaining a fixed concentration of the reactants and measurement of the extent of reaction with alteration of pressure, or maintaining a constant pressure and measurement of the extent of the reaction with altered reactant concentrations [112]. Changes in the standard volume change with pressure, indicated by non-linearity in K with P, are indication of compressibility changes.

The effects of pressure on protein phenomena have been studied extensively [112-140]. From atmospheric pressure to approximately 2 kbar, pressure-dependent reversible changes in protein structure and dynamics can be examined. In this range of pressure, the complex effects of pressure on protein dynamics have been studied using fluorescence and NMR techniques [113-118]. This is the range of pressure amenible to the study of ligand binding and allosteric phenomena. At pressures between 2 and 4

kbar, multisubunit proteins commonly undergo dissociation [119-122]. At pressures above 5 kbar, proteins typically undergo unfolding [123-131]. The predominant forces involved in pressure perturbation of dynamic protein phenomena are cavity compression and electrostriction [124]. The former exploits imperfect packing within the protein to yield an overall reduction in protein volume. The latter involves reduction in solvation volume associated with increased charge separation in either the reactants or products. Thus the overall perturbation includes affects on the reacting species and the solvent medium.

An issue inherent to pressure measurements is the concept of conformational drift [112]. In an experiment in which pressure is first increased and then decreased, conformation, fluorescence properties, ligation state and other characteristics are commonly hysteretic. This phenomenon has raised issues with respect to the reversibility of the processes under study with pressure perturbation. These data have also led to the hypothesis that conformational drift of proteins may occur on long timescales, and this drift is exacerbated by pressure. A protein and a ligand may interact only in a given protein conformation, and the kinetic consequences of two competing rates: reassociation and conformational change, lead to reduction in the extent of protein binding [112].

Phosphofructokinase

Biological role

Phosphofructokinase (PFK) (EC number 2.7.1.11) catalyzes the MgATP-dependent phosphorylation of D-fructose-6-phosphate (F6P) to give fructose 1,6-bisphosphate (FBP) and MgADP. This reaction represents one of the most studied enzymes in one of the best-studied, most highly conserved metabolic pathways known [1]. The reaction represents the first committed step of the glycolytic pathway, as the only metabolic fates of FBP are dephosphorylation to F6P or oxidation to pyruvate.

$$\text{F6P} + \text{MgATP} \xrightarrow[\text{PFK}]{} \text{F-1,6-BP} + \text{MgADP}$$

The large, negative standard free energy ($\Delta G^{0\prime} = -17.2$ kJ/mol) and even larger, negative physiological reaction free energy ($\Delta G' = -25.9$ kJ/mol) of the reaction ensure that the process is irreversible [1,141]. Consequently, the PFK catalyzed reaction is under very tight control; the enzyme is allosterically regulated by a variety of effectors that differ between variants of the enzyme from different sources. This regulation is discussed in greater detail below. PFK catalyzes the phosphorylation reaction by inducing nucleophilic attack by the C1-hydroxyl of F6P on the γ-phosphorus of MgATP. Mg^{2+}

plays a critical role chelating the β- and γ-phosphoryl oxygen molecules (figure 1-9), and in most PFK isoforms Mg^{2+} is essential for activity. In species including Streptococcus lactis, Mn^{2+} and Zn^{2+} can be substituted with reduced activity [142]. The catalytic mechanism of the enzyme varies between source tissues. In prokaryotic and in Saccharomyces cerevisiae PFK, the reaction is catalyzed in a random sequential mechanism [143].

Evolutionary conservation

The glycolytic pathway is conserved among most organisms. PFK is likewise conserved, showing homology in many diverse organisms. While there are differences between prokaryotic and eukaryotic PFK in quaternary structure, size and regulation, the mechanism, sequence and fundamental mechanisms of regulation are highly conserved through evolution. Between prokaryotic and eukaryotic PFK, *B. stearothermophilus* PFK has 44% sequence identity to the N-terminal domain of rabbit muscle PFK and 35% identity to the C-terminal domain [144,145]. This has led to the hypothesis that mammalian PFK has undergone gene duplication at some point in evolutionary history [146]. Among prokaryotic PFK variants, *E. coli* and *B. stearothermophilus* have 55% identity, and *B. stearothermophilus* and *T. thermophilus* are 58% identical [144,147].

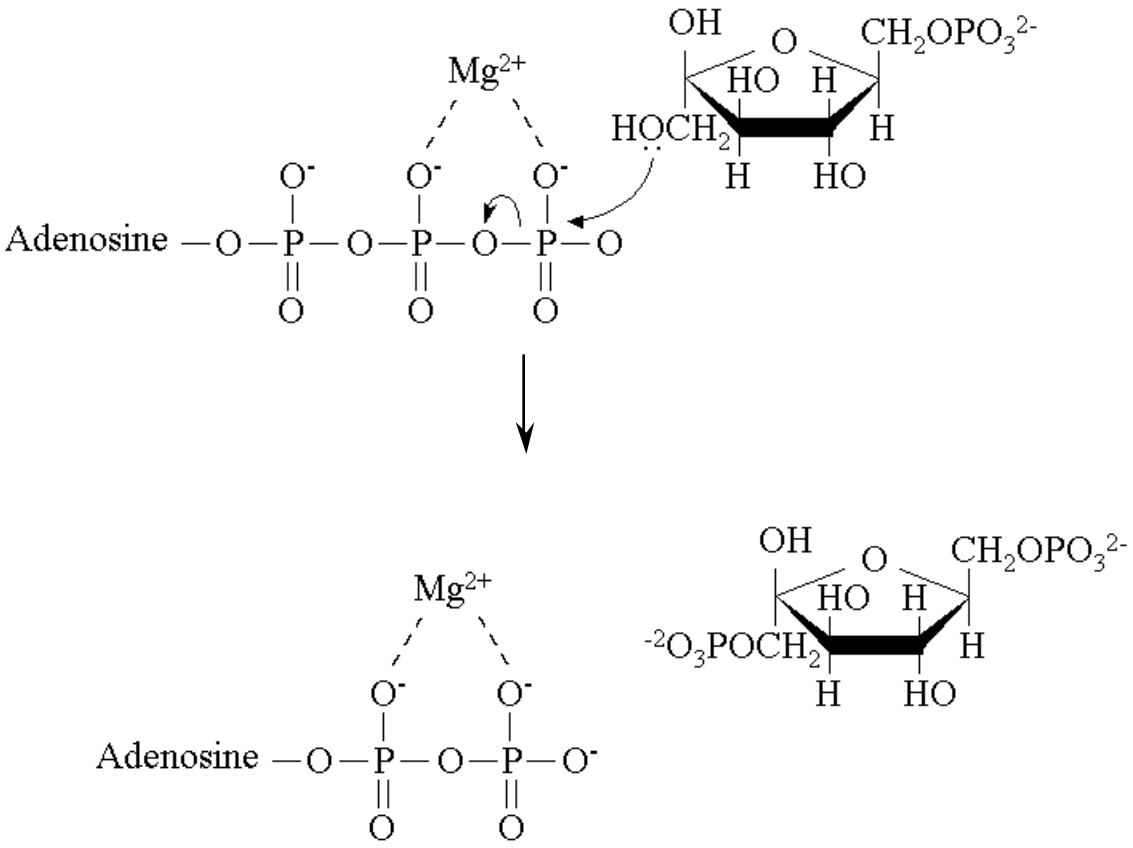

Figure 1-9: The mechanism of phosphofructokinase activity.
PFK catalyzes the MgATP ependent phosphorylation of F6P. The γ-phosphate of ATP undergoes nucleophilic attack by the C1-OH of F6P. The products are ADP and F-1,6-bisphosphate. Mg^{2+} serves to coordinate the β- and γ-phosphate oxyanions of the substrate ATP, and the α- and β-phosphate oxyanions in the product, ADP.

The high degree of sequence similarity and evolutionary conservation hints at the fundamental role PFK plays in the central metabolic pathways of all organisms.

Structure

The crystal structures of several prokaryotic variants of phosphofructokinase have been solved in various ligand-bound states, and the backbones of PFK isoforms from *L. delbrukeii* (LbPFK), *B. stearothermophilus* (BsPFK) and *E. coli* (EcPFK) essentially overlay [148-153]. The structures of two ligand-bound forms of BsPFK are presented in figure 1-10. Prokaryotic PFK is a tetrameric enzyme consisting of 4 identical subunits. Each subunit contains a large and small domain, and those are juxtaposed in adjacent subunits. Within the tetramer, each individual subunit makes significant protein-protein contacts with two other subunits, and minimal contact with the remaining subunit. The subunit molecular weight is approximately 34 kDa for the prokaryotic PFK isoforms listed, and varies only slightly between known prokaryotic variants. *Saccharomyces cerevisiae* PFK forms a $\alpha_2\beta_4\alpha_2$ octamer, and the component subunit molecular weights are 112 and 118 kDa, respectively [143]. Mammalian PFK isoforms form high order oligomers based on their ligation state and concentration, and

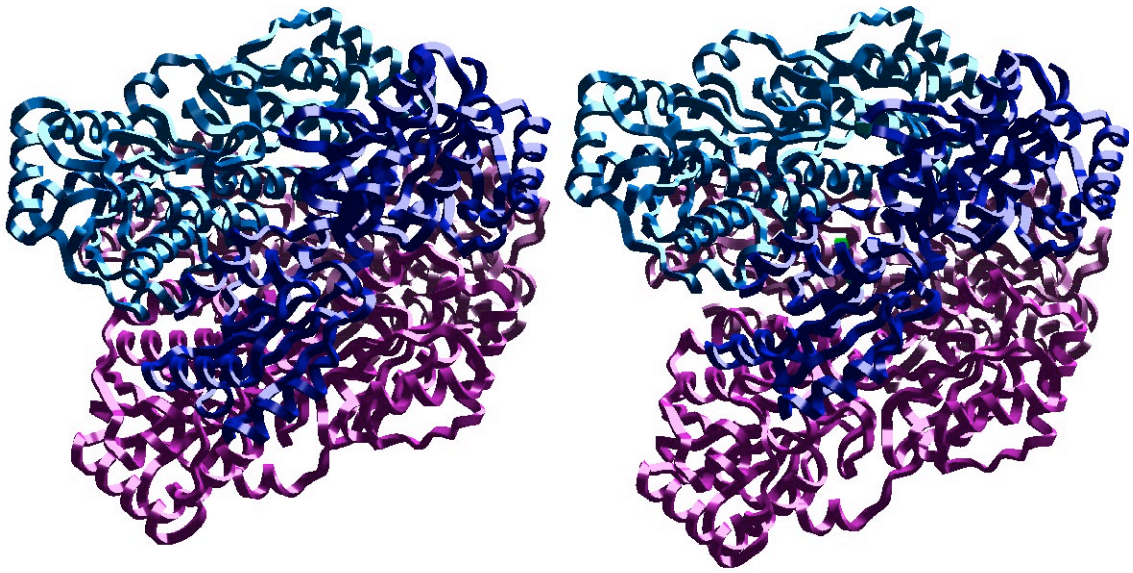

Figure 1-10: The crystal structures of BsPFK.
Panel A, the crystal structure of BsPFK with the allosteric inhibitor analog phosphoglycolate bound in the allosteric site. Panel B, BsPFK crystal structure with no allosteric ligands bound (a phosphate molecule is bound in the active site). The inhibitor-bound form shows a 7° rotation of the subunits around the active site interface relative to the uninhibited form [151,152].

each has a subunit molecular weight between 75 and 95 kDa. Human PFK isoforms, for example, are of three types: M-type (muscle) with subunit molecular weight of 79 kDa, L-type (liver) with subunit molecular weight of 74 kDa and C-type (fibroblast) with subunit molecular weight of 82 kDa.

As discussed previously, protein-protein interfaces commonly contain on the order of 1600 $Å^2$ of buried accessible surface area, contain a high degree of hydrophobicity, and significant numbers of hydrogen bonds. The PFK quaternary structure is an obligate tetramer; hence the interaction surfaces between subunits are high affinity interfaces. The characteristics and composition of the two dimer-dimer interfaces of both EcPFK and BsPFK are listed in table 1-1. For both enzymes, the allosteric site interface is approximately 40% larger than the active site, and contains more hydrogen bonds. This structural description leads to the prediction that for both *E. coli* and *B. stearothermophilus* PFK, the active site interface would possess lower affinity than the allosteric site interface. This prediction has been examined for the *E. coli* enzyme [154-155], and is still an issue under investigation for BsPFK. Interestingly, the interfaces are larger in BsPFK than in EcPFK. This may reflect a neccessity for thermal stability, an adaptation to the thermophilic environment in which

Table 1-1: Comparison of the subunit interfaces for phosphofructokinase, citrate synthase and malate dehydrogenase

Interface	ΔASA (Å^2)	% Aliphatic[a]	% Aromatic	% Charged	% Polar	Hydrogen Bonds	Hydrophobic Contacts
EcPFK							
Active	1150	35	15	31	12	9	60
Allosteric	1800	22	8	48	12	ND	ND
BsPFK							
Active	1400	25	5	31	18	13	65
Allosteric	2123	37	9	38	12	15	113
CTS	4773	43	8	21	17	42	313
MDH	1530	43	7	27	10	20	112

[a] *cys, gly, his and water are excluded from interface area*

B. stearothermophilus is found. Furthermore, the active site interface of BsPFK contains more charged and polar residues than does EcPFK. This may be pertinant to the dissociation of the tetramer at this interface, as discussed in chapter V.

Prokaryotic PFK contains 4 separate allosteric and 4 separate active sites. Each of the 4 allosteric sites lies along a single subunit interface and consists of residues from both subunits at the interface [148-152]. Similarly, each active site lies along the opposite interface and also consists of residues comprised of both subunits at its respective interface. The crystal structure of eukaryotic PFK is unknown, however the quaternary structure of the enzyme is highly dependent on the presence of allosteric ligands, and activator binding leads to high order aggregation [156-159].

The subunit arrangement of PFK has proven effective for studying association of the protein subunits. The active and allosteric sites are composed of amino acid residues from subunits on opposite sides of each interface; hence disruption of the interface leads to loss of the binding site. Using *E. coli* PFK, Le Bras and Garel have performed subunit association studies under conditions of mild chemical denaturation [154]. At low concentrations of the chemical chaotrope KSCN, enzyme activity is lost. At higher concentrations of KSCN, the intrinsic fluorescence intensity emanating from the single tryptophan near the allosteric site interface is lost. This loss of emission intensity is attributed to disruption of the allosteric interface and increased exposure of the tryptophan to solvent. These data have led to a model in which the active site interface

has a lower subunit affinity than does the allosteric site interface, as predicted from the structural description of the two interfaces. Binding substrate, F6P, or allosteric inhibitor, PEP, leads to decreased KSCN lability [154]. While ligand induced protein-protein interactions are ubiquitous in nature as discussed, the ligand-binding sites of PFK are contained within the protein-protein binding interface. PFK thus provides a functional model with which to interrogate the effects of ligand binding on subunit interactions specifically and protein-protein interactions in general. The subunit affinities of BsPFK, and the effects of ligand binding thereon, are discussed in detail in chapter V.

Thermus thermophilus PFK exhibits dissociation of the active site interface on binding the allosteric inhibitor PEP at the allosteric sites [160]. In opposite fashion, rabbit muscle PFK aggregates to vast extents during inhibitor binding. Based on the general observation that allosteric enzymes are often multimeric, ligand-induced subunit association is a possible general mechanism for allosteric inhibition as previously discussed. *B. stearothermophilus* undergoes a 7° rotation around the active site interface with an inhibitor analog bound (figure 1-10), and introduction of a tryptophan-shift mutation, W179Y/Y164W, imparts this enzyme with the same dissociation phenotype observed with *T. thermophilus* PFK [161]. Based on these collective data, it is possible that quaternary structural changes do represent a fundamental mechanism in the allosteric behavior of PFK. The various PFK isoforms have different degrees of responsiveness to

ligand binding, and it is possible that these enzymes demonstrate varying degrees of change in subunit association. We test this hypothesis for BsPFK and demonstrate for the first time a correlation between allosteric inhibition and subunit association.

Allosteric regulation

As the major regulation point of glycolysis, PFK is under tight regulatory control. The allosteric regulation of the enzyme imparts feedback control and integration of the metabolic pathway with the intracellular environment. While the metabolites that are responsible for regulation vary between organisms, most PFK isoforms are under allosteric regulation of some type and to some extent. In the context of linked-function thermodynamics, the structural or energetic basis for communication between active and allosteric sites for many of these PFK isoforms is an ongoing area of investigation [104,105]. Eukaryotic PFK-1 is allosterically activated by several metabolites including AMP, ADP and F-2,6-BP. ATP, citrate and phosphoenolpyruvate (PEP) allosterically inhibit the enzyme [143]. Most prokaryotic PFK is inhibited by PEP and is activated by MgADP. Other known activators of the various PFK isoforms include MgGDP, cAMP, $NH4^{+}$, and PO_4^{2-}, and other known inhibitors include 2- and 3-phosphoglycerate, ADP, AMP, ATP, citrate and PO_4^{2-} [141-143]. As discussed, many of the isoforms of PFK integrate intrasubunit interactions with ligand binding. Rabbit

muscle and rat liver PFK undergo vast aggregation that leads to lowered K_m for F6P under conditions of inhibitor binding or high protein concentration [157]. *Thermus thermophilus* PFK undergoes dissociation along the active site interface under conditions of inhibitor binding, leading to a similar overall effect on F6P binding [160].

In the regulation of BsPFK and EcPFK, the disproportionation equilibrium that defines this regulation has been extensively examined. The thermodynamic driving forces behind the allosteric inhibition of both of these enzymes have been determined by van't Hoff analyses (equation 1-47). The amino acids involved in binding substrate and effector have been extensively mutated and additional amino acids lying between active and allosteric sites have been mutated in an effort to highlight the through-protein pathway by which allosteric inhibition and activation are transferred [95,103-105,109,110,162,163]. Furthermore, the thermodynamic parameters of ligand and substrate binding and allostery have been determined as a function of temperature, pH, and recently have been perturbed using hydrostatic pressure [109-111]. Each of these various methods is utilized to disrupt the disproportionation equilibrium underlying the allosteric response and to study the effects thereon.

Despite their close structural, mechanistic and regulatory resemblance, a distinction between EcPFK and BsPFK exists in the thermodynamic driving forces that form the basis for their PEP inhibition. Van't Hoff analyses have demonstrated that the inhibition of EcPFK is driven by enthalpy and inhibition of BsPFK is governed by

entropy. In both cases, the overall free energy of coupling, ΔG_{ay}, is positive, as expected for inhibition, and is small in magnitude (the subscript, Y, denotes the specific allosteric ligand, PEP) [107,110]. This arises from a small difference between large, opposing contributions from entropic and enthalpic terms, a phenomenon referred to as entropy-enthalpy compensation. The inhibition of EcPFK is enthalpy driven; both entropy and enthalpy are positive and the ΔH_{ay} term is larger in magnitude than the ΔS_{ay} term, leading to positive ΔG_{ay}. The inhibition of BsPFK is entropy driven; both entropy and enthalpy are negative and the ΔS_{ay} is larger in magnitude than ΔH_{ay}, similarly leading to positive overall ΔG_{ay}.

Van't Hoff analyses have also revealed that an allosteric effector can undergo a temperature-induced inversion of allosteric effect. Below 16°C, F6P binding by BsPFK is inhibited by MgADP rather than activated [110]. Above 40°C, MgATP binding by EcPFK is inhibited by PEP, whereas activation is observed below this temperature [162]. Subsequently, other means of disruption of the disproportionation equilibrium have similarly been shown to induce inversion of allosteric effects. Low pH is predicted to cause the MgADP-dependent activation of F6P binding to become inhibition and the PEP-dependent inhibition of F6P binding by BsPFK to become activation [163]. The physicochemical dependence of the nature of the allosteric effect caused by an effector arises from different dependencies of the two thermodynamic parameters that lead to the overall coupling free energies. Either the entropic or enthalpic term in each case is more

sensitive to temperature or pH, thus as temperature or pH increases the free energy of coupling switches signs. At some critical value of perturbation the free energy of coupling crosses zero, at which point the inhibitor becomes an activator and *vice versa*.

To further examine the difference in thermodynamic driving forces between EcPFK and BsPFK; the temperature-pressure landscape of EcPFK ligand binding and allosteric coupling has been determined. Initial attempts to examine the pressure response of the disproportionation equilibrium for BsPFK have been hindered by the pH-sensitivity of the allosteric coupling for this enzyme. To mitigate this issue, a series of baroresistant buffer mixtures have been developed (chapter II).

The effects of hydrostatic pressure on PFK structure and function

The effects of hydrostatic pressure on EcPFK and BsPFK structure, ligand binding and regulation have been examined. EcPFK has been studied extensively using intrinsic tryptophan fluorescence [111,155], and recent research has illuminated differences between this enzyme and its *B. stearothermophilus* counterpart.

As discussed previously, in the range of pressure from atmospheric through 5 kbar, proteins undergo reversible changes in dynamics, subunit dissociation and denaturation. EcPFK undergoes subunit dissociation at approximately 1kbar, and this subunit dissociation is accompanied by irreversible denaturation at pressures exceeding

1.4kbar [111]. The reversibility of EcPFK subunit dissociation is improved by the addition of reducing reagents to the solution, as non-specific disulfide formation is hypothesized to play a major role in the irreversible denaturation [164]. F6P binding has also been shown to reduce the pressure-lability of the tetramer, and this observation supports the premise of LeBras and Garel regarding the relative subunit affinities of the active and allosteric site interfaces. At pressures below 800-1000 bar, reversible changes in protein structure and dynamics leading to modifications in binding and allosteric coupling can be examined. In this pressure range, the effects of hydrostatic pressure on the disproportionation equilibrium and hence the allosteric response of PFK can be determined.

The standard reaction volumes of ligand binding and allosteric coupling for EcPFK are summarized in table 1-2. The ΔV values for binding of the various ligands are 13-45 mL mol^{-1} [111]. The partial charge neutralization of the anionic ligands associated with binding leads to positive ΔV values for ligand-binding, as anticipated based on electrostriction effects. The overall ΔV values for all the allosteric couplings of the enzyme are negative. This is also expected, as the disproportionation equilibrium includes no free ligand; hence electrostriction effects are expected to be minimal.

The research presented herein addresses the effects of pressure on the entropic and enthalpic contributions to the coupling free energy of PEP inhibition. With pH and temperature, disparity between the sensitivity of the two thermodynamic parameters to

Table 1-2: Standard reaction volumes for ligand-binding and allosteric coupling

Ligand	Other saturating ligands	ΔV (ml/mol)
Binding		
F6P	—	45 ± 2
	PEP	18 ± 8
	MgADP	26 ± 5
PEP	—	40 ± 11
	F6P	13 ± 12
MgADP	—	44 ± 3
	F6P	25 ± 6
Coupling		
F6P/PEP		-27 ± 8
F6P/MgADP		-19 ± 5

the perturbant led to an inversion of allosteric effect. The hypothesis that similar effects would arise with pressure was the basis for this research as discussed in chapter III.

While the EcPFK tetramer is highly pressure-labile, BsPFK appears to be pressure-stable within the experimentally accessible pressure region from 1-3kbar [Quinlan, unpublished data]. Intrinsic tryptophan fluorescence is highly linear with pressure and surprisingly, hysteresis is not observed. *B. stearothermophilus* is a moderate thermophile, and BsPFK is correspondingly temperature-stable. The pressure and temperature stability of the enzyme may reflect the evolutionary requirement for enzyme stability under high environmentally imposed temperatures.

The strong pH dependence of the allosteric coupling between PEP and F6P has prevented the derivation of the temperature-pressure landscape for BsPFK as obtained for EcPFK. Initial research in this area has focused on the development of pressure-insensitive buffers to allow examination of this inhibition in the absence of pressure-induced pH effects. The development of these baroresistant buffers is discussed in chapter II.

Research Aims

The research presented herein has, as its overall goal, the aim of dissection of the thermodynamics of protein-protein interactions and the mediation of those interactions

by protein-ligand interactions. We specifically examine both transient and obligate protein-protein associations. The putative transient interaction between pig heart mitochondrial malate dehydrogenase and citrate synthase, and the effects of oxaloacetate binding on this interaction are examined using Fluorescence Correlation Spectroscopy. The obligate interactions between the subunits of the phosphofructokinase tetramer and the effects of ligand binding on those interactions are examined using a variety of biophysical techniques including fluorescence anisotropy, correlation spectroscopy, electrophoretic mobility shift assay, and FRET.

Protein-ligand interactions can also mediate other protein-ligand interactions, as exemplified by allosteric regulation of enzymes. We examine the thermodynamics of the disproportionation equilibrium for *E. coli* PFK, and perturb this equilibrium using hydrostatic pressure. To further extend the use of hydrostatic pressure in the examination of protein-ligand interactions, we have developed a series of pressure-insensitive buffer mixtures.

CHAPTER II

BARORESISTANT BUFFER MIXTURES FOR BIOCHEMICAL ANALYSIS AT NEAR-PHYSIOLOGICAL pH VALUES

Synopsis

Hydrostatic pressure is a useful tool in the study of such varied fields as protein aggregation, association, folding, and allostery. Application of pressure has a small but significant effect on the pK_a values of buffers commonly used for biochemical analysis. Consequently, cationic rather than neutral buffers are generally utilized in order to minimize pH effects; however even in these charged buffers pH effects may be consequential in highly pH-sensitive cases. Using fluorescence-based assays, we have systematically examined the effects of pressure on various buffers in the physiological pH range. We show that many commonly used cationic and Good's buffers increase in pH with pressure on the order of 0.1- 0.3 pH units/kbar in agreement with other published values. Carboxylates and phosphate decrease in pH to a similar extent. Buffer mixtures comprised of both cationic and neutral components are shown to be an order of magnitude less pressure-sensitive than individual buffers. Using various relative concentrations of Tris and either phosphate, tricarballylate or 1,1-cyclohexanediacetate at pH values between 7and 8 yields a baroresistant buffer mixture.

The buffer mixture can be optimized for a specific pH and a list of mixtures is presented for general laboratory use.

Introduction

Hydrostatic pressure has become an increasingly important tool in the study of biological and biochemical systems, allowing examination of chemical equilibria while maintaining both the chemical and energetic characteristics of the system. Pressure has been effectively used to study such varied phenomena as protein folding and association [112,119-131], nucleic acid thermodynamics [132-135] and dynamic protein behavior including allostery [113-118]. Furthermore, pressure is being examined as a potential tool in food preservation and as an anti-microbial agent [136-138].

The standard volume change (ΔV) for a reaction is related to the change in equilibrium constant with change in pressure. For an acid-base equilibrium, the ΔV is given by:

$$\Delta V = RT \frac{\Delta \ln K_a}{\Delta P} \qquad [2\text{-}1]$$

where K_a refers to the acid dissociation constant of the aqueous buffer. The change in ΔV with pressure, or compressibility, has been shown to be minimal at pressures less than 3-4kbar for most buffers studied [139,140]. Over the pressure range examined, changes in pH from pressure are attributed to changes in pK_a of the buffer [140].

$$\frac{\partial pH}{\partial P} \approx \frac{\partial pK_a}{\partial P} \qquad [2\text{-}2]$$

The effects of hydrostatic pressure have been exploited in broad fields of biochemical study. It has been shown that below 1kbar, proteins typically undergo reversible changes in dynamics [113-118]. At pressures of 2-5kbar, oligomeric proteins typically undergo dissociation [119-122] and above 5kbar, protein denaturation is observed [123-131]. These protein phenomena have been extensively examined using hydrostatic pressure in each of the respective pressure regimes. While proteins undergo dissociation under pressure, nucleic acids demonstrate pressure-stabilization over a similar pressure range [132-135]. Increased base stacking under elevated pressure leads to a small, positive volume change (ΔV) for the helix-coil transition. Moderate pressures and temperatures have also been widely studied in the inactivation of both viral and bacterial pathogens [136-138]. The titer of viable microorganisms is effectively reduced by pressure-induced disruption of the cell wall and/or cell membrane by pressures of 2-4kbar, often in concert with elevated temperatures or appropriate microbicides [136].

Application of hydrostatic pressure perturbs equilibria in the direction of smallest total volume. Consequently, in aqueous solution acid/base equilibria are driven by pressure in the direction of greatest charge separation [139,140, 164]. According to the theory of electrostriction, a fully charged species is encompassed by a tighter solvent array than that of a neutral or partially charged species. The charged species and its accompanying solvent sphere are therefore smaller in total volume than the neutral or

partially charged species with its associated solvent. When a neutral buffer is deprotonated, two charged species are produced from a single, uncharged species.

$$HA \rightleftharpoons H^+ + A^-$$

Electrostriction predicts a large change in pH with pressure, as pressure leads to increased charge separation and hence smaller net volume. Conversely, deprotonation of cationic buffers yields reduced electrostrictive effects.

$$HA^+ \rightleftharpoons H^+ + A$$

In this case, both sides of the acid dissociation equilibrium are similarly charged and no net charge separation occurs during the reaction.

Since the pioneering work of Walter Kauzmann [127,140], biochemical pressure research is typically performed in cationic buffers. The pH of a solution in Tris buffer, the most prevalent buffer utilized in pressure studies, increases >0.1 pH unit/kbar, and the pH change approaches half a pH unit over a typical 3-4kbar experiment [140]. While these pH effects are relatively minor, in particularly pH-sensitive cases the effects may be non-trivial. In some systems this may lead to a convolution of pressure and pH effects that may therefore complicate the interpretation of pressure effects.

In order to alleviate the effects of pressure on pH, a series of baroresistant buffers have been developed. An initial search of various biologically important buffers has

been undertaken to identify the buffers that are most baroresistant, and the effects of pressure on the pK_a values of these buffers at pH values near the respective pK_a of each have been determined. More significantly, the $\Delta pH/\Delta P$ of the respective buffers is utilized in the development of pressure-insensitive buffer mixtures. While the effects of pressure on many of the commonly used biological buffers have been known for many years, this study combines buffers of positive ΔV and negative ΔV in order to arrive at composite buffers with $\Delta V \sim 0$. The examination is constrained to pressure less than 3 kbar, the range most easily accessible with commonly available laboratory pressure apparatus, and the pH range near neutrality. The feasibility of our experimental method is demonstrated by comparison to published values for buffers previously studied using other techniques, and is extended to previously unstudied buffers and the baroresistant buffers that have been developed.

Several pH-sensitive fluorophores are available, and these can be used to determine pH at elevated pressure. The fluorescence properties of these fluorophores, including HPTS (8-hydroxypyrene-1,3,6-trisulfonic acid), SNAFL-1 (5&6-carboxy-seminaphthofluorescein-1) and fluorescein have been extensively utilized in determination of pH both *in vivo* and *in vitro* [139, 165-168]. The non-invasive character of a fluorescence-based assay for pH determination is the clear advantage of its use in this case. pH can be optically monitored within a sealed cuvette, allowing the application of hydrostatic pressure to the cuvette and sample within. Electrodes or conductivity meters need not be adapted for use in a pressure cell.

We present 3 specific baroresistant mixtures at pH values of 7, 7.5 and 8, and it is anticipated that these will be relatively simple to use in future high-pressure biochemical research. The relative concentrations of cationic and neutral buffer components in a specific mixture determine the pH value at which $\Delta pH/\Delta P$ is minimal. The systematic trend of molar ratio of the component buffers with pH allows formulation of buffer mixtures that are pressure-insensitive at all pH values between 7 and 8. It is further anticipated that additional baroresistant mixtures could be developed based on this technique at additional pH values or with other buffer mixtures, given the precise experimental requirements of the specific research carried out.

Materials and methods

Materials

The various buffers examined, including MOPS (3-[N-morpholino]propane sulfonic acid), HEPES (N- [2-hydroxyethyl]piperazine-N′-[2-ethanesulfonic acid]), CHES (2-[N-cyclohexylamino]ethanesulfonic acid), PIPES (2-[N-morpholino]ethanesulfonic acid) and MES (piperazine-N,N'-bis[2-ethanesulfonic acid) were purchased from Sigma-Aldrich as free acids. EPPS (N- [2-hydroxyethyl] piperazine-N′-[3-propanesulfonic acid]) was purchased from Acros Organics. The various carboxylic acids including acetic acid, succinic acid, oxalic acid, malonic acid, maleic acid, malic acid, 3-hydroxybenzoic acid, citric acid, tricarballylic acid and 1,1-

cyclohexanediacetic acids were purchased from Sigma as free acids. K_2PO_4 and $KHPO_4$ were purchased from EM Science. $NaHCO_3$ and Na_2CO_3 were purchased from Mallinckrodt. Ultra pure Tris (Tris-(hydroxymethyl)-aminomethane) was purchased from Research Organics as a free base. Cacodylic acid was purchased as a sodium salt trihydrate from Fluka. All buffers were reagent or spectrophotometric grade. HPTS (8-hydroxypyrene-1,3,6-trisulfonic acid), SNAFL (5&6-carboxy-seminaphthofluorescein-1) and fluorescein were purchased from Molecular Probes. Ethanol was purchased from AAPER and was stored in glass containers. Buffers were made with distilled, deionized water and pH was adjusted using either HCl or KOH.

Fluorescence apparatus

Data were collected using an ISS (Champaign, IL) Koala spectrofluorometer in photon counting mode, with excitation from a xenon lamp source. Slit widths were 0.5 mm in the excitation and 1.0 mm in the emission path corresponding to 4nm and 8nm bandwidths, respectively. Temperature was controlled at 25°C using a circulating water bath. Emission intensity was determined in L-format using a single grating monochromator. An ISS pressure apparatus with quartz windows connected to an Automated Pressure Products (APP-PMI, Ithaca NY) automated pressure generator allowed hydrostatic pressure to be applied to the sample by injection of ethanol. Pressure was applied to the sample in a sealed cuvette using a flexible plastic cap, as first described by Paladini and Weber [119]. Data were collected using a batch file in macro

acquisition mode and were analyzed using ISS acquisition software or Kaleidagraph (Synergy Software, Reading IL).

Data analysis

For experiments using HPTS, total emission intensity was determined by integrating emission spectra between 465 nm and 700 nm. HPTS has a pH-dependent excitation spectrum, with peaks at 403 nm for the protonated species, 450 nm for the deprotonated species and an isosbestic point at 413 nm [164-167]. The pH was determined by measuring the relative fluorescence emission intensities under excitation at both 450 nm and at the isosbestic point of 413 nm. As pH increases, the excitation peak at 450 nm increases, hence the emission arising from excitation at that wavelength increases relative to excitation at 413 nm. For experiments using SNAFL-1, the excitation wavelength was 525 nm, and emission spectra were measured from 535 nm to 700 nm. From the spectra, the emission intensity at 545 nm and 625 nm were obtained. The emission intensity at 545 nm is pH-dependent, and intensity at 625 nm is isosbestic, therefore the ratio of these two intensities was used to determine pH [167-169]. For experiments using fluorescein, total emission intensity was determined by integrating emission spectra between 505 nm and 700 nm, with excitation wavelengths of 435 nm and 500 nm [139,164, 169]. 435 nm represents an isosbestic point in the pH-dependent excitation spectra of fluorescein, and 500 nm is the excitation maximum. Thus for each fluorophore, ratiometric fluorescence measurements were used to determine pH. Standard fluorescence vs. pH curves were constructed at atmospheric pressure for each

of the three fluorophores. The standard pH curves were corrected for the effects of pressure on a solution of each fluorophore in water at approximately pH 7, producing a corrected standard pH curve at each pressure. The pH was determined for each buffer at each pressure by fit to the pressure-corrected standard curve. The calculated pH of each buffer was plotted as a function of pressure and fit to a linear equation in most cases, the first derivative of which gave $\Delta pH/\Delta P$.

Experimental method

Samples were prepared using distilled, deionized water and were adjusted to the indicated pH with either KOH or HCl at atmospheric pressure at 25°C. The pH was measured with a Fisher scientific model AB15 pH meter with an Accumet Calomel Microprobe electrode immediately prior to the experiments. In all cases, total buffer concentration was 50 or 100 mM as indicated in the text, and fluorophore concentration was ~500 nM. Buffer concentration an order of magnitude above and below this value did not alter the observed pH changes. Observed pH changes were independent of fluorophore concentration. Samples were filtered using a 0.22 μm syringe-driven filter prior to addition to the pressure cuvette and cuvettes were visually inspected to avoid air bubbles. Cuvettes containing the buffer-fluorophore mixtures were allowed to equilibrate at 25ºC for 30 minutes prior to the application of hydrostatic pressure. Samples were allowed to equilibrate at each pressure for 15 minutes prior to acquisition of spectra. Additional equilibration time did not alter the acquired spectra. Calculated

pH values at each pressure were independent of the direction of pressure application. Buffer mixtures were made from 100 mM stock solutions of each of the respective component buffers to the final relative concentrations indicated.

Results and discussion

Several pH sensitive fluorophores have been utilized in the measurement of buffer pH, each with a unique fluorescence response. The fluorophores utilized include HPTS (8-hydroxypyrene-1,3,6-trisulfonic acid) or SNAFL-1 (5&6-carboxy-seminaphthofluorescein-1) and fluorescein. The excitation spectrum of HPTS features maxima at 450 nm for the deprotonated species, 403 nm in the protonated form and an isosbestic point at 413 nm (figure 2-1a). SNAFL-1 has a pH dependent emission with the emission maximum evident at 545nm when protonated. The emission of the deprotonated species is evident at the isosbestic point of 625 nm (figure 2-1b). The emission maximum of fluorescein occurs at 505 nM when the fluorophore is deprotonated. The protonated species has negligible fluorescence emission (figure 2-1c).

For each of the fluorophores, ratiometric fluorescence measurements were obtained at both a pH-sensitive wavelength and an isosbestic point. Solutions of the indicator fluorophore at serial pH values were used to develop a standard pH curve for each fluorophore at atmospheric pressure (figure 2-2). The standard curve was fit to a modified acid-dissociation equation:

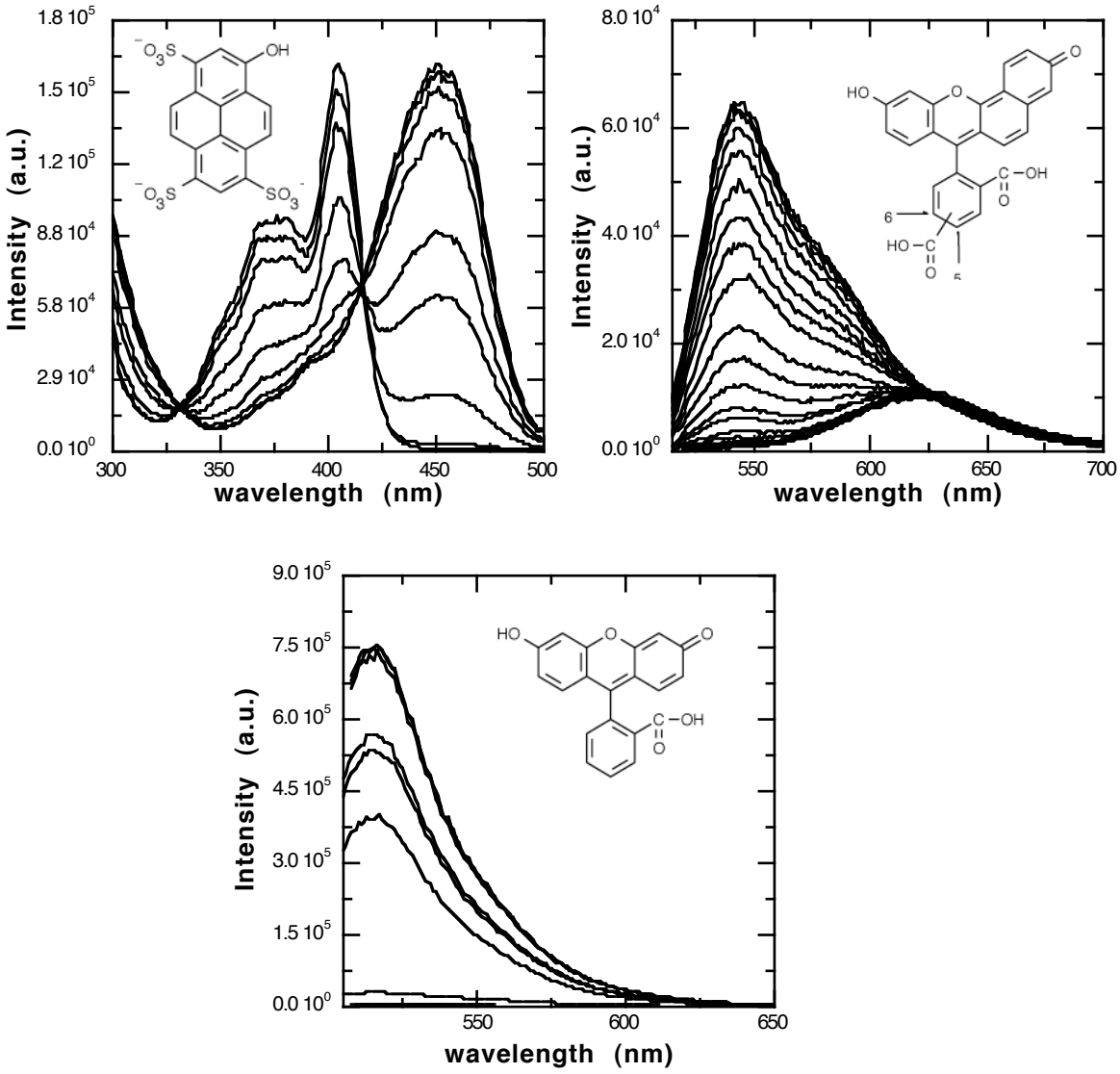

Figure 2-1: The spectra and structures of HPTS, SNAFL-1, and fluorescein as a function of pH.

Panel A shows the excitation spectra of HPTS from pH 5 - 9.5, excitation maxima are apparent at 450 nm and 403 nm, and an isosbestic point is evident at 413nm. Panel B shows the emission spectra of SNAFL-1 from pH 6.4 - 10.3. The emission maximum is 545 nm, and the isosbestic point is at 625 nm. Panel C shows the emission spectra of fluorescein from pH 3.4 - 10.6, with emission maximum at 520 nm. The chemical structure of each fluorophore is shown inset.

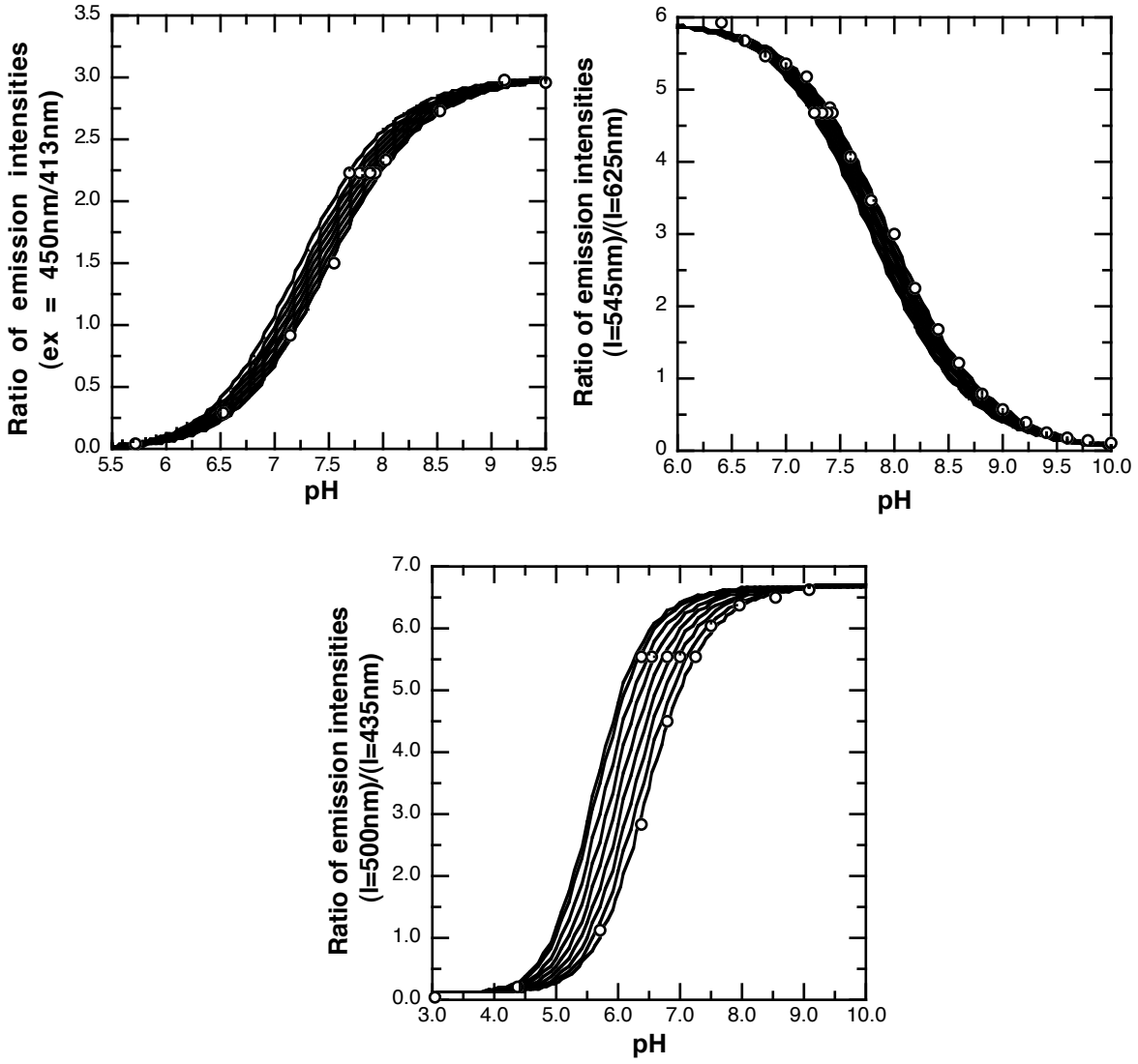

Figure 2-2: The corrected standard pH curves of HPTS, SNAFL-1 and fluorescein. The standard pH curves of (A) HPTS, (B) SNAFL-1 and (C) fluorescein are shown corrected for the effects of pressure on the individual fluorophores in water. Atmospheric pressure pH points are shown, as are the points for the fluorophore in water, used to correct the curves for pressure effects. Curves are presented from atmospheric pressure through 3 kbar.

$$F = \frac{(F_\infty - F_0)pH^\chi + F_0(pK_a + pH)^\chi}{(pK_a + pH)^\chi} \qquad [2\text{-}3]$$

where F is the ratiometric fluorescence intensity for each of the fluorophores as described.

Hydrostatic pressure has been shown to alter the pK_a values of both water and fluorescence indicators including fluorescein and naphthol [139,140,164]. Consequently, a solution of each fluorophore in water was examined for changes in pK_a with pressure. In all cases, the pH of these mixtures decreases with pressure, as reported for water and for other fluorophores studied [139, 140, 169]. The change in the pH of aqueous solutions of each fluorophore was used to correct each standard curve, as shown by the shift in standard pH curves with pressure (figure 2-2). The apparent pK_a of the standard curve was shifted by the effect of pressure on the pK_a of the fluorophore in water at each pressure:

$$F = \frac{(F_\infty - F_0)pH^\chi + F_0((pK_a * P(\Delta pK_a/\Delta P)) + pH)^\chi}{(pK_a(P(\Delta pK_a/\Delta P) + pH))^\chi} \qquad [2\text{-}4]$$

The spectral curves of fluorophore in each buffer examined showed monotonic increases or decreases with pressure, and the isosbestic points remained fixed over the pressure ranges examined (figure 2-3). As representative data, the excitation spectra of HPTS in Tris at pH 7.50 (figure 2-3a) and the emission spectra of SNAFL-1 in CHES at pH 8.50 (figure 2-3b) are shown at pressures between 1bar and 2kbar. The excitation

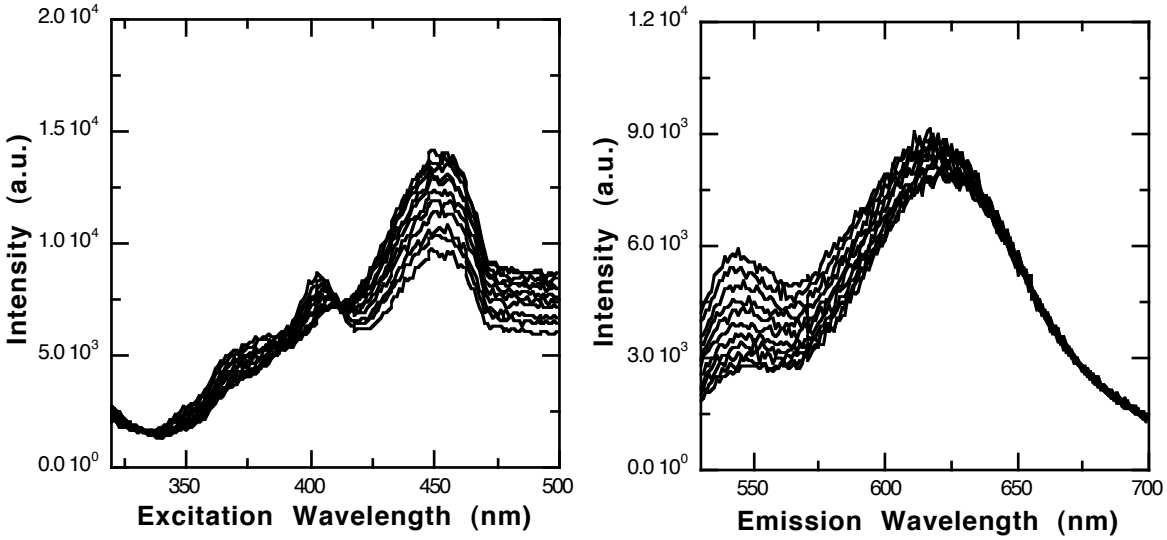

Figure 2-3: The spectra of HPTS and SNAFL-1 as a function of pressure.
Panel A shows the excitation spectra of HPTS (pH 7.5) as a function of pressure from 1 bar – 2 kbar. Panel B shows the emission spectra of SNAFL-1 (pH 8.5) over the same range of pressure. In each panel, spectra are presented from atmospheric pressure through high pressure. Isosbestic points and local maxima are constant over the range of pressures examined.

spectrum of HPTS has a maximum at 450nm, corresponding to the excitation maximum of the deprotonated species and this peak increases in intensity with pressure. The isosbestic point at 413 nm is pressure-independent. The ratio of emissions following excitation at 450 nm to 413 nm would consequently increase with pressure, indicating an increase in solution pH. The emission spectrum of SNAFL-1 in CHES has a maximum at 545 nm and an isosbestic point at 625 nm. The emission peak at 545 nm increases in intensity with pressure, whereas the isosbestic point is pressure-independent. The increase in the ratio of emission at these two wavelengths suggests that the pH of the solution increases with pressure. For each buffer examined at each pH examined, a solution of ~500 nM fluorophore was made up in 100 mM buffer. The solution was subjected to hydrostatic pressure, and the fluorescence intensity was measured as described. The pH at each pressure was determined by fit of the fluorescence ratio to the appropriately corrected standard curve. The pressure-dependent change in pH of the buffer solutions was quantified by linear fit of pH vs. pressure plots (figure 2-4). A linear fit was accurate for all buffers examined under the pressure range examined.

The $\Delta pH/\Delta P$ for many of the various biologically relevant buffers examined is positive and on the order of 0.1-0.3 pH units/kbar (figure 2-5a). All of the "Good's" buffers and cationic buffers examined have a $\Delta pH/\Delta P>0$ at pH values near their pK_a values, between 7 and 8. It is also evident that the cationic buffers examined have the smallest overall magnitude of $\Delta pH/\Delta P$, as expected. Phosphate buffer has a $\Delta pH/\Delta P$ of the same magnitude, but is negative in sign. These data are in agreement with reported

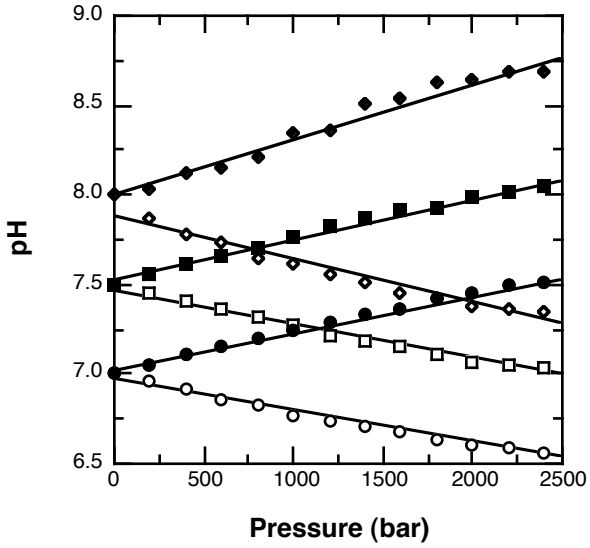

Figure 2-4: pH as a function of pressure.
The change in pH with pressure is shown for MOPS (closed symbols) and phosphate buffers (open symbols). Circles: pH 7.0, squares: 7.5, diamonds: 8.0.

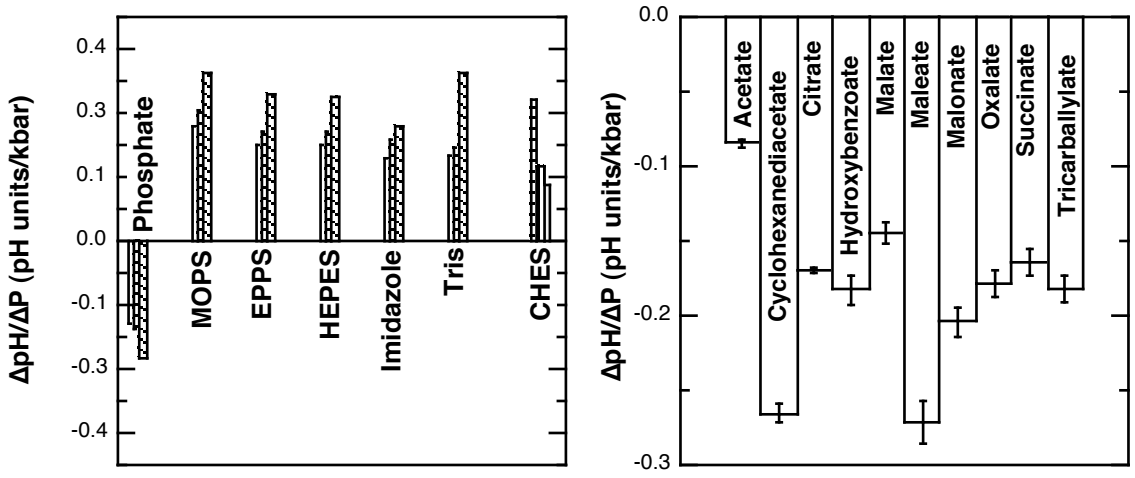

Figure 2-5: The change in pH with pressure for various buffers.
In panel A, the change in pH with pressure for various commonly used buffers is presented. Solid white: pH 7.0, left hatch: pH 7.5, right hatch: pH 8.0, horizontal hatch: pH 8.5, vertical hatch: pH 9.0, dots: pH 9.5. In panel B the changes in acidity with pressure for various carboxylate buffers at pH 7 are presented. Data are presented in ΔpH units / kbar. Error bars represent the standard errors of fits to the respective pH-pressure plots.

values for the buffers that have previously been examined [139, 140] demonstrating the validity of the experimental technique.

For many of the buffers examined, the ΔpH/ΔP has a smaller absolute magnitude at pH values below the pK_a of the respective buffer. CHES buffer, on the other hand, had a lower ΔpH/ΔP at pH values above its pK_a. The pK_a of CHES is ~9.3, well above the pK_a value of SNAFL-1, the fluorophore used. At pH values well above or below the pK_a of the indicator, precise pH determination is complicated by the small changes in fluorescence intensity produced by comparatively large changes in pH (figure 2-2b). This ambiguity is reflected in the large error bars at pH values of 9.0 and 9.5. While the cationic and neutral buffers increased in pH with pressure, carboxylates decrease in pH with pressure (figure 2-5b). The ΔpH/ΔP values for the various carboxylic acids examined ranges from -0.08 / kbar for acetate to -0.26 / kbar for 1,1-cyclohexanediacetate and maleate. These measurements were made at pH 7.0, which may be significantly above the respective pK_a values of many of the carboxylates studied. Presumably, buffer capacity would be negligible for these carboxylates under these conditions. They are included in the examination as they may be biologically relevant as enzyme substrates; or they may be a common component of biochemical buffers. Furthermore, the apparent ΔpH/ΔP of several carboxylates was altered by the presence of ammonium counter-ions at neutral pH. The high pH makes the pK_a of ammonium (9.25) [170] significant relative to that of the carboxylate under study. To avoid this confusion, free acids were used. As with the cationic and Good's buffers, the

ΔpH/ΔP data for the carboxylates we studied are consistent with other carboxylates previously examined [140].

The observation that pressure has opposing effects on cationic buffers and carboxylates leads to the prediction that pressure insensitivity might be achieved in a mixture of the two buffer types. Since the cationic buffers afforded the smallest positive ΔpH/ΔP, Tris was used as the cationic component in each mixture. Phosphate, tricarballylate (1,2,3-tricarboxylate) and CDA (1,1-cyclohexanediacetate) were selected as counter buffers. These three buffers have both a negative ΔV and a relatively high pK_a value, approaching the physiological pH values under examination. Various relative concentrations of each combination were tested at pH 7.0, 7.5 and 8.0 (figure 2-6). Increasing the relative concentration of the carboxylate diminishes the ΔpH/ΔP at each of the pH values tested. For each of the three mixtures, a specific mole fraction of the two component buffers can be derived at which ΔpH/ΔP = 0. The relative buffer concentrations that yield a minimal change in pH with pressure can be determined by solving the polynomial fits to the pH-mole fraction curves at each pH for each combination. As the solution pH increases, a higher relative concentration of phosphate or carboxylate is required to reach pressure- insensitivity. The solution conditions that yield pressure insensitive mixtures are tabulated and gram weights are presented to allow easy laboratory use (table 2-1).

The specific baroresistant buffer mixtures were tested using the same method. In each case, at each pH value tested, a very small ΔpH/ΔP is achieved using the relative concentrations derived (figure 2-7). These combination buffers in many cases have a

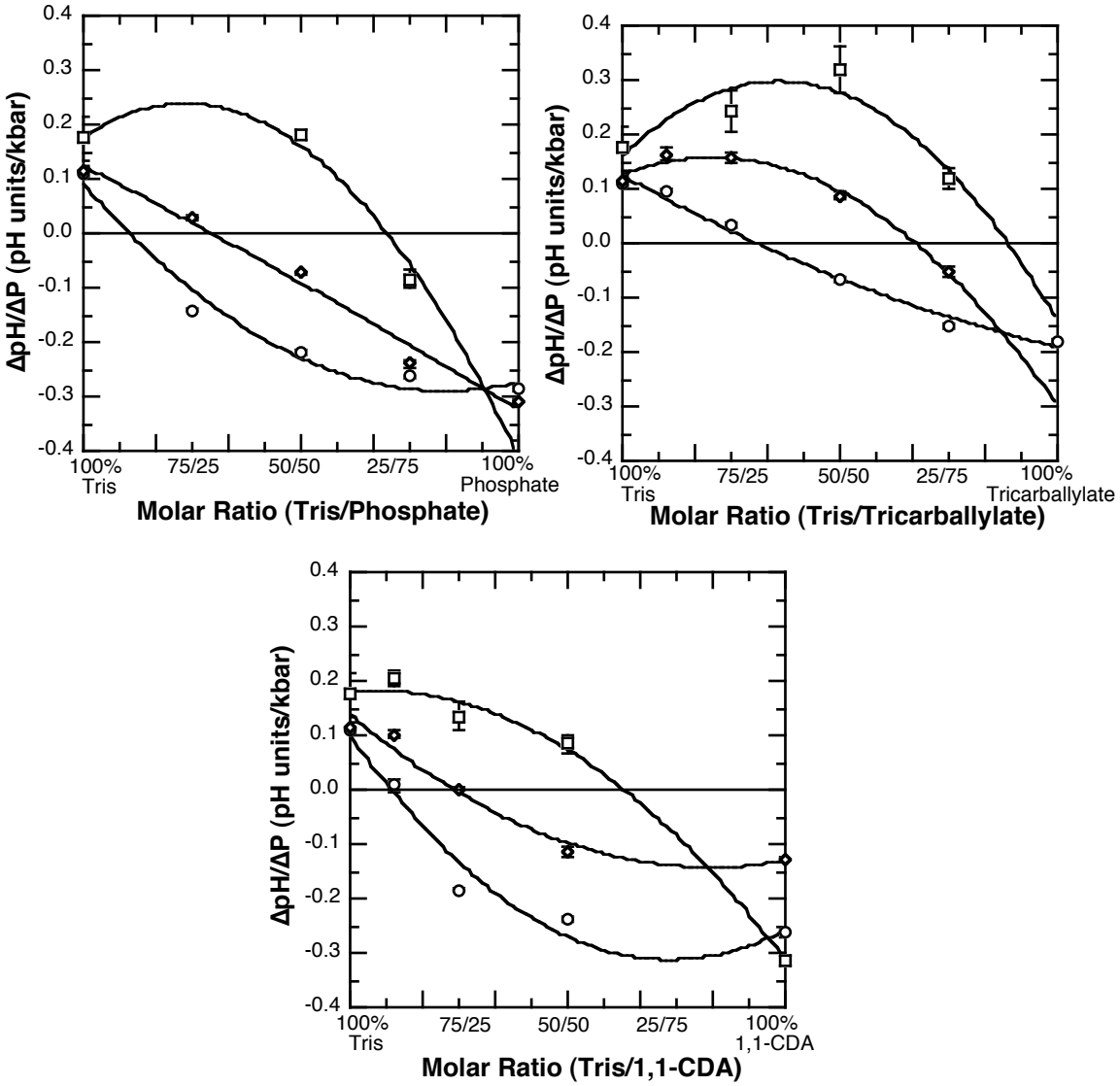

Figure 2-6: The change in pH with pressure for various 2-component buffer mixtures.

In each panel the change in acidity with pressure is plotted as a function of molar ratios of various buffer mixtures. Circles: pH 7.0, diamonds: 7.5, squares: 8.0. In panel A, Tris and phosphate data are presented. In panel B, Tris and tricarballylate mixtures are shown. In panel C, mixtures of Tris and 1,1-cyclohexanediacetic acid are presented. In all three binary mixtures, a different molar ratio of the two components yields a minimal $\Delta pH/\Delta P$ at each pH value and at each pH value, a different mole fraction of the two components yields a minimal $\Delta pH/\Delta P$.

Table 2-1: Composition of pressure-insensitive buffer mixtures

	pH	Volume 100mM X (ml)	Volume 100mM Tris (ml)	Mass X ($*10^{-5}$g) [a]	Mass Tris ($*10^{-5}$g)
Tris/ Tricarballylate	7.0 7.5 8.0	30.95 67.35 88.58	69.05 32.65 11.42	1.757 3.824 5.030	5.702 2.696 0.943
Tris/ Phosphate	7.0 7.5 8.0	10.62 29.40 74.98	89.38 70.60 25.02		7.381 5.830 2.066
Tris/ 1,1-CDA	7.0 7.5 8.0	9.45 23.87 62.94	90.55 76.13 37.06	0.472 1.192 3.143	7.477 6.287 3.060

[a] *100mM Phosphate buffer was made at each pH as described [178].*

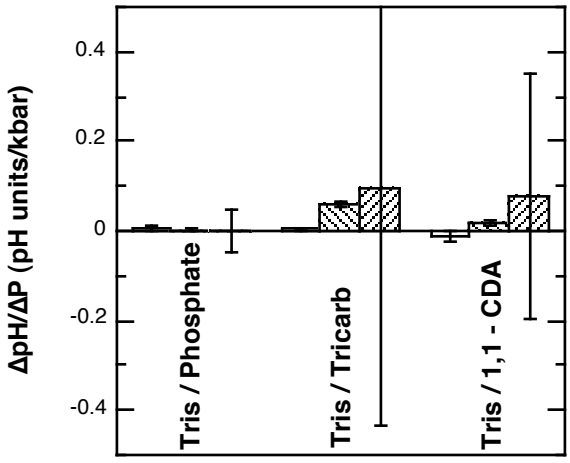

Figure 2-7: Confirmation of the baroresistance of 2-component buffer mixtures. Buffer mixtures with relative buffer concentrations as determined were tested for change in pH with pressure. Solid white: pH 7.0, left hatch: 7.5, right hatch: 8.0.

$\Delta pH/\Delta P < 0.01$ pH units / kbar. This represents an improvement over each individual buffer of approximately an order of magnitude, therefore in a typical pressure experiment with total pressure change of 3-4kbar; each buffer mixture will change in pH < 0.1 pH units.

Conclusions

In all commonly used biological buffers examined, pH was significantly altered by pressure, increasing 0.1 - 0.3 pH units/kbar in most cases. As expected, cationic buffers including Tris and imidazole showed the smallest $\Delta pH/\Delta P$. Buffers containing phosphate and the carboxylates that were examined decreased in pH with pressure, with a similar magnitude of change. The pressure effects on pH for a given buffer are reduced at pH values below the respective pK_a value in most cases. Mixing phosphate, tricarballylate or 1,1-cyclohexanediacetate with Tris yields a pressure-resistant buffering system. Altering the relative component concentrations can optimize the pH at which the pressure response of each individual buffer system is minimal. This suggests that in future pressure experiments, a buffer can be tailored to the pH optimum of the system to minimize buffer pH effects.

CHAPTER III

THE EFFECTS OF HYDROSTATIC PRESSURE ON THE ENTROPIC AND ENTHALPIC CONTRIBUTIONS TO THE FREE ENERGY OF ALLOSTERIC INHIBITION OF *E. coli* PHOSPHOFRUCTOKINASE

Synopsis

Tetrameric *E. coli* phosphofructokinase (EcPFK) has a single tryptophan residue per subunit, and the fluorescence of this tryptophan is sensitive to ligand binding. Steady-state fluorescence has been used to examine the thermodynamics of allosteric coupling of EcPFK as a function of both temperature and pressure. The binding of substrate, fructose-6-phosphate (F6P), is allosterically inhibited by the binding of phosphoenolpyruvate (PEP). Van't Hoff analyses of F6P and PEP binding, as well as the coupling between the binding events, demonstrate that not only is coupling free energy positive at 25º C, as expected for inhibition, but both entropy and enthalpy components are positive as well. The coupling free energy is also pressure dependent, becoming less positive with increasing pressure. This indicates an associated negative standard volume change. F6P binding is further examined in both the presence and absence of inhibitor PEP. Despite the overall decrease in coupling free energy, both entropy and enthalpy components increase with pressure. The decrease in magnitude of the inhibition must therefore derive from increasing entropy-enthalpy compensation, as

entropy increases more steeply with pressure than does enthalpy. Examination of the steady-state anisotropy of each of the ligation states of the enzyme as a function of pressure suggests that within the disproportionation equilibrium that defines the allosteric response the increase in coupling entropy is predicted by a concomitant decrease in anisotropy.

Introduction

Prokaryotic Phosphofructokinase (PFK) is a homotetramer with subunits containing both two partial active and two partial allosteric sites. Tetramer formation enables the juxtaposition of the partial binding sites to create four functional active and four functional allosteric sites. There is a single native tryptophan residue at position 311 near the active site in PFK from *Escherichia coli* (EcPFK), and the fluorescence from this tryptophan is sensitive to ligand binding at the active site [94,108,164]. By examination of the intrinsic fluorescence intensity, the degree of substrate saturation of the enzyme can be determined [94].

As the first committed step in glycolysis, EcPFK activity is under judicious regulation. EcPFK is allosterically activated by adenosine diphosphate (MgADP) and is inhibited by phosphoenolpyruvate (PEP) in a classic example of K-type allosteric regulation. Each of these regulatory molecules has an opposite effect yet bind the same allosteric site [94,163].

K-type allosteric inhibition is, by definition, an increase in the K_d of an enzyme for substrate while an inhibitor is bound in the allosteric site. This is accompanied by a reduction in the magnitude of the free energy of substrate binding. Conversely, activation leads to a decrease in K_d and concomitant increase in the absolute value of binding free energy. Consequently, a coupling energy can be defined which relates the substrate binding energies when effector is bound to the binding energy in the absence of effector [98,99,102]. From this linked-function analysis, the disproportionation equilibrium that defines the allosteric response can be derived:

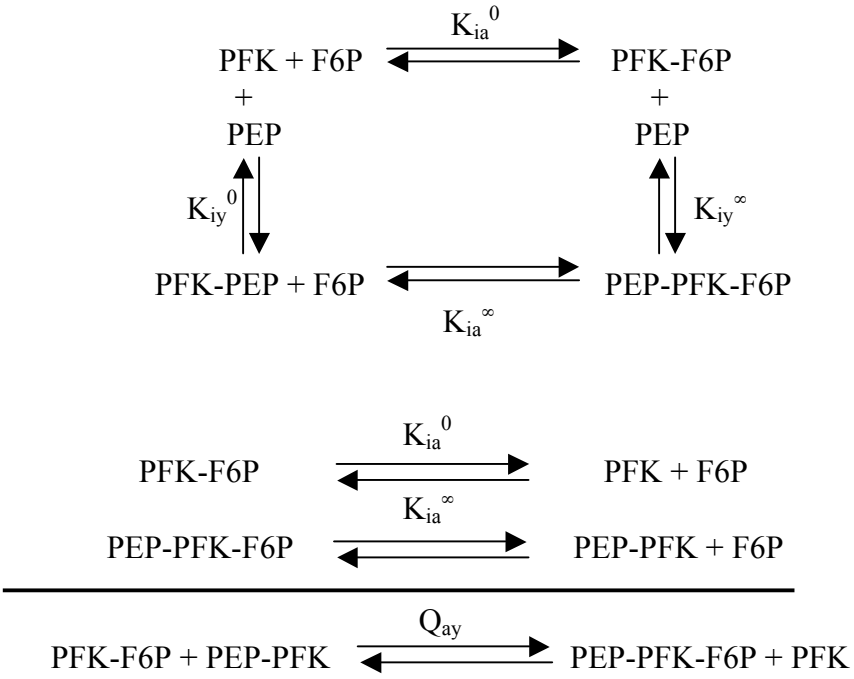

$$Q_{ay} = \frac{K_{ia}^{0}}{K_{ia}^{\infty}} \qquad [3\text{-}1]$$

where K_{ia}^{0} represents the thermodynamic dissociation constant for substrate in the absence of allosteric effector, K_{ia}^{∞} is the dissociation constant with allosteric effector saturating the enzyme and Q_{ay} is the ratio of these two parameters. It is evident from the equations that Q_{ay} also represents the equilibrium constant for the disproportionation equilibrium. The free energy of each of the equilibria can be derived from the respective dissociation constants.

This equilibrium has been studied by perturbation in various manners: mutation of the amino acid residues involved in catalysis, binding or allosteric communication, alteration of the pH, and alteration of temperature [104,110,163]. In the present study, the pressure-temperature landscape of both the ligand-binding equilibria and the disproportionation equilibrium that defines the allosteric response are determined. The standard reaction volume (ΔV) for allosteric inhibition and of multiple ligand binding equilibria is calculated from the change in these equilibrium constants with pressure.

Hydrostatic pressure is a widely utilized tool in such broad fields as protein aggregation and association [119-122], folding and denaturation [123-131], nucleic acid thermodynamics [132-135] and ligand binding [112]. Increasing pressure, as predicted by Le Chatelier, shifts chemical equilibria in the direction of smallest overall volume. For proteins, it is anticipated that pressures <1 - 2 kbar will generate reversible compression changes in the overall structure and perturb the dynamics of the enzyme [113-118]. In a pressure range of 2 – 5 kbar, subunit dissociation of multisubunit enzymes is expected [119-122]. Above 5 kbar, irreversible denaturation of the tertiary structure of most enzymes is anticipated [123-131]. Below the dissociation threshold,

proteins undergo reversible changes in dynamics. Under the conditions of moderate hydrostatic pressure, the effects of pressure on ligand binding and allostery can be examined. The predominant forces involved in pressure perturbation of dynamic protein phenomena are cavity compression and electrostriction [113]. The former exploits imperfect packing within the protein to yield an overall reduction in protein volume. The latter involves reduction in solvation volume associated with increased charge separation in either the reactants or products. Thus the overall perturbation includes affects on the reacting species and the solvent medium.

Tetrameric EcPFK dissociates at pressures ~1.2 kbar, and that dissociation becomes irreversible at 1.4kbar at which point denaturation is assumed to occur. Below 1 kbar, effects of pressure on ligation and allostery have been reported [111]. The ΔV for binding of the various ligands is 13-45 ml mol^{-1}, as predicted for partial charge neutralization of the anionic ligands associated with binding. The overall ΔV for the disproportionation equilibrium defining the allosteric response of the enzyme is negative. In this case, the effects of electrostriction are expected to be minimal as both ligands are protein-bound, hence partially charge-neutralized on both sides of the equilibrium. The standard volume change for the disproportionation reaction therefore represents significant changes in the protein volume for the doubly liganded and free vs. the two binary complexes.

We have determined the temperature-pressure landscape for the allosteric coupling between PEP and F6P, and the individual binding interactions that compose this coupling. From van't Hoff analyses, the enthalpic and entropic components of

ligand binding and of coupling free energy are determined. Furthermore, the steady-state anisotropy of all 4 species comprising the disproportionation equilibrium have been determined as a function of pressure.

Materials and methods

Fructose-6-phosphate, phosphoenolpyruvate, ammonium chloride, magnesium chloride and EDTA were spectral or reagent grade and were purchased from Sigma. Ethanol was purchased from AAPER. Tris was purchased as a free base from Research Organics.

Data were collected using an ISS Koala spectrofluorometer in photon counting mode, with excitation from a xenon lamp source. Slit widths were 0.5 mm in the excitation and 1.0 mm in the emission path, corresponding to bandwidths of 4nm and 8nm respectively. Temperature was controlled using a circulating water bath. Total emission intensity was determined in L-format using a Schott WG-345 cut-on emission filter, with excitation at 300 nm. An ISS pressure apparatus with quartz windows connected to an Automated Pressure Products (Ithaca, NY) automated pressure pump allowed hydrostatic pressure to be applied to the sample by ethanol injection. Pressure was applied to the aqueous sample in a sealed cuvette via a flexible polystyrene cap, as described by Paladini and Weber [119]. Data were collected using a batch file in macro acquisition mode and were analyzed using either ISS acquisition software (Champaign, IL) or Kaleidagraph (Synergy Software, Reading, IL). Steady-state anisotropy was measured with a similar instrumental arrangement, with external Glan-Thompson

polarizers in L-format using a square quartz pressure cuvette. Data were collected in batch mode and were corrected for birefringency [171]. Data collected in the pressure cuvette were normalized to data collected at atmospheric pressure in Uvonics $1cm^2$ quartz cuvettes. Fluorescence intensity data were fit to a modified Hill equation [88]. Standard volume changes were given by the change in association constant with respect to pressure [112]:

$$\Delta V = -RT\left[\frac{\Delta K_a}{\Delta P}\right] \qquad [3\text{-}2]$$

where ΔV is the standard volume change for association, ΔK_a is the change in association constant and ΔP is the change in pressure.

E. coli PFK was purified as described [173], with several modifications. Following Mimetic blue dye affinity chromatography and overnight dialysis, peak fractions were applied to a Pharmacia Mono Q anion-exchange column and were eluted with a linear salt gradient from 0 - 1 M NaCl. Peak fractions were extensively dialyzed into buffer composed of 50 mM Tris, 10 mM $MgCl_2$, 10 mM NH_4Cl, 0.2 mM EDTA. Purity was confirmed by SDS-PAGE and protein was quantified as described [94].

Samples were prepared using distilled, deionized water and were adjusted to the indicated pH with either KOH or HCl at atmospheric pressure. Samples contained 2.6 μM PFK, and were filtered using an Amicon 0.22 μM syringe-tip filter prior to addition to the pressure cuvette. The cuvette was visually inspected for the absence of air

bubbles. The pressure cuvette was allowed to equilibrate at the indicated temperatures for 30 minutes prior to data acquisition. During the pressure experiments, samples were allowed to equilibrate at each pressure for 15 minutes prior to the acquisition of spectra. Additional equilibration time did not alter the observed intensities. Sample activity was periodically checked following pressurization and was found to be recoverable.

Results

Effects of hydrostatic pressure on substrate binding

To determine the effects of pressure on substrate binding, F6P titrations were performed at pressures between 0 and 1.1 kbar. Above 1.2 kbar, the protein dissociates [111,155], whereas below 1.1 kbar the reversible pressure effects on ligation can be determined. Upon F6P binding, the intrinsic tryptophan fluorescence intensity is decreased ~30%. The degree of F6P saturation of the enzyme can therefore be assessed by determination of the fluorescence intensity. At all F6P concentrations examined, the intrinsic fluorescence intensity increases with pressure (figure 3-1a). At intermediate F6P concentrations, upward curvature is observed in the intensity plots. At both saturating F6P and very low concentrations of F6P, no change in slope is observed over the pressure range examined. In the presence of high concentrations of allosteric inhibitor, PEP, fluorescence intensity similarly increases with pressure (figure 3-1b). In this case, however, slopes are constant at all pressures examined.

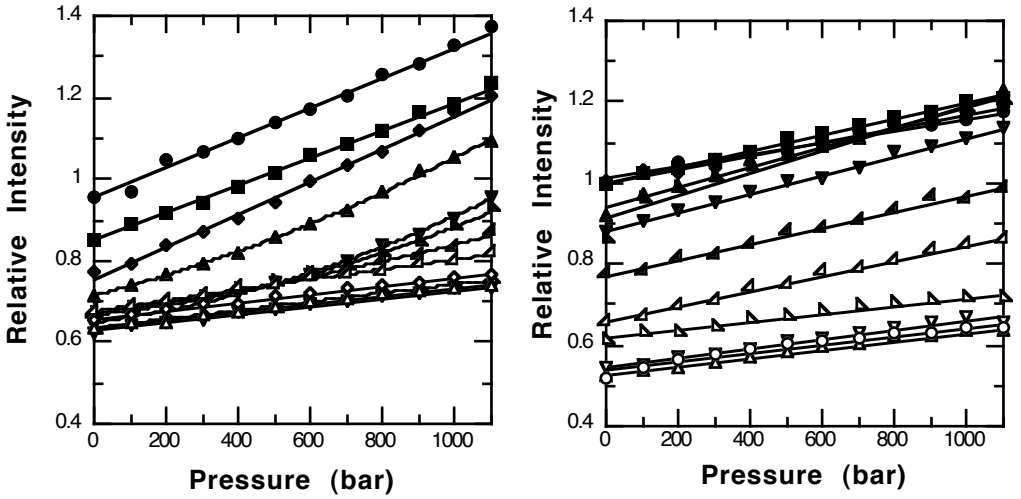

Figure 3-1: The effects of hydrostatic pressure on the intrinsic tryptophan fluorescence of *E. coli* PFK under varying ligation states.
In panel A, fluorescence intensity is plotted as a function of pressure at varying concentrations of F6P between 0 and 2 mM. Closed symbols: circles: 0 μM, squares: 4 μM, diamonds: 8 μM, triangles: 15 μM, inverted triangles: 30 μM, left triangles: 50 μM, right triangles: 100 μM. Open symbols: right triangles: 200 μM, left triangles: 400 μM, inverted triangles: 800 μM, triangles: 1 mM, diamonds: 2 mM F6P. In panel B, fluorescence intensity is plotted as a function of pressure at various F6P concentrations between 0 and 4 mM in 25 mM PEP. Symbols are as in (a), with open circles representing 4 mM F6P.

From the plots of fluorescence intensity vs. substrate concentration, the binding affinity can be derived at each pressure. F6P binding isotherms show an outward shift with increasing pressure at low temperature and in the absence of allosteric inhibitor (Figure 3-2a). The outward shift in binding curves, and the reduction in substrate-binding affinity this represents, is augmented at higher temperatures (Figure 3-2b). Conversely, in the presence of PEP, the F6P binding isotherms are nearly constant with pressure at low temperatures (Figure 3-2c) and are shifted modestly by pressure at higher temperatures (Figure 3-2d). The outward shift of each of the binding curves reveals the weakening binding affinity with pressure under all conditions.

The binding constants for F6P in the absence of PEP (K_{ia}^{0}) are dramatically increased with pressure, particularly at higher temperatures (figure 3-3a) and lower pressures. As pressure increases, K_{ia}^{0} values show reduced variation with pressure and ultimately plateau at pressures above 700 bar. In the presence of near saturating PEP concentrations, F6P-binding affinity (K_{ia}^{∞}) is largely pressure-independent. At high pressures, binding affinities appear to approach similar values in both the presence and absence of PEP, particularly at higher temperatures.

The effects of hydrostatic pressure on allosteric coupling

The allosteric coupling between PEP and F6P derives from the ratio of substrate binding affinities in the absence and saturating presence of PEP (equation 3-1). Consequently, since K_{ia}^{∞} is relatively constant and K_{ia}^{0} is strongly temperature and

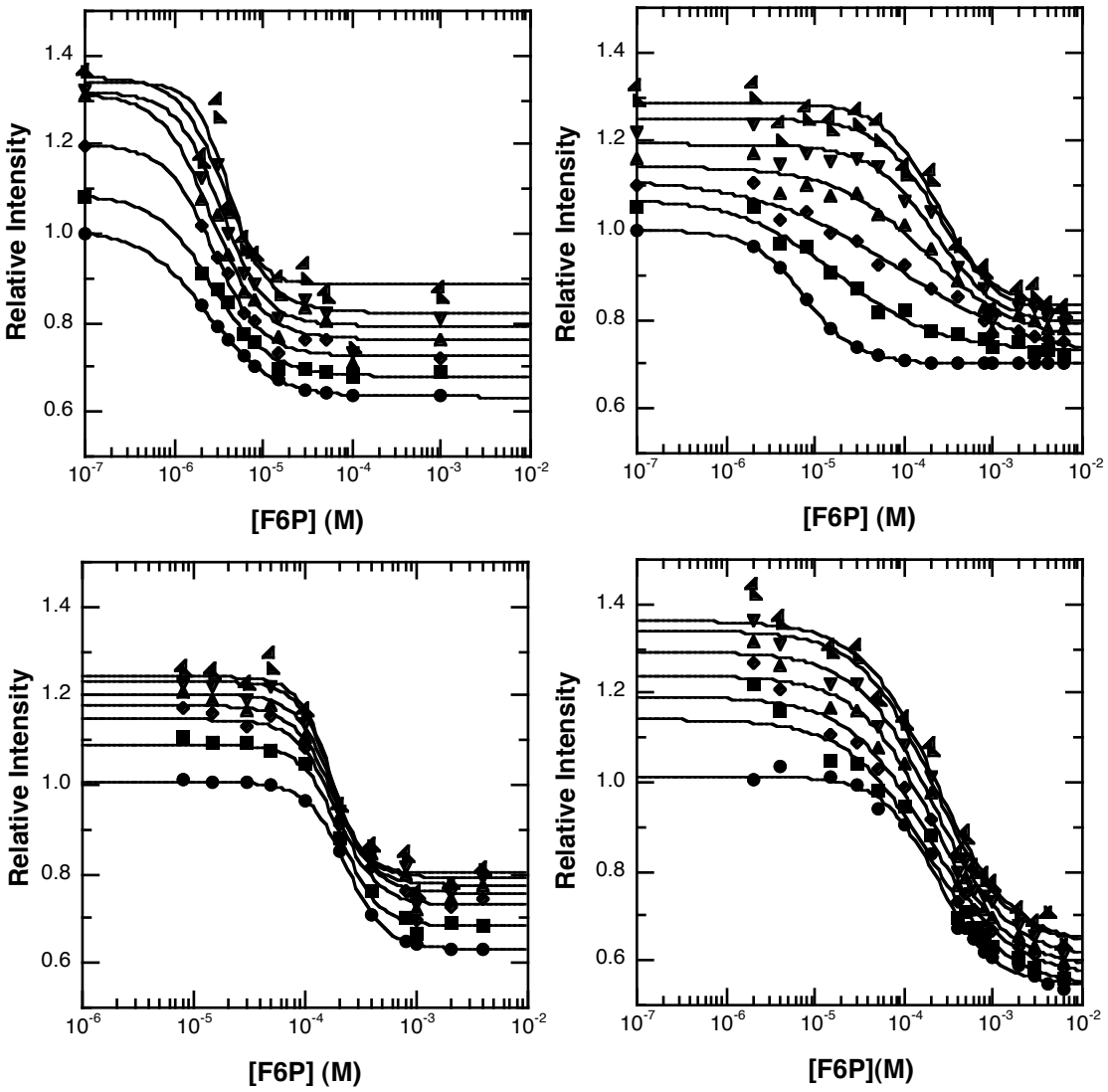

Figure 3-2: F6P binding titrations as a function of pressure.
In panels A and B, F6P binding isotherms at pressures between 1 bar and 1 kbar at temperatures of 15°C and 35°C are presented. In panels C and D, similar isotherms are presented for binding in the presence of 25 mM PEP. Circles: 1 bar, squares: 200 bar, diamonds: 400 bar, triangles: 600 bar, inverted triangles: 800 bar, left triangles: 1 kbar, right triangles: 1.1 kbar.

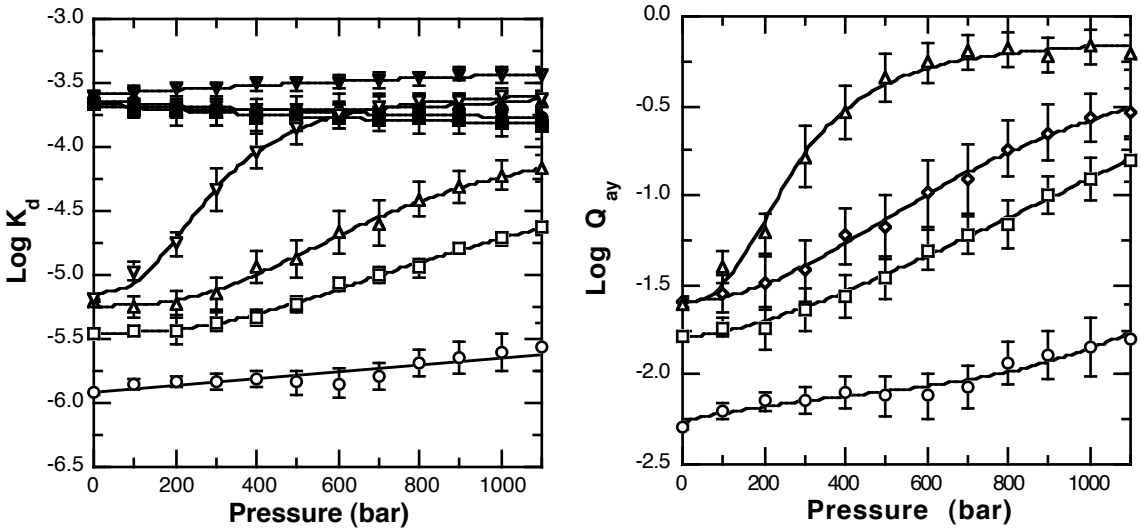

Figure 3-3: Binding constants as a function of pressure.
In panel A, log K_{ia}^{0} (open symbols) and log Kia^{∞} (closed symbols) values are shown as a function of pressure at various temperatures between 15°C and 35°C. Panel B shows the coupling constant, Q, as a function of pressure. In each plot, circles: 15ºC, squares: 20ºC, diamonds: 30ºC, triangles: 35ºC. Data fits are arbitrary.

pressure dependent, the variance in the coupling constant Q mirrors that of K_{ia}^{0} (Figure 3-3b). The coupling constant increases with pressure at all temperatures, suggesting that inhibition becomes less significant. This implies that as pressure increases PEP becomes a weaker inhibitor. Furthermore, as temperature increases, the pressure-dependence of Q increases at low pressures.

Standard volume changes of binding and allosteric coupling

The change in binding constant with pressure determines the standard volume change for the reaction. The ΔV for F6P binding (ΔV_{Kia}^{0}) is positive at all temperatures and increases at higher temperatures (Figure 3-4). The ΔV for F6P binding in the presence of saturating PEP ($\Delta V_{Kia^{\infty}}$) is near zero and is essentially unchanged with temperature. The ΔV of coupling (ΔV_{Q}) is negative and decreases with increasing temperature. The net change in volume for the allosteric response becomes smallerwith increasing temperature.

The thermodynamics of binding and allosteric coupling

Van't Hoff analyses of K_{ia}^{0}, K_{ia}^{∞} and Q were performed as a function of pressure in order to elucidate the effects of pressure on the thermodynamic contributions to ligand-binding and coupling. Both the K_{ia}^{0} and Q show strong pressure-dependence on both entropy and enthalpy, which are proportional to the y-intercept and slope of their van't Hoff

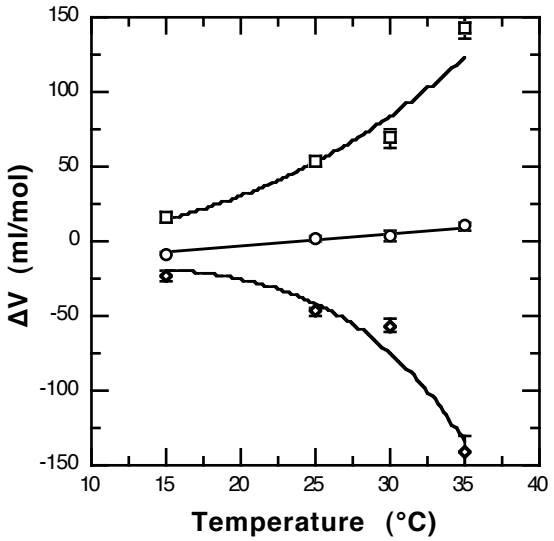

Figure 3-4: Standard volume changes of binding and coupling as a function of temperature.
Standard volume changes of ligand-binding and allosteric coupling are shown as a function of temperature. Circles: volume change for K_{ia}^{∞}, $\Delta V_{Kia^{\infty}}$, squares: volume change for K_{ia}^{0}, $\Delta V_{Kia^{0}}$, diamonds: volume change for the coupling constant Q, ΔV_{Q}. Fits are arbitrary.

plots, respectively (Figure 3-5a,c). Conversely, the thermodynamic parameters of K_{ia}^{∞} are largely pressure-insensitive (Figure 3-5b) as indicated by the minor changes in slope and intercept of the van't Hoff plot. In all cases, the apparent heat capacity is minimal, however the curvature in the van't Hoff plot of K_{ia}^{∞} is relatively larger given the small net change in K, as shown on an expanded scale (figure 3-5b, inset).

The pressure-dependencies of the thermodynamic parameters are summarized in figure 3-6. The entropy and enthalpy of K_{ia}^{0} and Q are highly non-linear with pressure, increasing sharply at low pressure, reaching a maximum at 700 bar, and decreasing at high pressure (figure 3-6a,b). The entropy and enthalpy of K_{ia}^{∞} increase linearly with pressure. The free energies of K_{ia}^{0} and Q decrease with pressure linearly, whereas the free energy of K_{ia}^{∞} is almost completely pressure-insensitive (Figure 3-6c). The interplay between ΔH and $T\Delta S$ give rise to the small and linear change in ΔG. In each case both ΔH and $T\Delta S$ increase with pressure, whereas the magnitudes of ΔG for binding and coupling decrease. These data suggest that a compensatory effect is occurring between entropic and enthalpic effects. The decreasing magnitude of ΔG arises from a greater pressure-dependent contribution from the $T\Delta S$ term than from the ΔH term. Entropy increases more dramatically with pressure than does enthalpy.

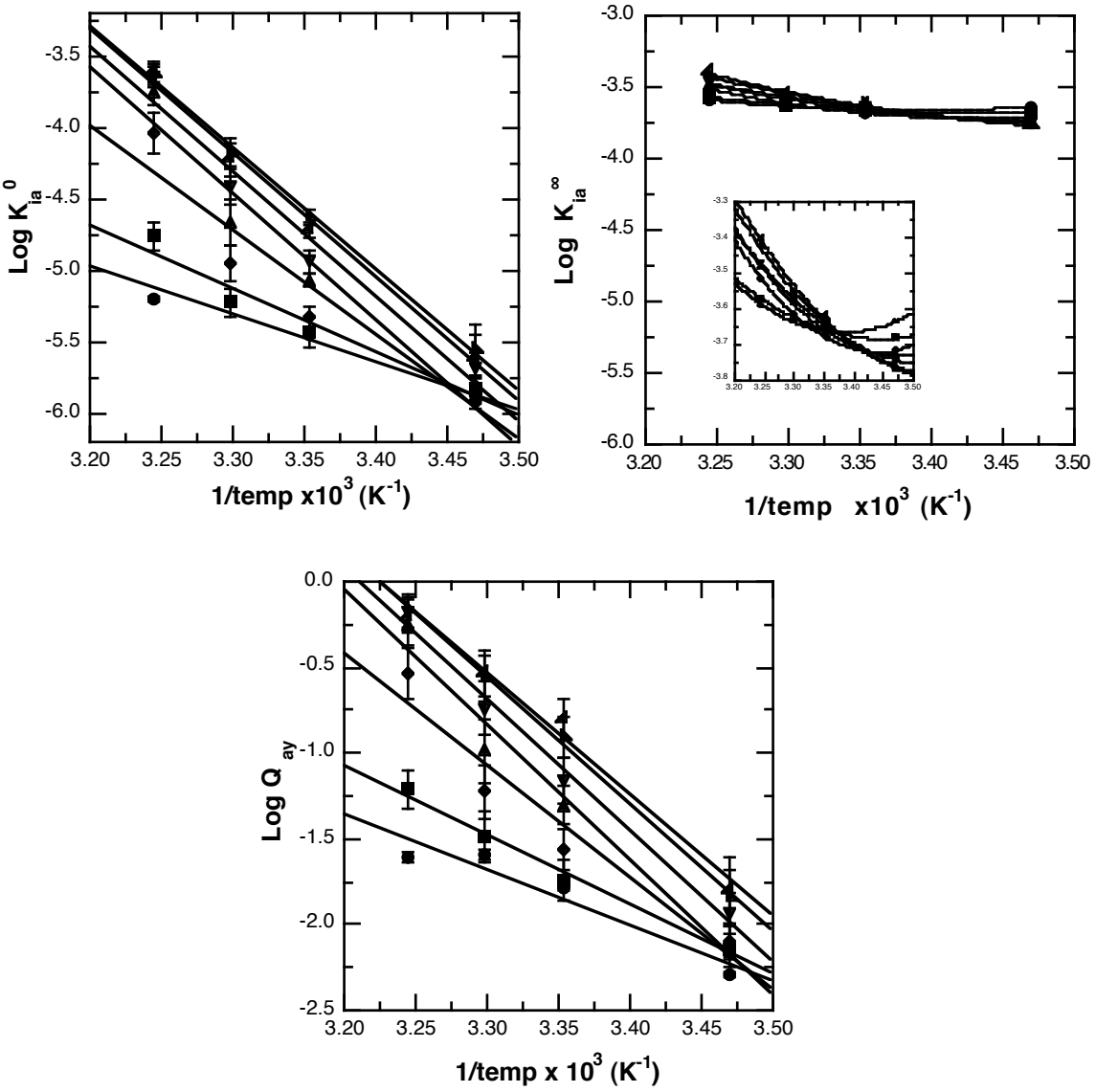

Figure 3-5: Van't Hoff analyses of ligand-binding and allosteric coupling.
In panel A, van't Hoff plots for K_{ia}^{0} are shown as a function of pressure. In panel B, K_{ia}^{∞} data is presented (expanded scale inset). Panel C shows the van't Hoff plot for the allosteric coupling constant, Q. Circles: 1 bar, squares: 200 bar, diamonds: 400 bar, triangles: 600 bar, inverted triangles: 800 bar, left triangles: 1 kbar.

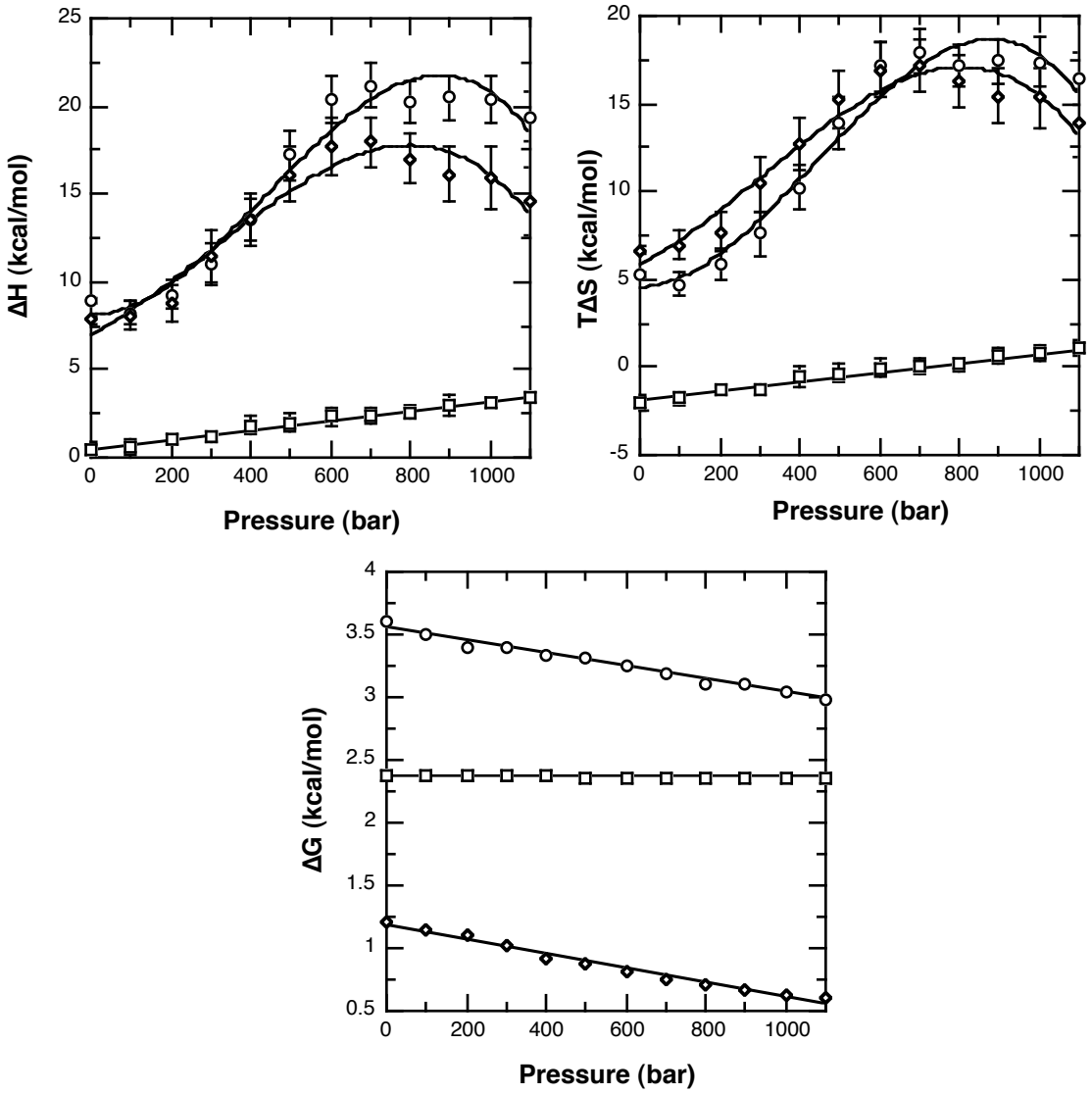

Figure 3-6: Pressure dependencies of the thermodynamic parameters of binding and allosteric coupling.
In panel A, the enthalpy of K_{ia}^{0} (open circles), K_{ia}^{∞} (open squares) and Q_{ay} (open diamonds) are shown as a function of pressure. In panel B, the entropy of the same parameters is shown as a function of pressure. In panel C, the Gibb's free energies of binding and coupling are shown.

Notably, several interesting thermodynamic phenomena occur at approximately 700 bar. At this pressure, the TΔS term of K_{ia}^{∞} is zero; therefore the entropy of Q becomes equivalent to the entropy of K_{ia}^{0}. At this pressure, the enthalpies of both K_{ia}^{0} and Q are also maximal.

The steady-state anisotropy of the components of the disproportionation reaction

In order to further examine the effects of pressure on allosteric coupling, the steady-state fluorescence anisotropy of the single native tryptophan was measured as a function of pressure. The pressure-dependence of the anisotropy of each of the individual components of the disproportionation equilibrium was measured and corrected for the effects of birefringency (figure 3-7a). The anisotropies of the free enzyme and the ternary complex are smaller and decrease more sharply with pressure than those of either of the two binary complexes. The PEP-bound enzyme has the smallest anisotropy-pressure slope of the enzyme ligation states. The sum of the anisotropy values of products minus reactants for the disproportionation reaction is negative and decreases linearly with pressure (Figure 3-7b) as expected, given that the anisotropies of both products are smaller in magnitude and are more pressure-sensitive than those of the reactants.

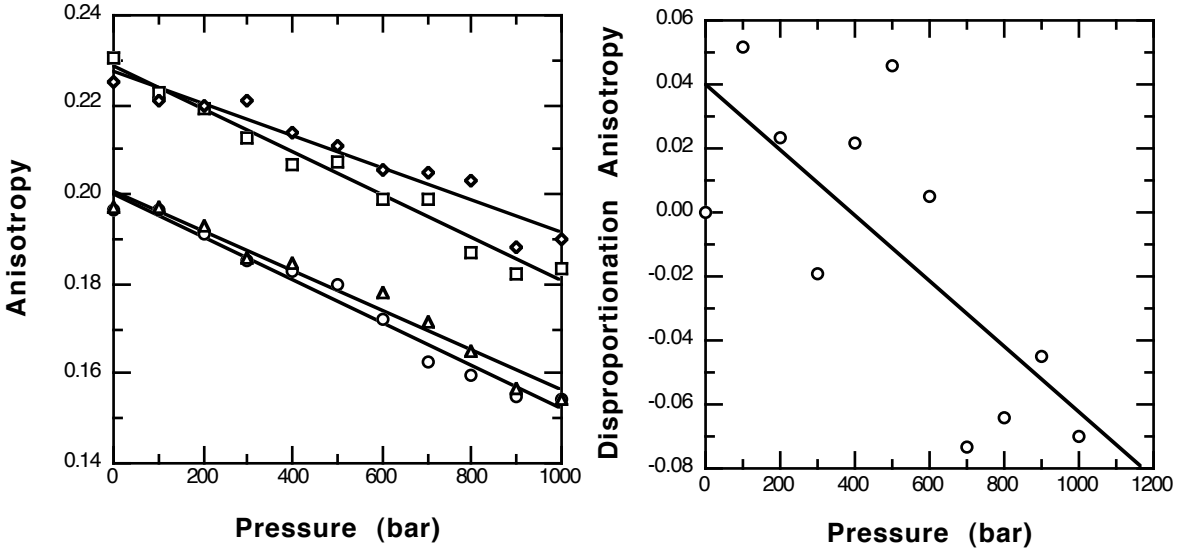

Figure 3-7: The steady-state anisotropy of the disproportionation equilibrium as a function of pressure.
In panel A, the anisotropies of the various ligand-bound species of the disproportionation equilibrium are shown. Open circles: PFK, squares: PFK-F6P, diamonds: PEP-PFK, triangles: PEP-PFK-F6P. In panel B, the anisotropy of the overall disproportionation ($r_{products} - r_{reactants}$) is shown.

Discussion

In the pressure range below ~1 kbar, the reversible effects of pressure on protein structure and function can be examined for *E. coli* PFK. The effect of pressure on the thermodynamics of multiple ligand-binding equilibria has been examined as a function of temperature.

At all F6P concentrations, the intrinsic tryptophan fluorescence intensity increases with pressure. Protein compression by pressure leads to tighter hydrophobic packing near the tryptophan residue, and hence higher intrinsic intensity would be predicted. In the absence of PEP, upward curvature in intensity-pressure plots is observed at intermediate F6P concentrations, whereas at both saturating F6P and very low concentrations of F6P, no change in slope is observed. In the absence of PEP, the substrate-binding affinity is strongly reduced by pressure. The curvature in the intensity-pressure plots can therefore be rationalized by the decreasing F6P affinity at higher pressures. As pressure increases, the increasing slope reflects increased intensity arising from both greater hydrophobic packing and F6P dissociation from the enzyme. At saturating F6P concentrations, no net dissociation is observed, and at low F6P concentrations the minimal extent of saturation leads to a very minor change in intensity due to F6P dissociation. In the presence of allosteric inhibitor, fluorescence intensity similarly increases with pressure, however slopes are constant at all pressures examined. This is due to the nominal change in F6P affinity with pressure observed in the saturating presence of inhibitor.

The binding of substrate in the presence of inhibitor, K_{ia}^{∞}, is essentially constant with pressure, whereas substrate binding in the absence of inhibitor, K_{ia}^{0}, is highly-pressure sensitive at lower pressures and becomes less so as pressure increases. Interestingly, K_{ia}^{0} values approach K_{ia}^{∞} values at high pressure, a phenomenon that may be attributed to either dissociation or compressibility. Pressure causes PFK subunit dissociation at ~1.2 kbar, therefore the maximal K_{ia}^{0} may simply reflect competing processes of ligand-binding and protein dissociation. As the affinities are equivalent at approximately 700 bar, this equivalency may be more reasonably attributed to changes in compressibility of the various enzyme forms. Compressibility refers to the rate of change in reaction volume with respect to pressure. The K_{ia}^{∞} is pressure-insensitive, suggesting that the reaction volume is small and compressibility is negligible. K_{ia}^{0} is highly pressure-sensitive at pressures below 700 bar, but becomes pressure-insensitive above this pressure, at which point compressibility approaches zero. Given that these characteristics occur at approximately the same pressure, these data suggest that pressure may be causing the enzyme to adopt a conformation that approaches that of the inhibitor-bound form.

The role of entropy-enthalpy compensation in varied biological functions, including the allosteric response, has been well-documented [97,163]. Small differences in large, opposing thermodynamic forces lead to allosteric effects. Various perturbations including pH and temperature have been shown to invert the effects of various allosteric ligands at some critical value. As with these other experimental parameters, the compensatory effect between enthalpy and entropy in EcPFK allostery increases with

pressure. The trend of increasing coupling constant with pressure suggests that pressure may induce a similar inversion of allosteric effect. The overall free energy of coupling decreases, yet both ΔH and ΔS terms increase. The compensation between entropy and enthalpy increases with pressure, leading to an overall reduction in the allosteric inhibition of the enzyme by PEP. The entropic term increases more strongly with pressure than does the enthalpic term. Based on these data, it is possible that at some critical pressure, an inversion of allosteric effect would occur whereby an allosteric inhibitor such as PEP may actually activate the enzyme to some extent. This possibility may be superseded by the apparent reduction in compressibility that leads to smaller change in Q with pressure at high pressures and which may prevent this inversion.

The increase in entropy with pressure is itself intriguing, as pressure would intuitively decrease rather than increase entropy. Increased pressure leads to protein compression and cavity reduction, which would leads to reduced conformational flexibility and lower entropy. The increasing entropy suggests that pressure is causing greater flexibility both for ligand-binding and allosteric coupling.

Several interesting thermodynamic phenomena occur at approximately 700 bar. At this pressure, the TΔS term of K_{ia}^{∞} is zero; therefore the entropy of Q becomes equivalent to the entropy of K_{ia}^{0}. Also at this pressure, the enthalpies of both K_{ia}^{0} and Q_{ay} are maximal.

The standard volume change of binding for both substrate and allosteric effector is positive, and its magnitude increases with temperature. Given the general effects of electrostriction, this is unsurprising. Since a charged ligand undergoes partial charge

neutralization during binding, the binding equilibrium would be anticipated to shift in favor of dissociation under pressure. Conversely, the ΔV of coupling (ΔV_Q) is negative in sign and its magnitude decreases with temperature. In this case, the disproportionation equilibrium has both ligands bound on either side of the equation, thus the electrostriction effects are hypothesized to be negligible. As pressure increases, the coupling decreases, suggesting that PEP becomes a weaker inhibitor. Stated another way, at high pressure the effects of bound effector on the binding affinity for substrate are smaller. The reaction volume for the allosteric response becomes more negative with increasing temperature. This may imply higher flexibility in the products of the disproportionation reaction at higher temperatures.

The reduction of coupling at high pressure derives from a strong pressure dependence of binding in the absence of inhibitor relative to a comparatively pressure-insensitive substrate affinity when inhibitor is bound. There are two possible, yet conflicting, explanations for this phenomenon. The first hypothesis is that with PEP bound, the enzyme itself becomes more rigid and hence less responsive to pressure effects. Bound PEP causes the protein to be more inflexible, in essence locking the active site in place. Increasing pressure would be largely ineffective in altering the binding properties of the rigid enzyme for substrate. A second possible hypothesis is the opposite: that bound PEP causes PFK to be more rather than less flexible. Each of the four ligation states of the enzyme as well as the overall disproportionation equilibrium decrease in anisotropy with pressure. This net decrease derives from the relative slopes of the component anisotropies as the two individual binary complexes, PFK-PEP and

PFK-F6P have smaller net decreases in anisotropy with pressure than both the ternary complex and the free enzyme. Since steady-state anisotropy reflects motion, these data imply that an increase in relative motion with pressure is occurring. These data, taken with the pressure-dependent increase in entropy of both ligand binding and allosteric coupling, suggest that the ternary complex and free enzyme are more conformationally flexible than the binary complexes and support the hypothesis that the enzyme is more flexible with PEP bound. The addition of allosteric inhibitor increases dynamic motion within the protein and the overall pressure-insensitivity of the PEP-bound state is due to compensation by increased protein flexibility.

A less likely possibility is that the substrate and ligand are less desolvated in the ternary complex than in either of the binary complexes. This explanation seems unlikely given that the active and allosteric sites do not undergo gross conformational shifts on binding [148,149], which might suggest that either or both of the ligands are more solvent exposed in the ternary complex than in the singly bound state.

The precise structural effects of pressure on the each of the various free and ligand-bound enzyme forms have yet to be determined, and may shed light on this subject.

Conclusions

The pressure-temperature landscape of ligand-binding and allosteric coupling by the enzyme EcPFK has been examined. The thermodynamics of allosteric coupling show a weaker coupling as a function of pressure, and it remains to be determined if an

inversion of allosteric effects may occur at high pressure. The weakened coupling arises from entropy-enthalpy compensation, and both thermodynamic parameters increase with pressure. Entropic contributions to free energy increase faster with pressure than do the enthalpic contributions, a phenomenon that is further clarified by the associated increase in steady-state anisotropy of the intrinsic tryptophan. Whether this increased compensation is a generalized protein response of multiple ligand binding equilibria to pressure or whether this is unique to the allosteric coupling of EcPFK remains to be determined.

CHAPTER IV

EXAMINATION OF A TRANSIENT INTERACTION BETWEEN PIG HEART MITOCHONDRIAL MALATE DEHYDROGENASE AND CITRATE SYNTHASE USING FLUORESCENCE CORRELATION SPECTROSCOPY

Synopsis

While the existence of transient interactions between many of the enzymes of intermediary metabolism has been hypothesized, demonstration of these associations has proven difficult in many cases. We have examined the interaction between pig heart citrate synthase (CTS) and mitochondrial malate dehydrogenase (MDH) using multi-photon, dual-channel Fluorescence Correlation Spectroscopy. Using G(0) analyses of cross-correlation and autocorrelation data, an association between CTS and MDH is demonstrated in polyethylene glycol (PEG). The affinity of these proteins is on the order of 10^{-7} M at <10% PEG, and is highly PEG dependent. Extrapolation to free solution suggests a protein affinity weaker than detectable by conventional methodologies. The apparent affinity between the enzymes is increased by low concentrations of the intermediate oxaloacetate (OAA), and decreased at concentrations above the K_m for OAA. At high concentrations of OAA or NaCl and PEG,

heterogeneous, nonspecific aggregates are observed suggesting that solid-state precipitates may not reflect the 1:1 interaction observed in the soluble phase.

Introduction

The existence of weak or transient protein-protein interactions between many of the enzymes of intermediary metabolism and the concomitant channeling of common intermediates between those enzymes has been debated for several decades [10-14]. Many if not all of the enzymes that function in the eukaryotic citric acid cycle have been implicated in transient interactions of some form [10,20-23]. Interactions of metabolic enzymes with cytoskeletal and motor proteins have also been demonstrated [24, 25]. In many cases, these weak interactions have been difficult to demonstrate experimentally, leading to hypotheses concerning fundamental differences between solution measurements *in vitro* and actual physiological conditions [11-13].

Despite the inherent difficulties in detection and quantification of transient or very weakly interacting species, those interactions may be physiologically significant. Transient interactions have been implicated in the channeling of common metabolic intermediates; a function that serves several purposes in the cell. Firstly, hydrophobic or membrane-soluble intermediates are commonly sequestered in long tunnels between active sites, preventing their loss to the extracellular environment, as shown with the

enzyme Trp synthase [14]. Secondly, labile intermediates are prevented from exposure to solvent [14]. Finally, kinetic rates for certain critical metabolic pathways are increased or are more tightly controlled by sequestering an intermediate from exposure to competing, non-productive enzyme activity [13, 27]. The obvious biological utility of both substrate channeling and transient protein-protein docking has driven research in this area for many years, even prior to the presence of experimental evidence suggesting such.

The sequential citric acid cycle enzymes malate dehydrogenase (MDH) and citrate synthase (CTS) have been shown to interact under conditions of enzyme precipitation [26, 27]. A molecular model of this protein association has been proposed, wherein an electrostatic channel between active sites allows catalysis to occur without release of their common intermediate oxaloacetate (OAA) to bulk solution [32]. Crystal structures of citrate synthase have been solved in two conformations, an "open" and a "closed" form [44]. OAA binding induces the change from the open to the closed form, leading to the formation of the acetyl-CoA binding site [44, 45]. If an interaction between MDH and CTS leads to substrate channeling of OAA as proposed, it is therefore anticipated that the open conformation is most likely to interact [32].

Based on the transient nature of this interaction, and under the hypothesis that the interaction would persist on a micro- to millisecond timescale, a systematic

examination of this putative association was performed to determine if the interaction could be directly observed using Fluorescence Correlation Spectroscopy (FCS).

Multi-photon, multi-channel Fluorescence Correlation Spectroscopy is a technique in which fluctuations in fluorescence intensity are interrogated and temporally variable characteristics including diffusion are determined [74-82]. Small numbers of fluorescent particles diffusing randomly from a larger volume through a small volume of excitation cause fluctuations around the average fluorescence intensity. Autocorrelation analysis on time resolved fluorescence acquisition from a small, precisely defined laser focal point yields a time-dependent decay from which apparent diffusion coefficient and particle number can be determined. The equation for the fluorescence correlation is given by:

$$G_{ij}(\tau) = \frac{< \partial F_i(t) \partial F_j(t+\tau) >}{< F_i(t) >< F_j(t) >} \qquad [4\text{-}1]$$

where G is the autocorrelation function at time τ, $<\partial F_x>$ are the average fluctuations of fluorescent species i and j respectively and $<F_x(t)>$ are the average fluorescence intensities of fluorescent species i and j [76,78]. The individual autocorrelation function for either of the two respective wavelength channels is given by equation 4-1 with i=j, and the cross correlation function is given by equation 4-1 with $i \neq j$ [79,80]. Based on a

Gaussian distribution of particles in free solution, the amplitude of the autocorrelation function is inversely proportional to concentration, and the amplitude of the cross correlation function is directly proportional to a species that is fluorescent in both red and green wavelength regimes [80]. For fluorescent-labeled biomolecules, the cross-correlated species represents a double-labeled biomolecule or an interaction between two biomolecules individually labeled with differing fluorophores. The ratio of these two amplitudes represents the fraction of bound to total biomolecules and can be used to quantify the degree of association in a bimolecular interaction.

In these experiments, the size of the focal volume is minimized by the two-photon nature of excitation utilized [78]. Use of fs-timescale pulsed excitation in the near-IR allows the simultaneous absorption of two excitation photons necessary for excitation only at the focal point of the objective lens. This focal volume minimization allows resolution of fluctuations at higher fluorophore concentrations than would be optimal in conventional confocal FCS. The limitations imposed by the higher protein concentrations necessary for the study of weak or transient interactions can thus be overcome to a large extent using multiphoton methodology.

An ongoing topic of debate in the examination of protein interactions is the veracity of solution measurements relative to conditions *in vivo* [11,12]. The intracellular or intraorganelle environments may differ greatly from conditions used for determination of protein-protein and protein-ligand interactions *in vitro*. Concentrations of polyanions

and polycations, localized protein and ion concentrations within sequestered organelles, and the presence of carbohydrates or lipids are factors that are seldom included in solution measurements [11]. Consequently, interactions may occur *in vivo* that would be overlooked in solution measurements because the localized or sequestered concentrations within a cell are above those accessible in a cuvette

Materials and methods

Materials

PEG 8000 was purchased from Fluka. $KHPO_4$ and K_2PO_4 were purchased from EM Science. Oxaloacetate was purchased from USB. Alexa-488 and Texas Red were purchased as C_2-maleimide derivatives from Molecular Probes Inc. (Eugene, Oregon). Pig heart malate dehydrogenase was purchased from Roche Biochemicals as a glycerol solution or ammonium sulfate suspension. Pig heart citrate synthase was purchased from Sigma as an ammonium sulfate suspension.

Enzyme purification

Commercially available pig heart mitochondrial malate dehydrogenase was found to contain sufficient impurities to warrant additional purification. Following extensive dialysis of the glycerol or ammonium sulfate stock, mMDH was further purified by cation exchange chromatography using a Pharmacia Mono-S column, equilibrated with 5 mM phosphate at pH 7.5 and eluting with a linear gradient of NaCl from 0 - 250 mM. Activity was assayed as described [27], at 25°C. SDS-PAGE and intrinsic tryptophan fluorescence intensity confirmed purity. Cytoplasmic MDH (cMDH) contains tryptophan residues whereas mMDH does not; therefore the absence of intrinsic fluorescence was used to indicate purification of the mMDH isoform [40]. MDH was fluorescently labeled with Alexa-488 C_2-maleimide via thiol-modification as described [40,169]. Citrate synthase was deemed sufficiently pure for use based on SDS-PAGE analysis. CTS activity was monitored as described [27]. Ammonium sulfate suspensions of CTS were extensively dialyzed in phosphate buffer and the enzyme was fluorescently labeled with Alexa568 C_2-maleimide.

Fluorescence Correlation Spectroscopy

Fluorescence Correlation Spectroscopy was performed using an ISS Alba Correlation instrument (ISS, Champaign, IL). Measurements were performed on a Nikon Eclipse TE300 inverted microscope with a 60X, 0.7 NA Nikon air gap objective lens. A mode-locked Spectra Physics Tsunami Titanium-Sapphire pulsed-laser with <100 fs pulse-length at 830 nm was used as the two-photon excitation source. The Ti:Sapph was optically pumped using a Spectra Physics Millenia-X 532 nm Nb:YVO_4 CW laser. The excitation beam was collimated using a Newport HB-4XAR.16 beam expander and the excitation power was approximately 20 mW at the sample. The excitation and emission paths were separated using a Chroma Technologies E700SP-2P dichroic mirror. In multi-channel experiments, emission wavelengths were separated using a Chroma Technologies Q570lp dichroic onto parallel APD detectors and filtered using Chroma Technologies 545/30 and 610/75 bandpass filters in each channel respectively. Data were collected at 50 kHz, for ~30-60 seconds and were repeated 5 times. Data were analyzed using ISS ALBA correlation software (LFD, Champaign, IL) using a 1-component model and were plotted using Kaleidagraph (Synergy Software, Reading PA).

Sample preparation

Following labeling with the extrinsic fluorophore, labeled protein was separated from free dye by repeated chromatography on a 15ml Sephadex G-50 column. Absence of free label was confirmed by measuring fluorescence anisotropy between successive chromatography steps. Protein fractions were then centrifuged at room temperature and 13200 rpm (16100 x g) for 90 minutes to remove any contamination from denatured protein or residual Sephadex resin. Samples were diluted in 5mM phosphate buffer at pH 7.5, and PEG 8000 was diluted from a 30% w/v stock at pH 7.5. OAA was prepared in phosphate buffer and the pH was adjusted to 7.5 immediately before performing experiments. All samples were filter sterilized using a Millipore PES Express 0.22 μm syringe-driven filter and were incubated at room temperature for 30 - 60 minutes before fluorescence measurements were taken. Samples were prepared to a total volume of 400 μL in LabTek 8-well borosilicate culture slides.

Results and Discussion

The interaction between MDH and CTS was examined using 2-photon, multi-channel fluorescence correlation spectroscopy. Titrations of equimolar concentrations of MDH-alexa 488 and CTS-alexa568 were performed between the limiting concentrations

of ~0.5 nM and ~150 nM. The amplitudes of cross correlation and autocorrelation curves were examined for deviations from linearity that would be predicted to arise from association.

In the absence of the molecular crowding agent PEG, no cross correlation is observed beyond the anticipated spectral crosstalk at any protein concentration observable using this technique. The absence of cross correlation suggests that bimolecular interaction does not occur to any significant extent at the low protein concentrations necessary for correlation analysis, < 200 nM.

An interaction between MDH and CTS has been observed in moderate concentrations of polyethylene glycol [26]. In order to induce the association, PEG was added in concentrations between 0 - 10% (w/v), and at PEG concentrations greater than 5%, cross correlation is observed (figure 4-1). The measured diffusion coefficient for both individual enzymes is ~55 um^2/s, and this decreases with increasing PEG concentration and hence increasing viscosity. The diffusion coefficient for the cross-correlated species is ~35 um^2/s. The amplitude of the green channel autocorrelation (MDH-alexa488) is two-fold higher than that observed for CTS-alexa568 of the same concentration. This phenomenon is attributed to the weak fluorescence of the MDH derivative and to spectral crosstalk from green emission into the red detector channel. This crosstalk leads to higher count rates and lower correlation amplitude [80].

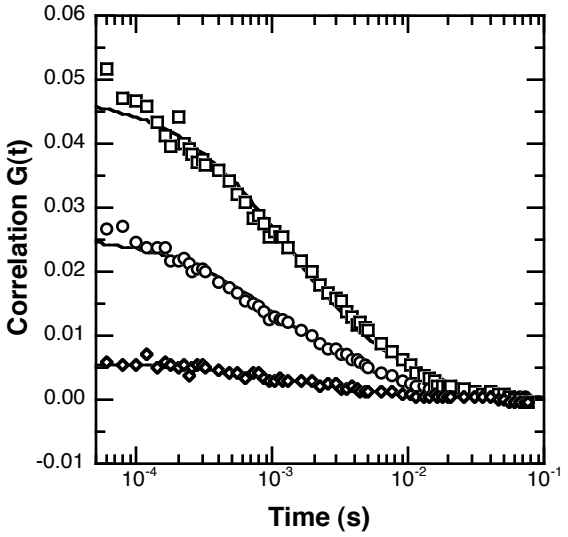

Figure 4-1: The autocorrelation curves of mMDH-alexa488 and CTS-alexa568.
Data presented were obtained in 7% PEG, 17 nM MDH, 17 nM CTS.
Circles: red channel autocorrelation, squares: green channel autocorrelation, diamonds: cross correlation.

At PEG concentrations between 5 and 10% (w/v), increased relative cross correlation between MDH and CTS is observed. The cross-correlation amplitude represents ~10-30% of the autocorrelation amplitude and the fraction increases with increasing protein concentration (figure 4-2). The non-linearity with concentration suggests the presence of a heteroassociation between the two proteins. Below 5% PEG no association is noted, and ≥10% PEG protein aggregation is observed. Between 5 and 10% PEG, increasing PEG concentration increases the apparent binding affinity for the heteroassociation (figure 4-2) as demonstrated by the shift in the apparent binding isotherms. The limited dynamic range of FCS prevents more accurate definition of saturation at lower PEG concentrations.

In order to demonstrate the specificity of the observed interaction, an excess of unlabeled MDH was added. In the presence of excess MDH, the cross correlation amplitude decreases sharply (fig 4-3a,b). Labeled CTS is saturated by unlabeled MDH, rather than binding to the cognate labeled protein, hence minimal cross correlation is observed. In the presence of excess unlabeled MDH, no change in cross correlation amplitude relative to the individual autocorrelation amplitudes is observed. Cross correlation is lost to competition with unlabeled MDH and hence remains constant with respect to the concentration of labeled enzyme (fig 4-3c).

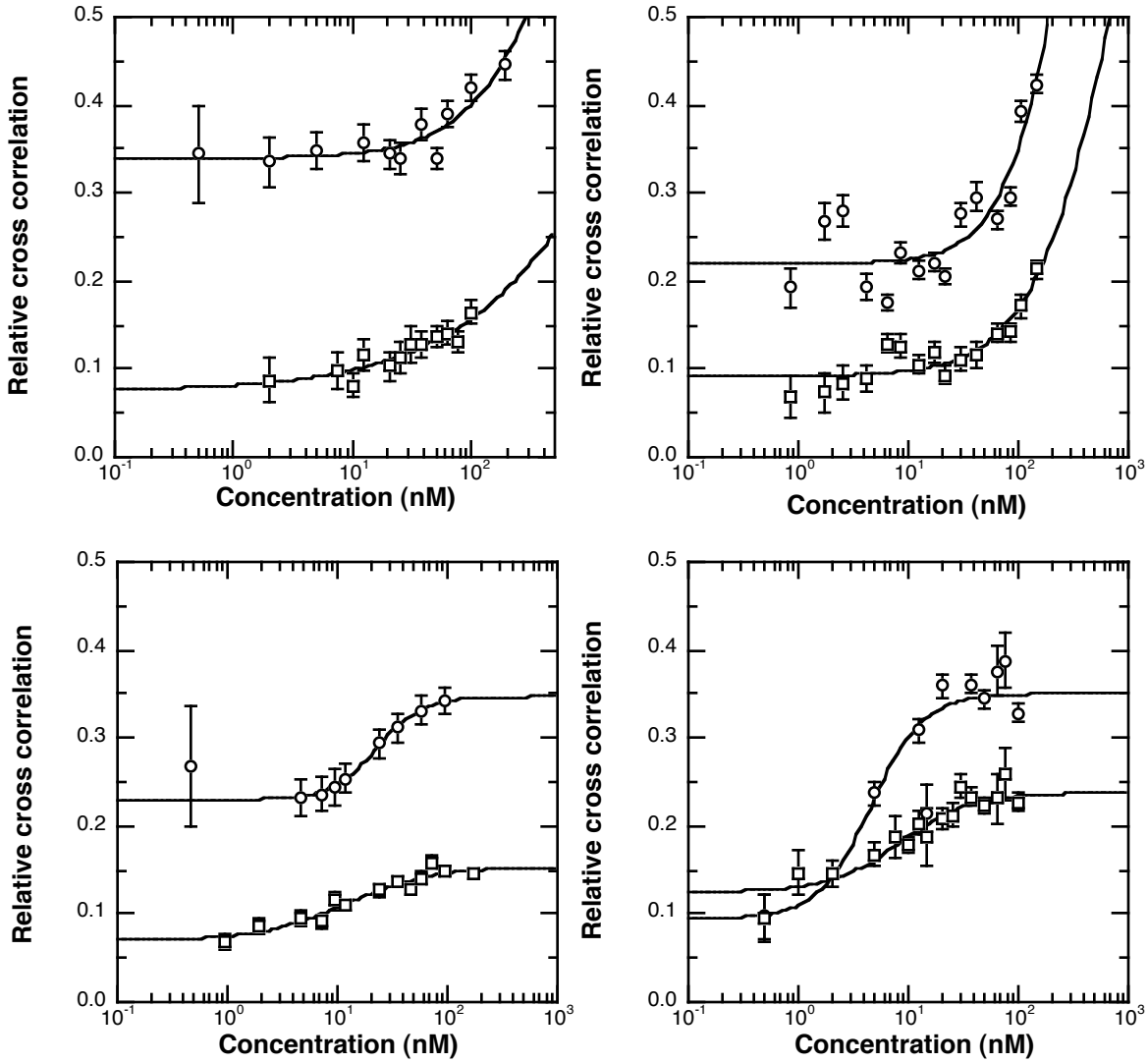

Figure 4-2: Binding isotherms for MDH and CTS at various PEG concentrations. In each panel the ratio of G(0) autocorrelation/cross correlation is presented as a function of protein concentration. Green channel G(0) autocorrelation/cross correlation is shown in open circles, red G(0) autocorrelation/cross correlation is shown in open squares. Panel A: 5% PEG, panel B: 6% PEG, panel C: 7% PEG, panel D: 9% PEG.

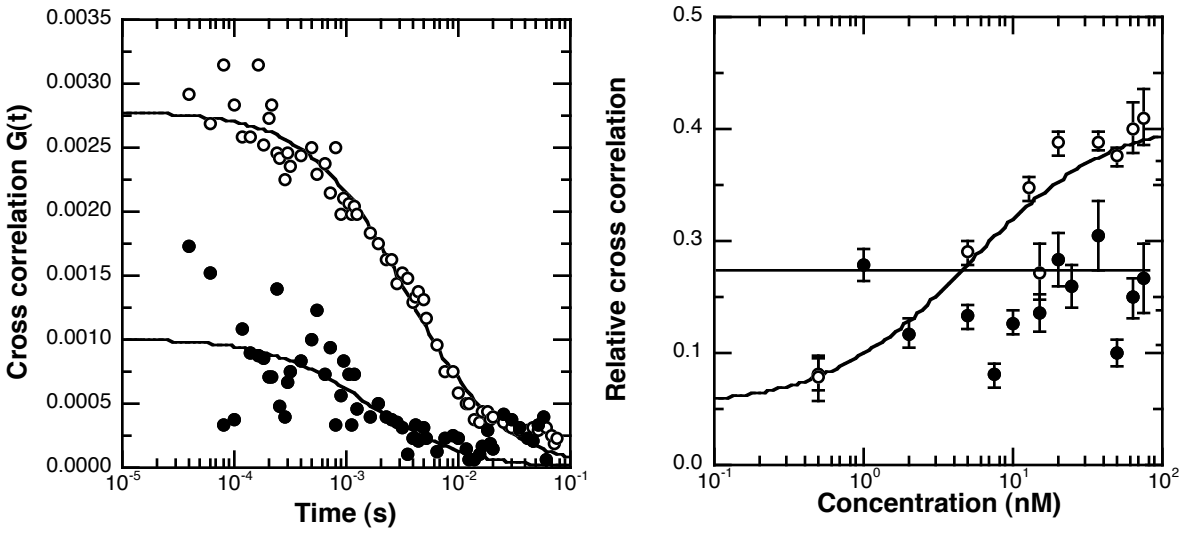

Figure 4-3: The specificity of the MDH-CTS interaction.
In each panel, correlation data is presented in the presence of excess unlabeled MDH (closed circles) and without excess MDH (open circles). In panel A, cross correlation curves from 50 nM MDH-CTS in 6% PEG with and without excess unlabeled MDH are shown. In panel B, the binding isotherms are shown with excess unlabeled MDH and without.

Substrate channeling has been reported for MDH-CTS interaction; therefore the effects of the common intermediate, oxaloacetate, on the interaction have been examined. At micromolar concentrations of OAA, the extrapolated protein-protein affinity increases. Conversely, at concentrations of OAA above the K_m of citrate synthase for the intermediate the extrapolated protein-protein affinity is reduced, and approaches the protein affinity in the absence of ligands (figure 4-4). These data suggest that the "open" conformation of CTS is responsible for the interaction, and increasing concentrations of OAA result in conversion of CTS to the "closed" conformation and hence loss of protein-protein affinity. A linear extrapolation is arbitrarily used to fit the K_d vs [PEG] data, and this extrapolation predicts an apparent affinity of ~10 mM in the absence of PEG and OAA. At OAA concentrations below the CTS K_m, this extrapolated affinity increases to ~0.5 μM. This value reasonably matches the affinity of 0.8 μM reported by Tompa *et al*. [33]. In the absence of ligands, however, our data suggests a very weak affinity between the two enzymes that would make observation by conventional methodologies difficult. The extrapolated affinity under these conditions differs widely from the 1 μM value previously reported [33].

At high concentrations of either OAA or PEG, large MDH-CTS aggregates are observed. Merz *et al*. observed similar aggregates at much higher protein concentrations, 1 mg/mL, using dynamic light scattering [26]. The aggregates contain both MDH-alexa

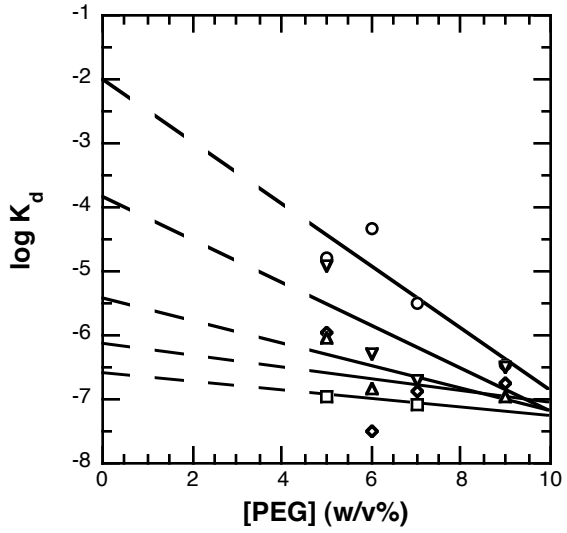

Figure 4-4: The effects of PEG and OAA on the apparent binding affinity between MDH and CTS.
Log K_d is plotted vs. [PEG] at [OAA] between 1 μM and 100 mM. Circles: 1 μM, squares: 5 μM, diamonds: 10 μM, triangles: 100 μM, inverted triangles: 10 mM.

488 and CTS-alexa 568, as intensity is evident in both red and green channels of the time-resolved intensity plot to an extent greater than spectral cross talk. The relative change in intensity arising from MDH-alexa 488, given by the integrated area under the aggregate intensity peaks, is much greater than that observed for CTS-alexa 568. This suggests that the stoichiometry of the aggregate may not be 1:1. Each individual protein species was therefore examined for aggregation in the absence of the other. No aggregation is noted for CTS in the absence of MDH, however aggregates of MDH are observed absent from CTS under similar solution conditions. Furthermore, the stoichiometry of the aggregates, while indecipherable by FCS, can be estimated by integration of the peak intensities. The peaks are highly heterogeneous, as one would predict based on random diffusion through a fixed volume, but on average yield a 15:1 ratio of MDH:CTS. These data suggest that MDH is forming non-specific aggregates under conditions of high OAA and PEG, and that the MDH-CTS interaction is non-specific under these conditions. Previous studies have used conditions of precipitation as a substitute for the putative 1:1 complex in solution and have done protection assays under these conditions. These data suggest that under conditions leading to precipitation, the aggregates observed are non-specific and non-stoichiometric. The correlation curves that derive from the observed aggregates are not adequately described by a simple exponential decay diffusion model (figure 4-5a). To more accurately determine the diffusion characteristics of the aggregating species, diffusion simulations were performed in which a small fraction of the

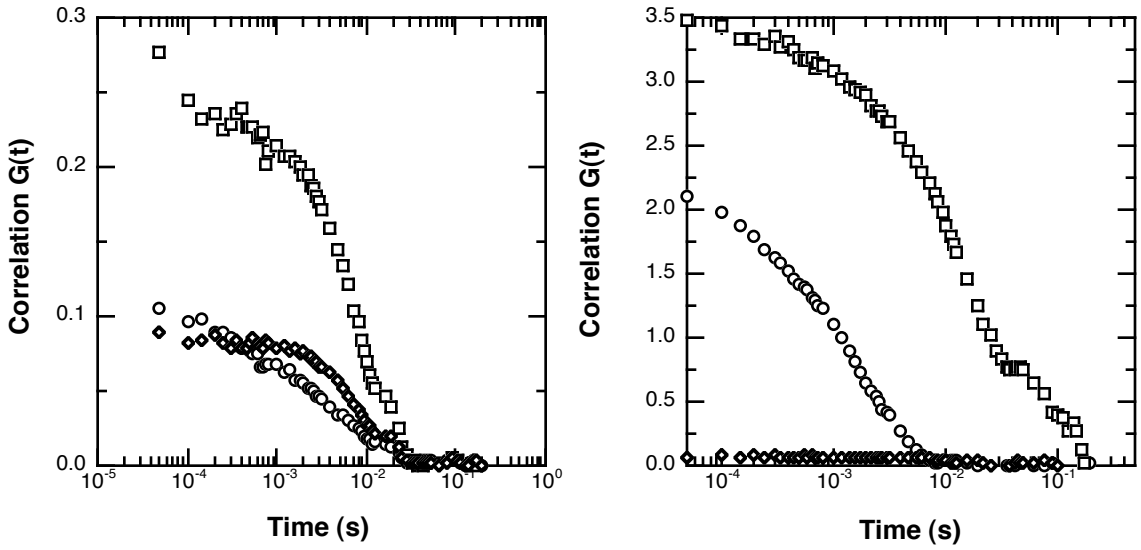

Figure 4-5: The autocorrelation curves for aggregated MDH-CTS.
In panel A, actual data obtained at 30 nM total protein, 25 mM OAA in 7% PEG are shown. In panel B, simulated correlation curves based on 10X lower molecular weight species (dimer D = 30 $\mu m^2/s$) to high order aggregate (D = 1 $\mu m^2/s$) are shown.

total fluorophores were assumed to have very high fluorescence intensity and low diffusion coefficient (figure 4- 5b). The simulations predict that the diffusion coefficients of the aggregates are on the order of 1 $\mu m^2/s$.

To further examine the creation of the aggregates, a systematic survey of PEG concentration, OAA concentration and protein concentration was undertaken. Equimolar concentrations of MDH and CTS were incubated with various concentrations of PEG and OAA. A high concentration of any of the components was sufficient to induce aggregate formation (figure 4-6). At an OAA concentration of 75 mM, aggregates were observed in PEG concentrations as low as 5%. Addition of NaCl at a comparable ionicstrength to the OAA added at each PEG concentration yields an equivalent extent of protein aggregation, therefore the OAA effects on aggregation can be attributed to a general salt effect.

The cross correlation data presented demonstrate that an interaction does occur in the presence of PEG, however in the absence of the crowding agent no association could be detected using FCS. Previous examinations of this interaction have utilized protein concentrations much higher than necessary or even accessible by FCS, and the observation of cross correlation at the low concentrations of enzyme utilized does imply a specific interaction. In a competition assay with excess unlabeled enzyme, cross correlation was lost, further confirming the specificity of the interaction between MDH

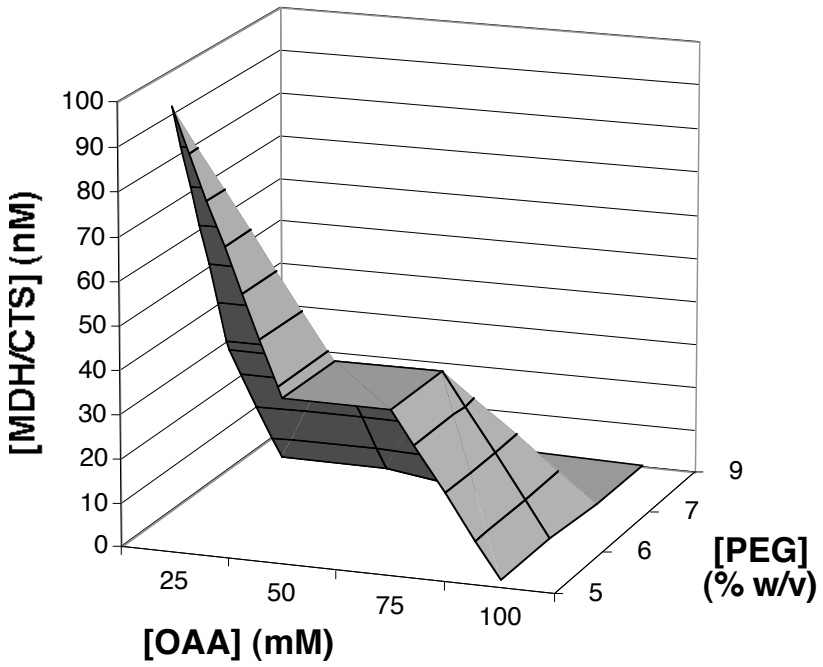

Figure 4-6: Solution conditions yielding MDH-CTS aggregation.
The 3-dimensional plot shows the solution conditions that yield aggregates of MDH and CTS. Total protein concentration is shown on the X-axis, OAA concentration is on the Y-axis, and PEG concentration is on the Z-axis.

and CTS under the conditions examined. Using a linear extrapolation to zero PEG, the protein-protein affinity is 10 mM in the absence of substrate and 0.5 μM at 5 μM OAA. These data suggest that in the absence of substrate or high salt concentrations the concentrations necessary for association are likely beyond those at which the protein is soluble. In the presence of substrate concentrations below the K_m of citrate synthase for OAA, however, the interaction is likely to occur.

Ongoing research with FCS aims to bridge the gap between the low concentrations of fluorophore required to observe fluctuations of sufficient magnitude in a fluorescence background and the high concentrations of biomolecule necessary to observe interactions of biological relevance [177]. In this examination, we further extend the capabilities of a two-photon FCS experiment by chemically inducing association using the molecular crowding agent polyethylene glycol. It is anticipated that this strategy may be useful for the examination of other such weak or transient biomolecular interactions.

Conclusions

We have systematically examined the putative interaction between sequential citric acid cycle enzymes mMDH and CTS. We show conclusively that at concentrations of PEG greater than 5% (w/v), an association does occur. Extrapolation

to free solution suggests the affinity of the interaction is sufficiently low as to elude most commonly utilized techniques for quantification of protein association. The low affinity does not preclude such an interaction *in vivo per se*, as considerations such as the sequestered protein concentrations and the presence of polyanions/cations must be taken into account. At micromolar concentrations of OAA, the protein-protein affinity is increased by the presence of the common intermediate whereas at millimolar concentrations of OAA, the protein association is diminished. At much higher concentrations of OAA, aggregates are observed. PEG precipitates of MDH-CTS have been used as a model of specific associations in solution. These data suggest that the aggregates are non-specific and heterogeneous and do not reflect a direct 1:1 interaction. Protection of OAA from oxaloacetate decarboxylase activity observed in PEG-induced MDH-CTS precipitates may reflect a more general steric protection than direct channel of OAA between MDH and CTS active sites.

CHAPTER V

RESOLVING THE IMPACT OF PROTEIN-LIGAND ASSOCIATIONS ON THE PROTEIN-PROTEIN INTERACTIONS OF *B. stearothermophilus* PFK USING MULTI-LABELED ENZYME

Synopsis

Development of methodologies for the determination and quantification of protein-protein interactions is of fundamental importance in Biochemistry, Proteomics and Molecular Biology. As a model system for protein-protein interactions, we have examined the subunit affinities of a multisubunit enzyme using several biophysical and spectroscopic techniques including 2-photon, dual channel Fluorescence Correlation Spectroscopy. *B. stearothermophilus* phosphofructokinase (BsPFK) is a homotetramer arranged as a dimer of dimers. The enzyme contains 4 active sites and 4 allosteric ligand-binding sites, each of which lies at one of the two potential dimer interfaces. The enzyme is thus ideally arranged to address the issue of subunit association and the effects of ligand binding thereon. We have developed a labeling and hybridization technique to generate a tetramer with subunits containing two different extrinsic fluorophores simultaneously in known subunit orientations. Fluorescence Cross Correlation Spectroscopy is used to probe the multi-label hybrid enzyme, allowing the simultaneous identification of the specific interface disrupted and the determination of the interface affinity.

A crystal structure of the enzyme demonstrates that the quaternary structure shifts with an inhibitor bound. We demonstrate for the first time that bound allosteric inhibitor is sufficient to reduce the affinity of the active site interface. In the presence of inhibitor, the active site interface has nanomolar affinity, yet in the absence of inhibitor that affinity is tightened beyond the limits of experimental detection. The reduced interface affinity is specific for the inhibitor, as binding an activator at the same regulatory ligand-binding site causes no such effect. The weakened subunit affinity of the inhibited conformation allows the kinetics of dimer association to be elucidated.

Introduction

Phosphofructokinase catalyzes the MgATP-dependent phosphorylation of fructose 6-phosphate (F6P), producing fructose 1,6-bisphosphate and MgADP. This reaction represents the first committed step of glycolysis and hence is under judicious regulation. Most prokaryotic PFK is allosterically activated by ADP and is inhibited by phosphoenolpyruvate (PEP). The K-type allosteric response of the enzyme is characterized by reduction in F6P binding affinity when PEP is bound, and tighter F6P affinity when ADP is bound in the allosteric site. Interestingly, both allosteric effectors bind the same allosteric sites, but cause opposite effects on substrate binding.

Phosphofructokinase from the moderate thermophile *Bacillus stearothermophilus* (BsPFK) is a homotetramer consisting of 4 identical subunits, the orientation of which provides 4 identical active sites and 4 allosteric sites along the subunit interfaces. The active sites lie along a single dimer-dimer interface, while the allosteric sites lie along the

opposite dimer-dimer interface. Each respective binding site is composed of residues that belong to both subunits at the interface, such that each subunit contributes half of 2 active sites and half of 2 allosteric sites and the complete tetramer is required for all 8 sites. The subunit arrangement of PFK provides a unique system with which to study the effects of ligand binding on the protein-protein interactions.

The subunit associations of *E. coli* PFK (EcPFK) have been studied [111,155, 164]. The multisubunit composition of the substrate and ligand-binding sites allows the direct examination of the effects of ligand binding on protein-protein affinity. In a titration of the chemical denaturant KSCN, enzyme activity is more denaturant-sensitive than intrinsic tryptophan fluorescence. The active sites are composed of residues from two adjacent subunits, and LeBras *et al*. propose that disruption of the active site interface is responsible for the observed loss of activity. Since the native tryptophan in each subunit lies near the allosteric site in the 3-dimensional structure [148], loss of intrinsic tryptophan intensity is attributed to solvent-relaxation upon disruption of the allosteric site interface by KSCN [154]. Based on these denaturation data, the active site interface is hypothesized to have lower affinity than the allosteric site interface. In the presence of ligands, the active site interface is stabilized to KSCN dissociation by F6P, and is weakly stabilized by bound allosteric inhibitor, PEP [154].

The crystal structures of BsPFK have been solved both with a PEP analog, phosphoglycolate, bound in the allosteric site and in the absence of regulatory ligands with a phosphate ion present in the active site [151,152] (figure 5-1). The most striking structural difference between the two structures is a 7° rotation of the subunits relative to one another around the active site interface in the inhibitor-bound form. In this

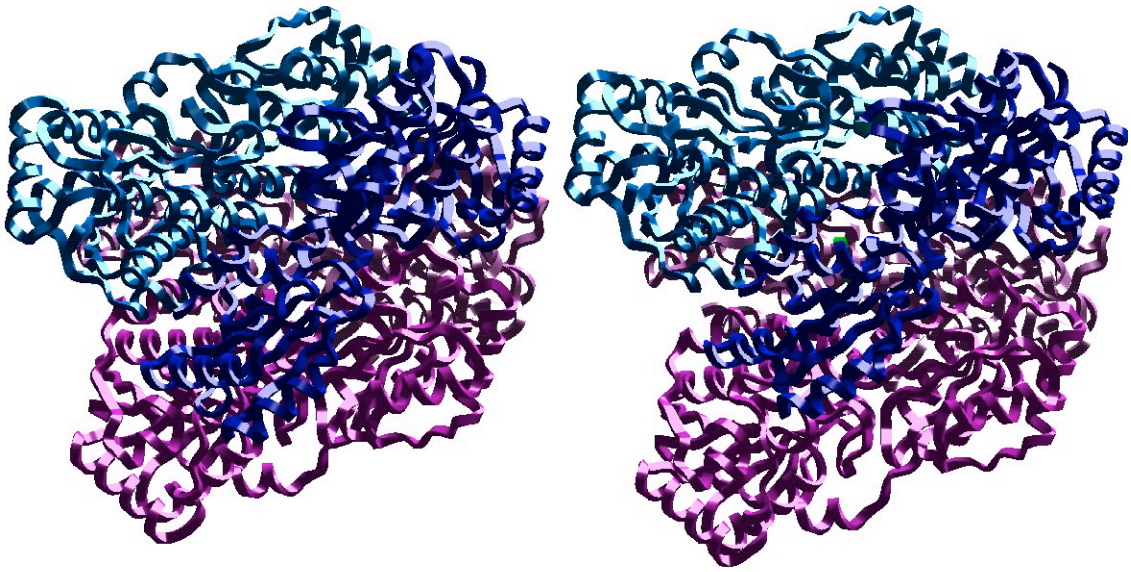

Figure 5-1: Comparison of PFK crystal structures.
Panel A shows the crystal structure of *B. stearothermophilus* PFK with no ligands bound. Panel B shows the structure of the same enzyme with PEP analog phosphoglycolate bound in the allosteric site. Subunits are colored in dark and light pink and blue. The allosteric site interface separates dark from light colored subunits, and the active site interface separates blue from pink colored subunits. A 7° rotation of the subunits around the active site interface is apparent between the inhibitor-bound form and the unliganded form [151,152].

examination we correlate significant loss of subunit affinity with the inhibitor-bound conformation.

Fluorescence Correlation Spectroscopy (FCS) is a technique that interrogates fluctuations in fluorescence intensity to determine diffusion and temporally variable characteristics. Small numbers of fluorescent particles diffusing randomly from a larger volume through a small volume of excitation produce fluctuations around the average fluorescence intensity. Autocorrelation analysis on time resolved fluorescence acquisition from a small, precisely defined laser focal point yields a time-dependent decay from which apparent diffusion coefficient and particle number can be derived. The amplitude of the autocorrelation function yields the particle number, which can then be utilized to determine concentration. The small excitation volume and the free diffusion of particles between that volume and the dilute solution that surrounds it combine to give this technique resolution that approaches single molecule.

Multi-channel FCS allows differentiation of multiple species with spectrally distinct fluorescence characteristics. Utilizing fluorophores with different emission wavelengths, and separating emission using a dichroic into 2 or more detector channels allows simultaneous correlation of each species in solution. Cross-correlation analysis interrogates the concommitant fluctuations between red and green spectral channels caused by direct interaction of these two fluorophores (or fluorophore-linked biomolecules) in solution. Cross-correlation of multichannel FCS data directly addresses molecular interaction, and the concentration of the interacting species can be derived from the cross-correlation amplitude [79-81].

Photon Counting Histogram (PCH) bases analysis on the intensity of fluctuations rather than their time-dependence. The histogram of photon counts vs. the number of counts yields two parameters; the particle number, N, and the molecular brightness, ε. During molecular association reactions, observed particle number is expected to decrease and molecular brightness correspondingly increases [82].

Placing multiple extrinsic fluorophores in known locations within the PFK tetramer will enable both the identification and quantification of subunit affinity within the tetramer. Two distinct fluorophores, Alexa488 and Texas Red, are used to modify the tetramer such that identical fluorophores are present on the two subunits associated at the allosteric site interface and opposite fluorophores are present on the two subunits associated at the active site interface. Dissociation at the active site interface is anticipated to separate a dimer of Alexa488-modified subunits from a dimer of Texas Red-modified subunits. This leads to loss of cross correlation, but constant apparent particle number and molecular brightness. Conversely, dissociation at the allosteric site interface leads to the formation of two dimers, each composed of a single Alexa488-labeled subunit and a single Texas Red-labeled subunit. In this case, dissociation causes loss of cross correlation and molecular brightness but an increase in apparent particle number.

A frequently observed characteristic of allosteric enzymes is their oligomeric quaternary structure. The crystal structures of BsPFK demonstrate that subunits in the inhibitor-bound form and the non-inhibited conformation move relative to one another. The question arises whether the intersubunit motion alters the subunit affinities, or plays a role in allosteric regulation of the enzyme. We demonstrate quantitatively that the

protein-protein affinities within a BsPFK tetramer are altered by ligation state, and those protein-protein interactions are correlated to the allosteric inhibition of the enzyme.

K-type allosteric inhibition is defined by decreased substrate affinity with an inhibitor molecule bound in the allosteric site of the enzyme. Relating the affinities with and without bound effector, a coupling parameter, Q, can be defined which quantifies the effect of effector binding on substrate binding [98,99,102]. From this linked-function analysis, the disproportionation equilibrium that defines the allosteric response can be derived:

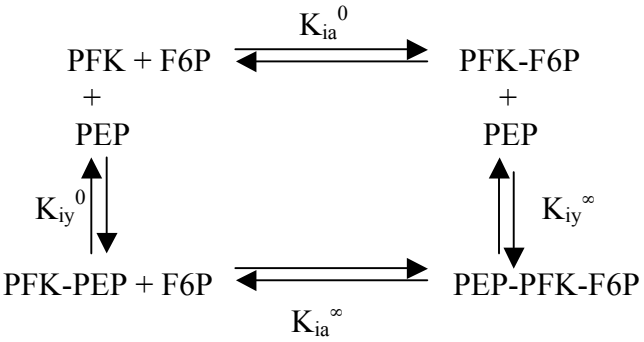

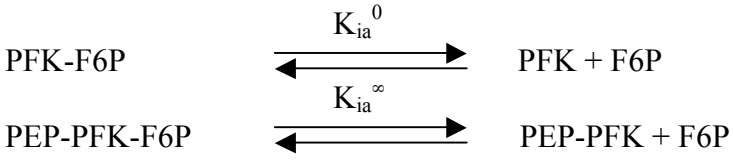

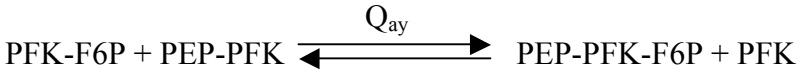

$$Q_{ay} = \frac{K_{ia}^{0}}{K_{ia}^{\infty}} \qquad [5\text{-}1]$$

$$\Delta G = -RT \ln Q_{ay} \qquad [5\text{-}2]$$

where K_{ia}^{0} represents the thermodynamic dissociation constant for substrate in the absence of allosteric effector, K_{ia}^{∞} is the dissociation constant with allosteric effector saturating the enzyme and Q_{ay} is the ratio of these two parameters. It is evident from the chemical equations that Q_{ay} also represents the equilibrium constant for the disproportionation equilibrium. The free energy of each of the equilibria can be derived from the respective dissociation constants.

The disproportionation equilibrium and the allosteric response that it defines have been studied by perturbation in various manners: mutation of the amino acid residues involved in catalysis, binding or allosteric communication, alteration of the pH, alteration of temperature and application of hydrostatic pressure [104,110,111,163]. We examine the role of subunit interactions in the PEP-dependent inhibition of BsPFK.

Materials and methods

Materials

EPPS was spectral grade and was purchased from Research Organics. $MgCl_2$, NH_4Cl, EDTA were spectral or reagent grade and were purchased from Sigma. AlexaFluor488 and Texas Red were purchased as C_2-maleimide derivatives from Molecular Probes (Eugene, Oregon).

Enzyme purification and labeling

Wild-type and K90,91E mutant BsPFK were purified as described previously [94] with the following modifications. Following Mimetic blue dye affinity chromatography and overnight dialysis, peak fractions were applied to a 10 mL Pharmacia MonoQ anion exchange column and eluted with a linear gradient of NaCl from 0-1 M. Activity was assayed as described [94,172]. Peak fractions were extensively dialyzed into buffer F (50 mM EPPS, 10 mM $MgCl_2$, 10 mM NH_4Cl, 0.2 mM EDTA). Purity was confirmed by SDS-PAGE and enzyme was quantified as described [REF]. PFK samples were thiol-labeled with AlexaFluor488 C_2-maleimide or Texas Red C_2-maleimide as described [169]. Labeling reactions contained 20-50 μM PFK, 1 mM F6P, 10% glycerol, and ~10X fluorophore in buffer F (Alexa488) or DMSO (Texas Red). 2 mL-labeling reactions were incubated for 2 hours at room temperature with slow stirring. Free fluorophore was separated from labeled protein using repeated applications to a 20 mL G-50 Sephadex column. Purity of the labeled enzyme was confirmed by measuring anisotropy between successive size exclusion columns and by SDS-PAGE visualized under UV excitation. Labeling stoichiometry was approximately 1:1 (>90%) fluorophore: subunit and the extrinsic fluorophore reduced the specific activity of the enzyme <30%.

Mixed tetramer formation

Multilabel enzyme was created by allowing dimer exchange between Texas Red labeled wildtype BsPFK and Alexa-488 labeled BsPFK-K90,91E. In this PFK mutant,

two surface glutamate residues have been changed to lysines by site-directed mutagenesis with minimal alteration of kinetic and allosteric properties [103,105]. Introduction of the surface lysines imparts two additional positive surface charges, which impart additional electrophoretic mobility to PFK tetramers containing subunits with these mutations. Furthermore, the surface charges allow PFK tetramers containing these subunits to be separated by anion exchange chromatography as described [103,105]. Incubation of BsPFK with 0.4 M KSCN and 1 mM PEP disrupts the active site interface while maintaining the integrity of the allosteric site interface to which the PEP binds. Incubation of wildtype-Texas Red with K90,91E-Alexa 488 under these conditions causes dimer exchange between the two protein species. Dialysis allows the reassembly of tetramers containing four wildtype, four K90,91E or tetramers containing two wildtype and two K90,91E subunits. Dimer exchange was confirmed by the presence of three bands on a non-denaturing PAGE gel. Following 30 minute incubation, the mixture was dialyzed extensively into 25 mM EPPS, 5 mM $MgCl_2$, 5 mM NH_4Cl, 0.2 mM EDTA. The solution of mixed tetramers was separated by anion exchange chromatography on a Pharmacia MonoQ column eluting with a linear salt gradient from 15 mM to 50 mM NaCl in 200 mL total volume. Peak fractions were identified by UV-Vis spectroscopy, were assayed for activity and were concentrated using Amicon centrifuge concentrators (Millipore, Billerica MA). In later experiments, dimer exchange was induced by incubation with 4 mM PEP for 4 hours at room temperature.

Non-denaturing PAGE

Non-denaturing PAGE was performed in 9% polyacrylamide gels (acrylamide: bisacrylamide 30:0.8). Running buffer consisted of Tris:glycine at pH 8.3. Samples were applied in glycerol/Coomassie/Tris pH 6.8. Samples were run at 120 V for 2 hours on ice and were visualized using UV excitation or were Coomassie-stained. Time-points were taken by incubation of the labeled protein indicated with the specified ligand for the indicated time prior to quenching of dimer-exchange by addition of 1 mM F6P. Densitometry was performed on the UV-exposed gels using an Alphaimager 950 (Alpha Innotech Corporation, San Leandro CA) and NIH Image V1.62f software, (NIH, Maryland).

Steady-state fluorescence

Steady-state fluorescence spectra, intensity and anisotropy were performed using either an SLM-8000 with an ISS Phoenix upgrade or an ISS Koala spectrofluorometer. Excitation was either 495 nm or 592 nm depending on the fluorophore utilized. Intensity was determined by integration of the blank-subtracted emission spectra. Spectra were taken at 1nm intervals with 1 sec integration time. Experiments using the ISS Koala had excitation slit widths of 0.5 mm and emission slit widths of 1 mm, corresponding to bandwidths of 4 nm and 8 nm respectively. Measurements were taken in L-format. The SLM modifications included a xenon lamp and power supply upgrade to ISS components, ISS X-1 photon counting detection and ISS Vinci acquisition and analysis

software. Spectra and intensity measurements performed using SLM instrumentation used excitation slit widths of 2 - 4 as appropriate and emission slit widths of 8. Anisotropy was determined in L-format using an appropriate cut-on filter: a Schott OG-530 for experiments using alexa-488 labeled enzyme, or a Melles-Griot 5-71 colored glass filter for experiments using Texas Red labeled enzyme. In anisotropy titrations, intensity was attenuated using neutral density filters in the excitation path. Anisotropy of unlabeled protein was determined using the SLM 8000 modified as described above with excitation wavelength of 300 nm, and emission measured through a Schott 345 nm cut-on filter. In each case, data were collected until the relative error in anisotropy was ≤ 0.02.

Frequency-domain fluorescence lifetime measurements

Frequency domain lifetime measurements were performed using an ISS Koala spectrofluorometer in L-format. A frequency-doubled, mode-locked Spectra Physics Tsunami Titanium-Sapphire (Ti: Sapph) pulsed-laser with <100 fs pulse-length and 80 MHz pulse frequency was used as the excitation source. The Ti: Sapph was optically pumped using a 10 W Spectra Physics Millenia-X 532 nm Nb:YVO4 CW laser. The pulse frequency was reduced to 4MHz using a Spectra Physics Model 3980 pulse selector. A Spectra Physics flexible harmonic generator was used to generate the second harmonic for visible fluorophore excitation and the third harmonic for intrinsic tryptophan excitation. Parasitic fundamental wavelength excitation was eliminated using a Corion FR-400-S bandpass filter. Spectra Physics model 3930 “lok-to-clock” electronics module was used to provide phased-lock loop stabilization to the Ti: Sapph

emission. The "lok-to-clock" module was coupled to an ISS linear broadband RF amplifier and Marconi Instruments model 2022D frequency synthesizer to synchronize the PMT detectors with the laser emission. The temperature was maintained at 25ºC using a circulating water bath. Data were collected at frequencies from 4 MHz to 320 MHz, and were fit using Globals software (University of Illinois, Champaign, IL). At each frequency, data were collected until the standard error was less than 0.1 in phase and 0.02 in modulation. The reference standard for each measurement was Rhodamine-6G in ethanol. Data collected on the extrinsically labeled proteins were fit to a 2-discrete lifetimes model, with one species representing a "zero-lifetime" scatter component. Intrinsic fluorescence lifetimes were fit to a 2-discrete lifetime model, as described previously [94] using p-tertphenyl as a reference standard.

Fluorescence Correlation Spectroscopy

Correlation spectroscopy was performed using a Nikon Eclipse TE300 inverted microscope with a 60 X, 0.7 NA Nikon air gap objective lens. A mode-locked Spectra Physics Tsunami Titanium-Sapphire pulsed-laser with <100 fs pulse-length at 800 nm was used as the two-photon excitation source. The Ti: Sapph was optically pumped using a 10 W Spectra Physics Millenia-X 532 nm Nb:YVO_4 CW laser operating at 7.6 W. The excitation beam was reduced in intensity using a Newport 10% beam splitter, and was collimated using a Newport HB-4XAR.16 beam expander. The excitation power was approximately 20 mW at the sample. The excitation and emission paths were separated using a Chroma Technologies E700SP-2P dichroic mirror. In multi-channel

experiments, emission wavelengths were separated using a Chroma Technologies Q570LP dichroic onto parallel APD detectors and filtered using Chroma Technologies 545/30 or 610/75 bandpass filters in each channel respectively. 400 μL samples were examined in Labtech 8-well borosilicate culture cuvettes. Data were collected at 50 kHz for 30-60 seconds and each acquisition was repeated 5 times. Data were analyzed using ISS-ALBA correlation software and were plotted using Kaleidagraph (Synergy Software, Reading, PA).

Results and discussion

Formation of mixed tetramers

As with any homotetramer, an examination of the subunit interactions of prokaryotic PFK is complicated by issues of symmetry. If a tetramer dissociates to dimers, regardless of which of the two potential dimer interfaces was disrupted, the product remains two dimers of identical monomeric composition. To address the issue of symmetry, we have introduced multiple fluorophores in known positions within the tetramer. In this manner, the subunit interfaces are uniquely identified by their orientation relative to the various fluorophores. In this manner, the interface that undergoes dissociation can be identified and its affinity can be quantified.

In 0.4 M KSCN and 1 mM PEP, the active site interface is preferentially weakened relative to the allosteric interface, such that dimer exchange occurs along that interface [173]. Incubation of BsPFK-Texas Red with K90,91E-Alexa488 under these

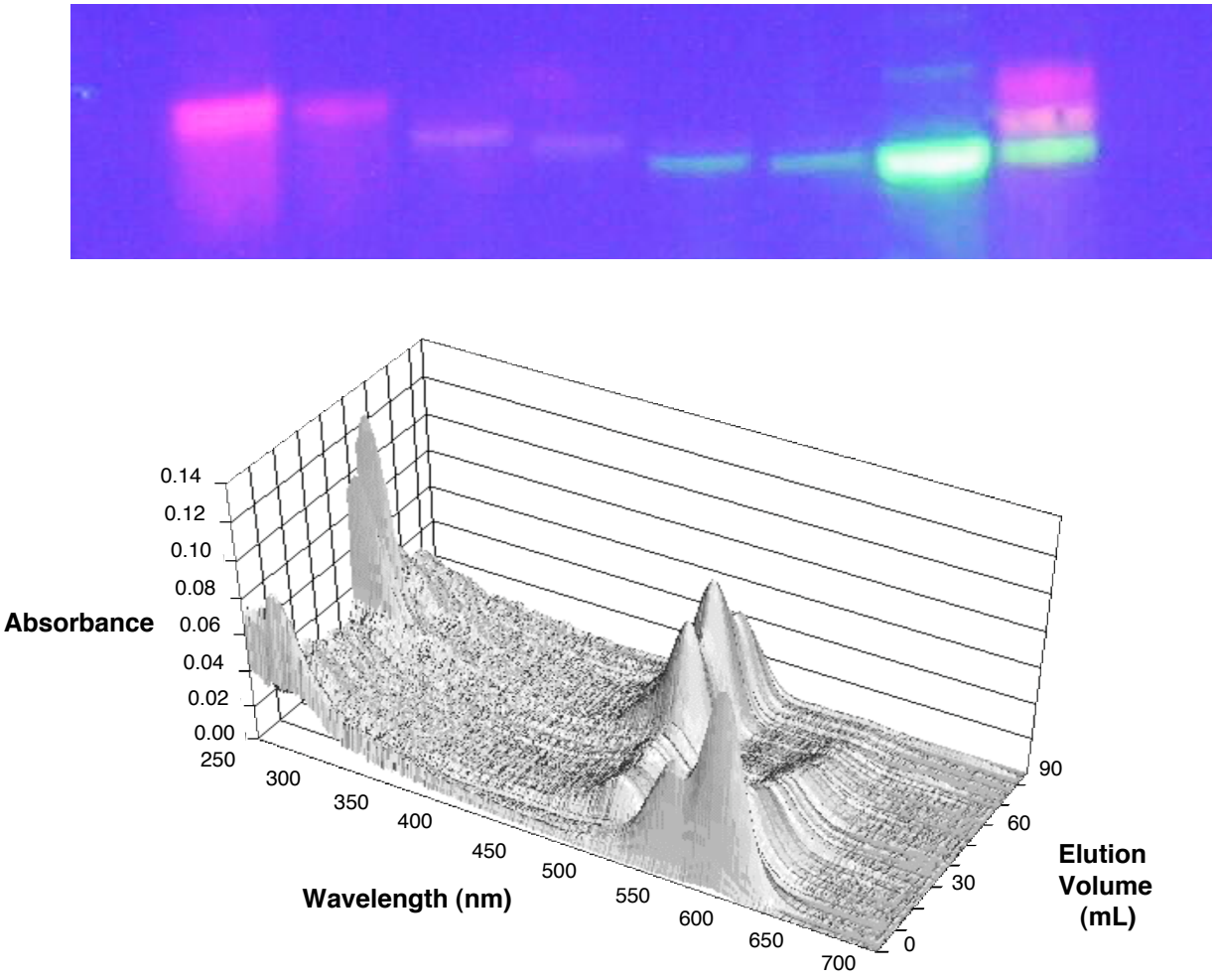

Figure 5-2: Formation of mixed tetramers.
Panel A shows a 9 - 12% gradient non-denaturing polyacrylamide gel of the mixed tetramer visualizing the fluorescent-labeled proteins under UV excitation. Lane 1: wildtype BsPFK-Texas Red, lane 2: fraction 5, lane 3: fraction 19, lane 4: fraction 25, lane 5: fraction 33, lane 6: fraction 42, lane 7: BsPFK K90,91E-Alexa488, lane 8: dimer exchange mixture following dialysis. Panel B shows the absorbance spectra of the anion exchange chromatography fractions. All protein-containing fractions show absorbance at 278 nm. Early fractions consist of BsPFK-Texas Red and show peak absorbance at the maximal absorbance wavelength of 592 nm. Late fractions consist of K90,91E-Alexa488 and show maximal absorbance at the Alexa488 peak of 496 nm. Intermediate fractions correspond to the mixed tetramer, and show two absorbance peaks corresponding to both Texas Red and Alexa488.

conditions induces dimer exchange between these two enzymes, and following dialysis, produces a mixed population of tetramers. The additional surface charges on tetramers containing K90,91E subunits impart higher electrophoretic mobility, and thus non-denaturing PAGE confirms the formation of mixed tetramers (figure 5-2a). Lane 8 of the UV-visualized gel shows the mixture of tetramers following dialysis, with those tetramers containing four K90,91E-Alexa488 subunits having highest mobility and appearing green, those tetramers containing four BsPFK-Texas Red subunits appearing red and having lowest mobility and those tetramers consisting of two of each subunits appearing yellow and having intermediate electrophoretic mobility. The presence of this intermediate yellow band verifies the presence of mixed tetramers.

The solution containing individually labeled, Texas Red and Alexa488 modified-tetramers and the mixed tetramers containing both fluorophores was resolved utilizing anion exchange chromatography. Once again exploiting the surface charge on the K90,91E subunits, additional K90,91E subunits increase the elution time in a linear salt elution gradient. Consequently, tetramers containing greater stoichiometry of the charged subunits are retained on the column at higher salt concentrations. Wildtype-Texas Red elutes in the lowest salt concentration, mixed tetramers elute in a higher concentration of salt, and the K90,91E-Alexa488 elute at highest salt concentration (figure 5-2b). Native PAGE confirms that the yellow fractions represent the mixed tetramer containing both Texas Red and Alexa488 labeled subunits, rather than a mixture of red and green-labeled tetramers (figure 5-2a, lanes 2-6). The yellow fractions run as a single electrophoretic species of intermediate mobility. UV-Vis spectroscopy confirms that these fractions contain absorbance corresponding to both Texas Red and Alexa488 (figure 5-2), whereas

those fractions with either red or green emission show absorbance corresponding to those respective fluorophores alone.

The effectiveness of multi-channel Fluorescence Correlation Spectroscopy in the measurement of dissociation of the mixed tetramer was confirmed by examination of mixed and singly labeled PFK (figure 5-3). FCS examines temporal fluctuations in fluorescence intensity that arise from changes in number density of fluorescent particles in the focal volume of a microscope lens. Autocorrelation analysis yields two parameters: concentration and diffusion coefficient. PCH analysis yields two additional parameters: molecular brightness and particle number. Cross correlation analysis determines the concentration of the double-labeled species, in this case the mixed tetramer, and the diffusion coefficient associated with that species. For the technique to be effective in examination of dissociation of the mixed tetramer, the cross correlation amplitude must represent a significant fraction of the autocorrelation amplitudes. The red tetramer shows minimal cross correlation amplitude relative to background (figure 5-3a). Conversely, the yellow tetramer has a high degree of cross correlation (figure 5-3b). Since red and green labeled subunits are separated by the active site interface, loss of cross correlation amplitude relative to the autocorrelation amplitude is indicative of dissociation at that interface.

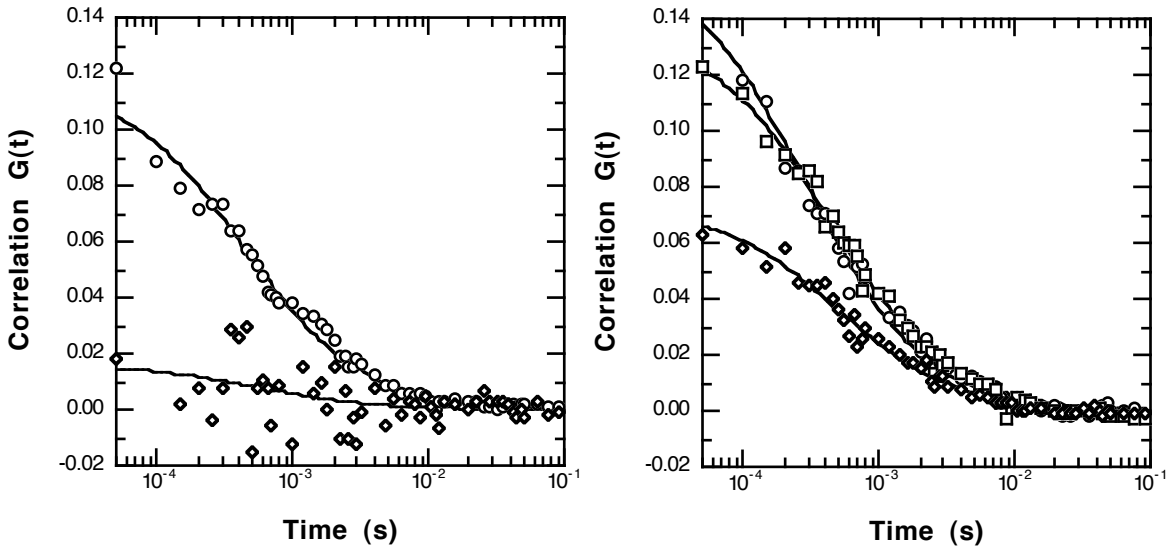

Figure 5-3: Correlation curves for mixed tetramers.
Panel A shows the autocorrelation and cross correlation curves for BsPFK-Texas Red. Circles: red channel autocorrelation, diamonds: cross correlation. In panel B, the autocorrelation and cross correlation curves for the mixed tetramer are presented. Circles: red channel autocorrelation, squares: green channel autocorrelation, diamonds: cross correlation.

Subunit dissociation by Fluorescence Correlation Spectroscopy

The mixed tetramer has a degree of asymmetry that allows differentiation of the two possible dimer-dimer interfaces in a dissociation titration. As the two green-labeled subunits are separated from each other by the allosteric site interface and are separated from the two red-labeled subunits by the active site interface, dissociation at either interface yields an observable fluorescence characteristic. Should the tetramer dissociate along the active site interface, green and red fluorophores will be separated from one another and the amplitude of cross correlation will be reduced. Oppositely, if the allosteric site interface is disrupted in a titration, the tetramer will dissociate into two dimers, each containing one red-labeled and one-green labeled subunit. The apparent particle number would increase and G(0) values would concomitantly decrease, with no apparent reduction in the degree of relative cross correlation.

FCS and PCH were used to determine the relative subunit affinities (figure 5-4) by measurement of G(0), molecular brightness and particle number as a function of PFK concentration. Within the accessible range of concentrations with this technique, no dissociation at either interface is observed. Both the particle number (figure 5-4a) and the G(0) values for each autocorrelation and cross correlation (figure 5-4b) remain linear with concentration. These data suggest that the two interfaces have subnanomolar affinities in 25 mM EPPS, 10 mM $MgCl_2$, 10 mM NH_4Cl, 0.2 mM EDTA at pH 8.0.

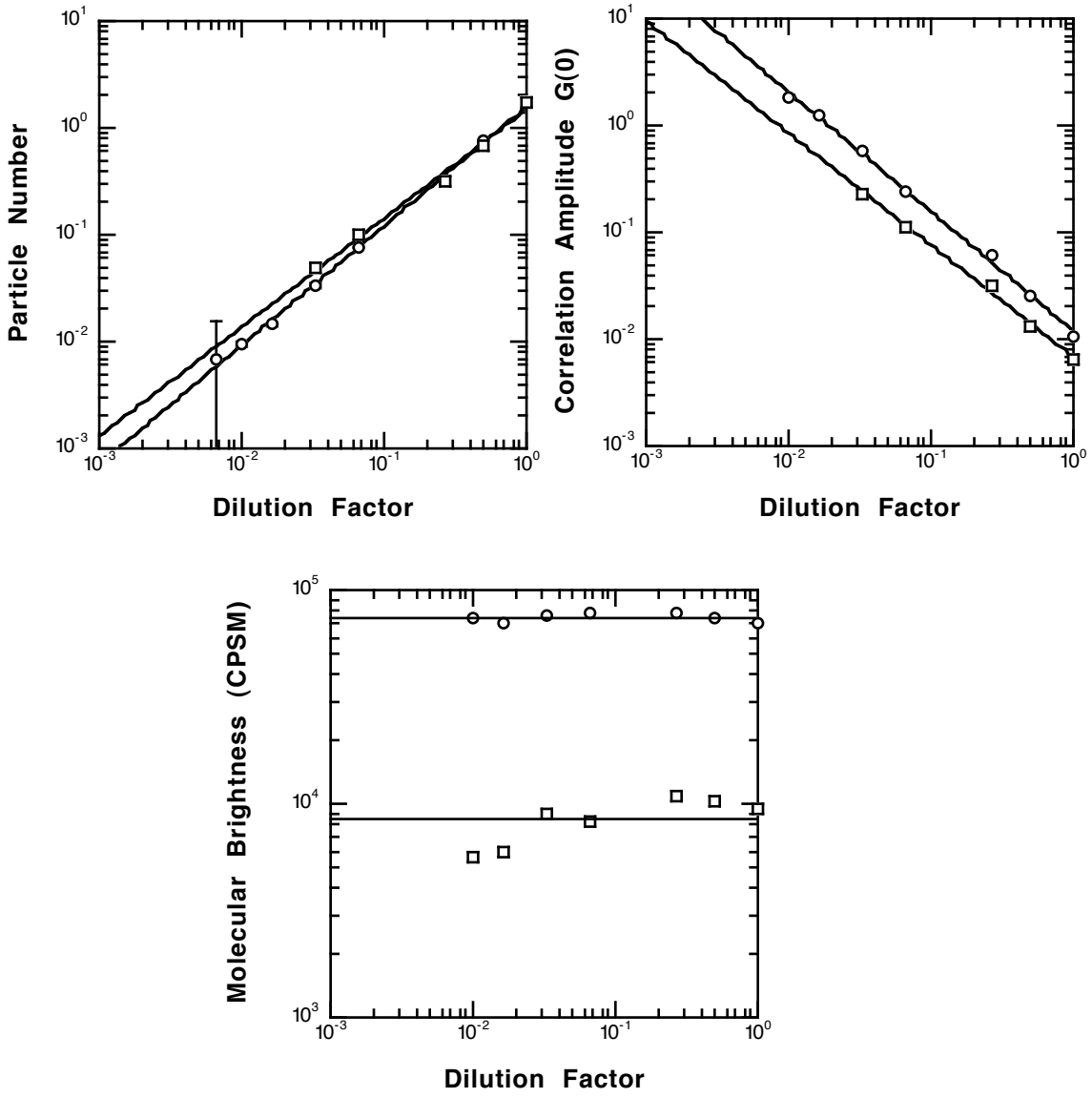

Figure 5-4: Fluorescence Correlation Spectroscopy of the mixed tetramer.
In panel A, a secondary plot of particle number vs. protein concentration is shown. In panel B, a secondary plot of G(0) values vs. protein concentration are shown. In panel C, the molecular brightness vs. protein concentration is shown. Open circles: red channel autocorrelation, open squares:green channel autocorrelation, open diamonds:cross correlation. Concentrations are given as monomer concentrations. In these plots, the slopes of the cross correlation and autocorrelation values are constant relative to one another, therefore no dissociation is observed under the concentration ranges accessible to FCS. Both red and green channel molecular brightness are constant with concentration, again indicating that no dissociation had occured.

Influence of ligands on subunit dissociation

The effects of ligand binding on the subunit affinities of BsPFK were examined using non-denaturing PAGE analysis. If dissociation and reassociation occurs in the presence of both PFK-Texas Red and K90,91E-Alexa488, dimer exchange between the two enzymes will occur, leading to the yellow intermediate band as observed in figure 5-1. Therefore, red and green-labeled proteins were incubated with the various substrate and allosteric ligands for various lengths of time. Samples at each time point were then subjected to native gel electrophoresis. In the absence of ligands or in the presence of saturating F6P, no dimer exchange is observed (figure 5-5a). In the presence of saturating PEP, however, a yellow band is observed at intermediate electrophoretic mobility and this band increases in intensity with time (figure 5-5b). These data are strong evidence that PEP is sufficient to induce dimer exchange and suggest that the bound allosteric inhibitor weakens the active site interface, thereby allowing dimer exchange. The disruption of the allosteric site interface alters the allosteric sites, and would abrogate PEP binding. The dissociation leading to dimer exchange must therefore occur at the active site interface. Interestingly, while both allosteric effectors bind to the same allosteric sites on the tetramer, the activator ADP does not induce dissociation (figure 5-5c). These data suggest that the effect is ligand specific. The crystal structure has been solved with F6P and ADP bound, and no quaternary shift is observed in this ligand-bound conformation [174]. While dimer exchange was observed using the native PAGE analysis, an independently stable dimer was not observed. When native PAGE in

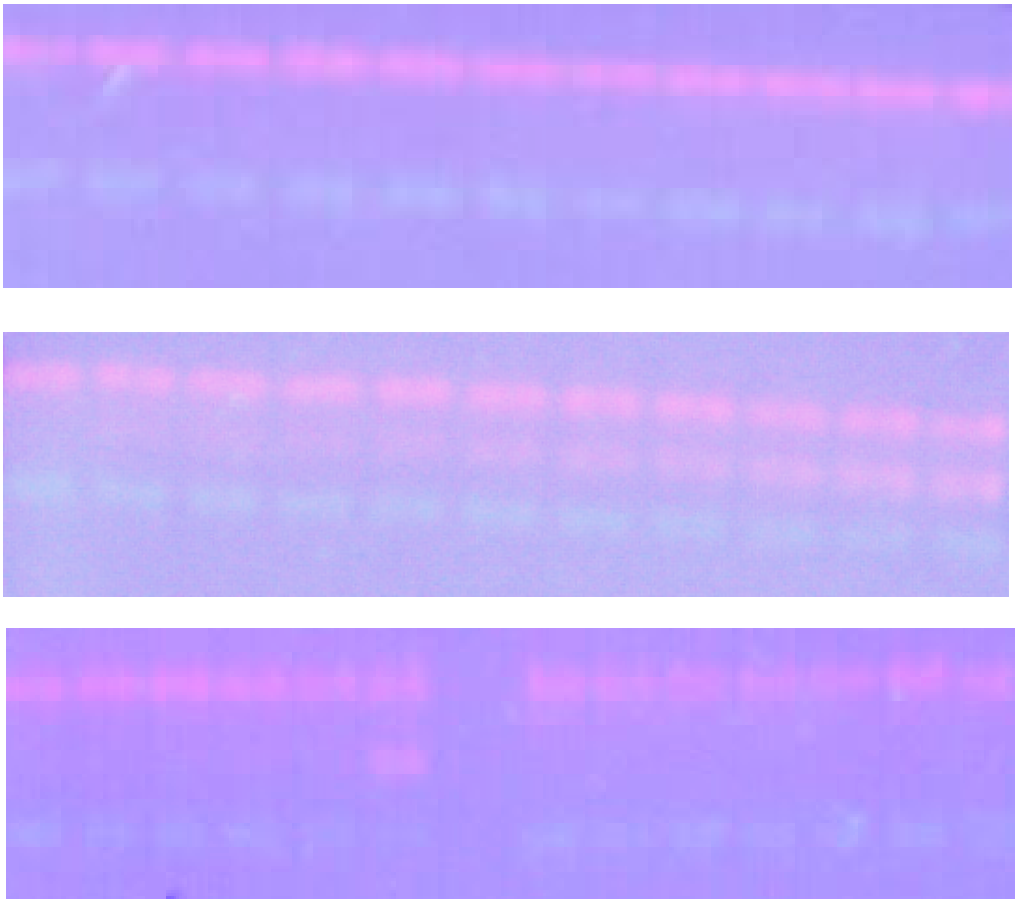

Figure 5-5: Ligand-induced subunit exchange in BsPFK.
In panel A, incubation time points from 0-4hrs without ligands are shown on a non-denaturing PAGE gel. No intermediate yellow bands are observed in any lane demonstrating that no dimer exchange has occurred. In panel B, time points in the presence of 4mM PEP are shown. In the presence of PEP, dimer exchange occurs, as is evident from the time-dependent development of a yellow band of intermediate electrophoretic mobility. In panels A and B, time points are: 0 minutes (lane 1), 3 minutes (lane 2), 6 minutes (lane 3), 9 minutes (lane 4), 12 minutes (lane 5), 30 minutes (lane 6), 1 hr (lane 7), 2 hrs (lane 8), 3 hrs (lane 9), 4hrs (lane 10). In panel C, the effects of ADP are shown. Lanes 1-6: 4mM PEP control time points. Time points are: 0 minutes (lane 1), 3 minutes (lane 2), 6 minutes (lane 3), 9 minutes (lane 4), 12 minutes (lane 5), 4hrs (lane 6). Lanes 8-14: 2mM ADP time points. Time points include: 0 minutes (lane 8), 1hr (lane 9), 2 hrs (lane 10), 3 hrs (lane 11), 4 hrs (lane 12), 5 hrs (lane 13), 20hrs (lane 14).

the presence of 4 mM PEP was attempted, the protein sample ran as a smear. This suggests that dissociation had occurred within the gel matrix, however PEP binding was not sufficient to produce an independently stable dimer. Interestingly, in the denaturation work of LeBras and Garel with *E. coli* PFK, weak PEP stabilization of the tetramer to KSCN-induced dissociation was observed. *B. stearothermophilus* PFK demonstrates strong PEP-induced destabilization of the enzyme.

To independently confirm the effects of these ligands on the stability of the enzyme, urea denaturation was performed (figure 5-6). In the presence of PEP, enzyme activity is lost at a much lower urea concentration, approximately 1 M, relative to the loss of intrinsic tryptophan fluorescence intensity, which is lost at approximately ~7 M urea. These data suggest that PEP is strongly weakening the active site interface while increasing the stability of the allosteric site interface. In the absence of ligands, the loss of activity and the loss of intrinsic fluorescence intensity occur at the same concentration of urea, approximately 4 M. These data suggest that in the absence of ligands, the transition from tetramer to monomer occurs in an apparent concerted dissociation. This is attributed to comparable relative affinities between the allosteric site interface of the dimer and active site interface of the tetramer.

Kinetics of dimer exchange

To quantify the rates of dimer exchange, the native PAGE gels were visualized under UV excitation, and the fluorescence emanating from each band was quantified by densitometry (figure 5-7). In the absence of ligands, no yellow band is observed hence

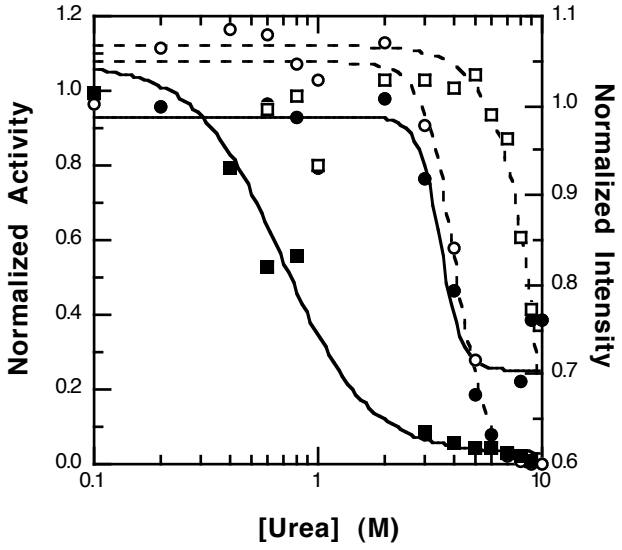

Figure 5-6: Ligand-binding effects on the structural stability of PFK.

A titration of urea into 330 nM PFK is shown. Open data points and dashed data fits represent intrinsic tryptophan fluorescence intensity and closed data points and solid data fits represent relative enzyme activity. Circles: no ligands, squares: 4 mM PEP. The PEP-induced weakening of the active site interface and strengthening of the allosteric site interface under conditions of urea denaturation is evident.

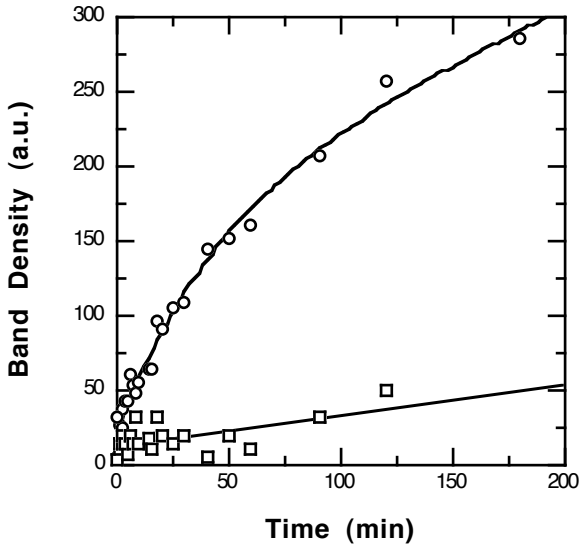

Figure 5-7: Quantitative native gel electrophoresis kinetic analysis of subunit exchange.
Densitometry was performed on the UV-exposed native PAGE gel. The quantification of the fluorescence of the yellow band corresponding to the mixed tetramer is plotted as a function of time. Fluorescence intensity from the PEP treated sample (open circles) is fit to a two-exponential increase and intensity from the sample in the absence of ligands (closed circles) shows no change with time and is fit linearly.

the intensity of the gel is near zero and is constant with time (figure 5-7). In the presence of PEP, the yellow band appears within minutes and the band intensity saturates in approximately four hours.

Based on the kinetic data obtained from native gel electrophoresis, dissociation was further examined under solution conditions. The mixed tetramer, containing Texas Red and Alexa488-labeled subunits on opposite sides of the active site interface would lose cross correlation in a dissociation of the active site interface, a phenomenon expected to occur in the presence of PEP. We thus monitored cross correlation amplitude as a function of time following PEP addition. Cross correlation amplitude decreases with time and the data are fit to a two-exponential decay (figure 5-8). The apparent rate constants closely match those obtained by gel electrophoresis. The loss of cross correlation confirms the electrophoretic mobility data, a non-equilibrium measurement, and demonstrates directly that the active site interface is the site of PEP-induced dissociation.

Within a mixed tetramer, two Texas Red-labeled and two Alexa488-labeled subunits are in close proximity, with cysteine residues separated by 30 Å to 70 Å, hence Förster Resonance Energy Transfer (FRET) would be predicted. Intersubunit FRET is used to confirm the kinetics of PEP-induced subunit exchange. Following PEP addition, the fluorescence emission from the acceptor decreases with time (figure 5-9a). As dimer exchange occurs, the mixed tetramer dissociates and reassociation of red with green labeled subunits would be expected in 50% of the tetramers, while 25% of the tetramers would be fully green-labeled and 25% would be fully red-labeled. The exponential decay of acceptor emission is fit to a single exponential model, and the rate replots

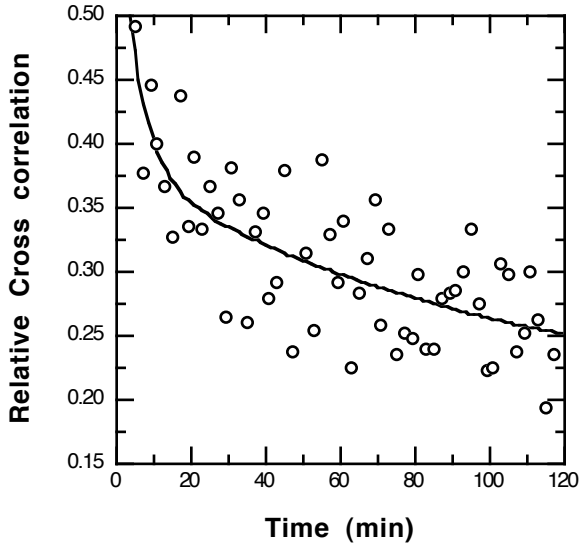

Figure 5-8: Cross correlation analysis of PEP-induced dissociation of the mixed tetramer.
The cross correlation amplitude of the mixed tetramer is plotted as a function of time following treatment with 4 mM PEP. The total protein concentration is 50 nM.

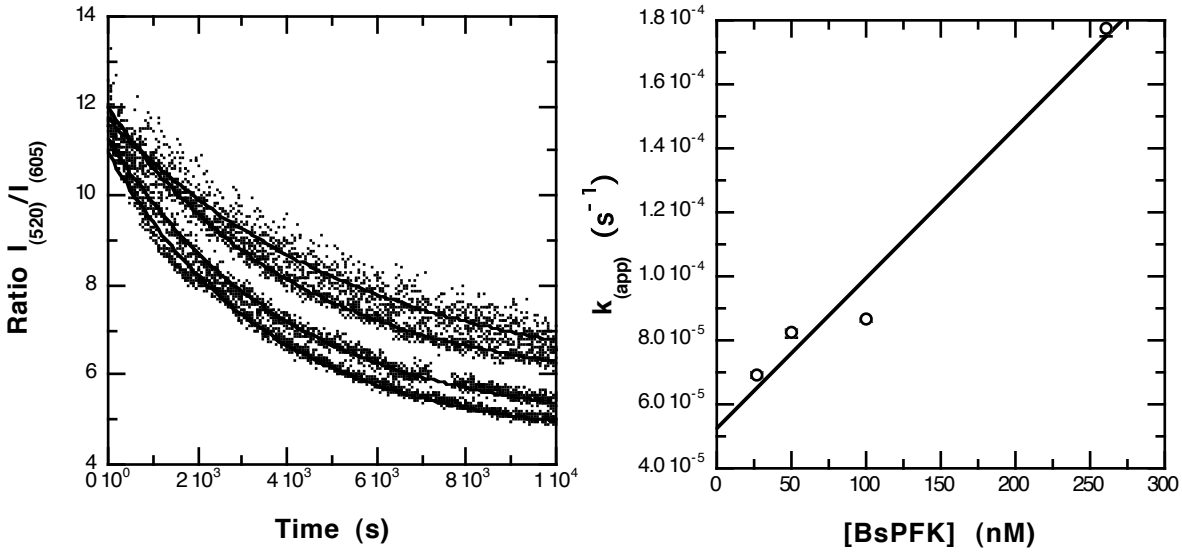

Figure 5-9: Förster Resonance Energy Transfer in the mixed tetramer.
In panel A, the loss of FRET with time following addition of PEP is demonstrated. The ratio of donor emission to acceptor emission (λ = 520 nm / 605 nm) is plotted vs. time, and the ratio decreases as the mixed tetramer dissociates and reassociates into a mixed population of red, green and mixed tetramers. Solid lines represent single exponential fits to the data. The curves represent total protein concentrations of 260 nM, 520 nM, 1 μM and 2 μM from top to bottom. In panel B, the apparent rate is plotted as a function of protein concentration.

The exponential decay of acceptor emission is fit to a single exponential model, and the rate replots (figure 5-9b) compare favorably to those obtained by FCS and quantitative electrophoresis, with $k_a = 4.67 \pm 0.60*10^2\ M^{-1}\ s^{-1}$ and $k_d = 5.29 \pm 0.85*10^{-5}\ s^{-1}$. These values correspond to an apparent K_d of 113±16.4 nM.

Subunit dissociation using fluorescence anisotropy

The subunit affinities have been examined by direct titration of the Texas Red modified tetramer using fluorescence anisotropy. BsPFK contains a single tryptophan per subunit; hence addition of the extrinsic fluorophore allows observation of protein at concentrations several orders of magnitude lower than those accessible to intrinsic fluorescence. The anisotropy of serial dilutions of BsPFK-Texas Red in the presence of various ligands are shown (figure 5-10). As tetrameric PFK dissociates, the anisotropy is anticipated to decrease, as the overall protein size decreases. At high protein concentrations, the anisotropy values of all the ligand-bound states of PFK-Texas Red are approximately 0.14, an absolute value much lower than anticipated. Allowing dimer exchange between BsPFK-Texas Red and an excess of unlabeled PFK increases the anisotropy from 0.14 to 0.21, and exchange to the level of monomers increases the anisotropy to 0.23. These data imply that the low anisotropy values are caused by homo-FRET between fluorophores on adjacent subunits. No change in anisotropy is observed in the absence of ligands and in the presence of F6P at any concentration of PFK examined. As protein concentration decreases in the presence of saturating PEP, a sharp increase in anisotropy is observed. The increase in anisotropy is attributed to loss of

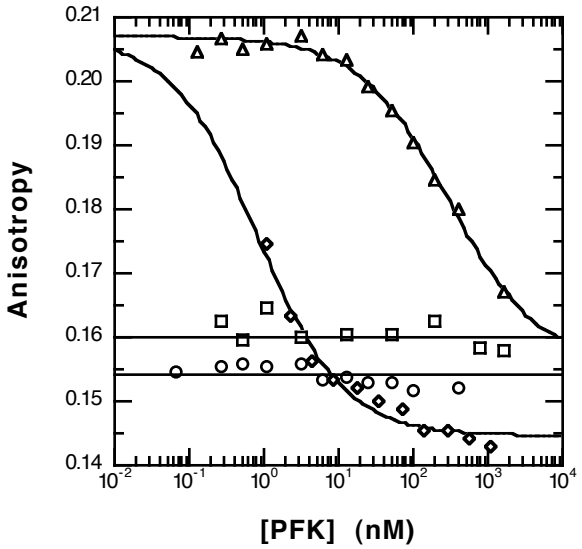

Figure 5-10: Anisotropy of the various ligation states as a function of protein concentration.
Anisotropy titrations of the various ligation states of BsPFK are shown. Circles: free enzyme:, squares: PFK + 1mM F6P, triangles: PFK + 4mM PEP, diamonds: PFK + 4mM F6P + 20mM PEP.

homo-transfer between subunits as dissociation occurs along the active site interface, and yields an apparent affinity of 107 ± 17 nM. This value corresponds well with the apparent K_d determined from the kinetics of dimer exchange. The ternary complex between PFK, F6P and PEP similarly increases in anisotropy, but at a much lower concentration of enzyme. The apparent K_d for the ternary complex is approximately 0.81 ± 0.12 nM. F6P binding by the enzyme thus stabilizes the active site interface to PEP-induced dissociation by 132-fold, or approximately 2.9 kcal/mol.

The role of subunit association in allosteric response

The disproportionation equilibrium defines the thermodynamics of the allosteric regulation. If the subunit interactions play a role in allostery as hypothesized, this must be apparent within the context of the disproportionation equilibrium. To demonstrate a link between subunit interactions and inhibition, an inequality between the subunit affinities of the components of the disproportionation equilibrium must be established.

$$\text{PFK-F6P} + \text{PEP-PFK} \rightleftharpoons \text{PFK} + \text{PEP-PFK-F6P}$$

$$\Delta G_{(\text{PFK-F6P})} + \Delta G_{(\text{PEP-PFK})} \neq \Delta G_{(\text{PFK})} + \Delta G_{(\text{PEP-PFK-F6P})} \qquad [5\text{-}3]$$

The terms of the equilibrium can be rearranged to show that the effect of subunit interactions, if any, must arise from differences between the ternary complex and free enzyme, and the sum of the two single ligand-bound forms and free enzyme:

$$PFK\text{-}F6P + PEP\text{-}PFK \rightleftharpoons PFK + PEP\text{-}PFK\text{-}F6P$$

$$(PEP\text{-}PFK\text{-}F6P - PFK) \rightleftharpoons (PEP\text{-}PFK - PFK) + (PFK\text{-}F6P - PFK)$$

$$\Delta G_{(PEP\text{-}PFK\text{-}F6P)} - \Delta G_{(PFK)} \neq (\Delta G_{(PEP\text{-}PFK)} - \Delta G_{(PFK)}) + (\Delta G_{(PFK\text{-}F6P)} - \Delta G_{(PFK)}) \qquad [5\text{-}4]$$

The PEP-induced dissociation of the active site interface has been demonstrated conclusively but the role of this effect in allosteric regulation remains unclear. The subunit affinities are determined from fits to the dilution dissociation curves (figure 5-10). In an examination of equation 5-4, each term in the equation contains the dissociation of free enzyme, a value that is beyond the limits of experimental detection. The reactant in the equilibrium is the ternary complex, which has a dissociation constant of 0.81 nM, and the products of the equilibrium consist of the two binary complexes; one of which has a dissociation constant of 107 nm and the other of which is too tight to determine. If the dissociation constant of free enzyme is assumed to be less than 0.05 nM, a reasonable upper limit based on the anisotropy data presented in figure 5-10, the following situation arises:

$$\Delta G_{(PEP\text{-}PFK\text{-}F6P)} - \Delta G_{(PFK)} \neq (\Delta G_{(PEP\text{-}PFK)} - \Delta G_{(PFK)}) + (\Delta G_{(PFK\text{-}F6P)} - \Delta G_{(PFK)})$$

$$(0.81nM - x) \qquad (107nM - x) + (y - x)$$

$$(-12.4 - \leq (-14.0))\ kcal/mol \neq (-9.5 - \leq (-14.0))\ kcal/mol) + (y - \leq (-14.0))\ kcal/mol)$$

$$1.6\ kcal/mol \neq 4.5\ kcal/mol + (y - \leq (-14.0))\ kcal/mol)$$

$$-2.9\ kcal/mol \neq (y - \leq (-14.0))\ kcal/mol)$$

$$y \leq -16.9\ kcal/mol \cong 0.4pM$$

This equilibrium would therefore represent an inequality if the subunit affinity of the F6P-bound enzyme form did not possess exactly 132-fold higher affinity than free enzyme, or based on the assumption that the free enzyme has affinity of at least 0.05 nM, less than or equal to 0.4 pM. While F6P stabilizes the enzyme to PEP-induced dissociation at 25°C (figure 5-5), and anecdotal evidence exists that F6P stabilizes the enzyme to thermal dissociation (data not shown) it is unlikely that F6P provides stabilization to this extent. If the subunit affinities of the free enzyme and the F6P-bound form are reasonably assumed to lie within 3 orders of magnitude of each other, then an inequality exists and PEP-induced subunit disruption may play a significant role in the allosteric inhibition of BsPFK.

Conclusions

The role of protein-ligand interactions in the mediation of protein-protein associations is a fundamental issue in biochemistry. We demonstrate conclusively that the binding of the allosteric inhibitor PEP causes a significant reduction of protein-protein affinity at a site distant from the binding site in BsPFK. Ligand-mediated loss of protein affinity of this type is common, and is observed in such generic biochemical phenomena as transcription factor association with nucleic acids. Ligand-binding has been shown to cause eukaryotic PFK aggregation to high order oligomers [156-159] and inhibitor-induced dissociation has been demonstrated for *Thermus thermophilus* PFK [160]. These data represent the first direct correlation between ligand-binding and

protein association for *B. stearothermophilus* PFK, and suggest that intersubunit interactions may play a general role in the regulation of multisubunit allosteric enzymes. While the effects of PEP binding on the subunit affinities of the active site interface is itself an allosteric property, the possible role of this effect in the allosteric regulation of catalysis must be considered. The crystal structures of the free enzyme and the inhibitor-bound enzyme show a quaternary shift in the orientation of the subunits around the active site interface, and this has been trumpeted as the structural model for the allosteric inhibition of the enzyme. We have quantitatively confirmed this hypothesis by direct measurement of the affinities of all the components of the disproportionation equilibrium.

CHAPTER VI

CONCLUSIONS

The effects of hydrostatic pressure on ligand binding and coupling of *E. coli* PFK

While much work has been done toward the elucidation of pressure effects on protein folding and protein association, the study of pressure effects on ligand-binding and dynamic phenomena is in its infancy. The initial study presented had as its aim the elucidation of the effects of hydrostatic pressure on allosteric regulation. It was anticipated that the use of pressure would lead to insights on the basis of the observed inversion of allosteric effects as a function of various perturbants including temperature and pH, and the apparent discordance between the thermodynamic driving forces of PEP-inhibition of *E. coli* and *B. stearothermophilus* PFK. The study has revealed surprising characteristics of the enzyme and the properties of its various ligation states.

The effects of pressure on substrate binding depend largely on the ligation state of the enzyme. In the absence of allosteric inhibitor, substrate binding is strongly reduced by pressure. This pressure-sensitivity is further influenced by temperature, and increasing temperature leads to greater reduction in binding affinity with pressure. The associated standard volume change for ligand binding is consequently higher at high temperature. In the saturating presence of allosteric inhibitor, PEP, the binding of substrate is largely pressure-insensitive. Likewise, increasing temperature has minimal affect on the affinity of the enzyme for substrate and the effects of pressure thereon. The

standard volume change with inhibitor bound is small, and essentially constant with temperature under the range of temperatures examined.

These data lead to hypotheses regarding the nature of the enzyme in the free and ligand-bound forms. The effects of pressure are, simply, to drive equilibria in the direction of smallest volume. Consequently, the large effects of pressure on K_{ia}^{0} lead to the conclusion that the sum of the partial volumes of F6P and free enzyme are larger than that of the enzyme bound substrate, as predicted by electrostriction. The surprising result is that bound PEP essentially eliminates this effect. K_{ia}^{∞} is pressure-insensitive, suggesting that the sum of the partial specific volumes of the PEP-bound enzyme and substrate are roughly equivalent to those of the partially charge-neutralized ternary complex.

Pressure has strong effects on allosteric inhibition by PEP, causing PEP to become a weaker inhibitor. While it was anticipated that an inversion of allosteric effect might occur with pressure, as has been observed with temperature and pH, none was apparent under the accessible pressure conditions. At all temperatures examined, pressure reduces the magnitude of the coupling constant, but dissociation of the tetramer obscures the absolute effects of pressure on coupling at pressures above 800 bar.

The free energy of coupling for PEP inhibition becomes less positive with pressure, a consequence of compensating entropic and enthalpic effects. While both entropy and enthalpy are positive, entropy has a higher pressure-dependence than does enthalpy leading to a decrease in the magnitude of inhibition. The increase in entropy

with pressure is itself an unexpected result, as increasing compression would be anticipated to result in tighter protein packing and restricted motion.

A long-term goal of the high-pressure studies was to more closely examine the differences in thermodynamic driving forces between EcPFK and BsPFK. Specifically, the aim was to compare the pressure responses of the van't Hoff entropy and enthalpy of allosteric coupling for the two enzymes. In this manner, the effects of pressure on EcPFK could be examined with respect to an enzyme with opposing thermodynamic response to temperature. It was anticipated that this would lead to insights into whether the observed pressure effects represent a general protein response to pressure, whether these effects would be inverse, or whether the effects were specific to the enzyme studied. Furthermore, while the *E. coli* enzyme is pressure-labile, the *B. stearothermophilus* enzyme resists pressure-induced dissociation to pressure greater than 3 kbar. We anticipate that with this more pressure-stable enzyme, pressure-induced inversion of allosteric effects will be experimentally observed if they occur. To this end, initial studies were performed with site-directed mutants of BsPFK in which a single tryptophan residue had been engineered at a location in which the extent of ligation could be observed by examination of fluorescence. Unfortunately, the high pH sensitivity of the allosteric regulation of BsPFK was a complicating factor that has only recently been overcome. The development of the pressure-insensitive buffer mixtures discussed in chapter II will allow the examination of the effects of pressure on the ligand binding and allosteric regulation of BsPFK.

It is of interest to note that this study directly connected many of the diverse research aims of Gregorio Weber at various points in his career. His initial work developing the theories of internal equilibria and ligand-binding, the use of hydrostatic pressure as a biochemical perturbant, and fluorescence spectroscopy all combined as the basis for this research.

The development of baroresistant buffer mixtures

With the initial aim of determining which of the pre-existing buffers was most pressure-insensitive, a systematic study of the effect of pressure on the pK_a values of various biochemical buffers was undertaken. This research confirmed earlier studies on the effects of pressure on various buffers, fluorophores and water, and was extended to previously unstudied buffers. Additionally, and most significantly, a series of binary mixtures were developed with greatly reduced standard reaction volumes, and hence minimal change in pH with pressure.

A series of pH-sensitive fluorophores were utilized to measure the pH of aqueous buffer solutions in sealed pressure cuvettes. This technique allowed pH to be monitored optically, and eliminated the need for modified electrodes or conductivity meters. At each pressure, a standard pH curve was corrected for effects of pressure on a solution of fluorophore.

The effect of pressure on most biochemically significant, aqueous buffers is to decrease the pK_a, leading to an increased solution pH. The magnitude of the change in

pH with pressure is typically 0.1 - 0.3 pH units/kbar, which corresponds to a total pH change of approximately 0.5 - 1 pH unit over a typical biochemical experiment of 3 kbar. For cationic buffers including Tris and imidazole, the $\Delta pH/\Delta P$ is smaller, as would be anticipated due to reduced electrostrictive effects. While in most cases, this pH change is insignificant, in particularly pH-sensitive cases the convolution of effects from pressure and pH perturbation can make interpretation of effects difficult. With respect to the initial aims of this research, a 0.3 unit change in pH would dramatically alter the allosteric regulation of BsPFK, rendering comparison with EcPFK difficult.

The effect of pressure on carboxylic acids and phosphate is the opposite of the effect observed for "Good's" and cationic buffers. While these buffers increased in pH with pressure, carboxylates and phosphate buffer decreased in pH. The magnitude of the change was similar to that of the "Good's" buffers.

From these two conflicting effects, mixtures were prepared using a buffer with a positive ΔV and a buffer with a negative ΔV to yield a mixture with a $\Delta V \sim 0$, and consequently minimal $\Delta pH/\Delta P$. Mixtures consisting of Tris and one of either phosphate, tricarballylate or 1,1-cyclohexanediacetate were tested at various molar ratios and at pH values around neutrality. For each mixture, at each pH, a specific mole ratio was derived at which the $\Delta pH/\Delta P$ of the mixture was zero. The systematic trend of $\Delta pH/\Delta P$ with relative concentration allows a specific mixture to be developed for all pH values in the range examined. These mixtures were tested for pressure effects, and the baroresistance of each was confirmed. Buffer components were tabulated for general laboratory use.

It is anticipated that other labs will use the buffers developed, and will develop buffers per their respective needs based on the principles outlined in chapter II. The use of phosphate as a component in buffer mixtures is specifically impractical for research with PFK, based on the catalytic function of the enzyme. Hence, it is also anticipated that other labs will explore other binary mixtures that will prove similarly effective. Based on the research discussed in chapters II and III, future pressure research will focus on BsPFK, enabling comparison to the EcPFK ligand binding and allostery discussed above.

Examination of the putative interaction between the sequential citric acid cycle enzymes malate dehydrogenase and citrate synthase using FCS

The existence of transient or weak interactions between sequential enzymes of various metabolic pathways, articulated in the metabolon hypothesis, has been debated for many years. While conclusive evidence exists for the channeling of substrates between active sites in bifunctional enzymes, much of the evidence for channeling in transient multi-enzyme complexes has been indirect. The transitory and hence weakly interacting nature of these enzyme associations has made their detection difficult *in vitro*, yet the rationale for their existence is plausible. Polyethylene glycol-induced association between the citric acid cycle enzymes mitochondrial malate dehydrogenase and citrate synthase had been demonstrated [26,27]. Based on the assumption that the putative transient interaction between these two enzymes exists on a milli- to

microsecond timescale, and that interactions on this timescale could be detected by correlation analysis, an examination of this interaction was undertaken using Fluorescence Correlation Spectroscopy.

Initial cross correlation experiments aimed to detect and quantify the interaction in the absence of PEG. Titrations performed in the absence of PEG under the concentration conditions accessible to the technique (~0.5 nM - 100 nM) showed no cross correlation, indicative of insignificant extent of association. Under conditions of 5% to 10% (w/v) PEG, cross correlation was observed. The presence of cross correlation is direct evidence of a heteroassociation between the two enzymes. The specificity of the interaction was demonstrated by competition with unlabeled MDH. The apparent binding affinity was highly dependent on the concentration of PEG, and increased with increasing PEG concentration. The protein-protein affinity in the absence of PEG was estimated to be approximately 10 mM, based on a linear extrapolation of K_d with PEG concentration.

Addition of the common intermediate, oxaloacetate, was predicted to increase the protein-protein binding affinity. Repeating the titrations with OAA revealed that at OAA concentrations below the K_m of citrate synthase for this substrate, the affinity was strongly increased. At successive OAA concentrations above the K_m, the MDH-CTS affinity decreased. These data suggest that the open conformation of CTS, the form to which OAA binds, is also the conformation to which MDH binds.

High concentrations of either OAA or PEG resulted in the formation of high order aggregates of MDH-CTS. These aggregates are shown by simulation to have an

apparent diffusion coefficient of approximately 1 $\mu m^2/s$, and are highly heterogeneous. Addition of NaCl at the same ionic strength as the OAA yields a similar extent of aggregation. Furthermore, in the absence of CTS, MDH forms similar aggregates under the same conditions. These aggregates have been previously reported, and in prior experiments have been used to simulate soluble MDH-CTS complexes. These data suggest that these aggregates are heterogeneous and salt-dependent, therefore they are unlikely the specific complexes observed at low protein concentration.

Examination of the subunit associations of *B. stearothermophilus* PFK and the effects of ligand-binding on these interactions

Dual-channel, multi-photon Fluorescence Correlation Spectroscopy was used to examine the high affinity subunit interactions of *B. stearothermophilus* PFK. The technique is ideally suited for the examination of low concentrations of fluorescent labeled biomolecules, and thus molecular associations with affinity in the nanomolar range. Cross correlation analysis, in concert with a labeling/hybridization technique wherein multiple fluorophores were introduced into the PFK tetramer, was anticipated to allow differentiation between dissociation at each dimer-dimer interface with a unique fluorescence response.

Modification of a hybridization scheme demonstrated by Kimmel [103], allowed dimers of BsPFK differentially labeled with either Alexa488 or Texas Red to reassociate in known orientations within the tetramer forming mixed tetramers composed of 2

Alexa488-labeled subunits and 2 Texas Red-labeled subunits. In a protein titration these mixed tetramers were anticipated to demonstrate loss of cross correlation relative to autocorrelation if dissociation occurred at the active site interface. Alternatively, cross correlation would be maintained, but non-linear particle number and molecular brightness would be observed if dissociation occurred at the allosteric site interface. In this manner, the binding affinities of both interfaces could be determined and the effects of ligand binding at either interface on those affinities could be resolved. The identity of the mixed tetramer was confirmed by native PAGE, UV-Vis spectroscopy and by FCS. In a protein titration, no dissociation was observed at either interface within the range of concentration accessible with the experimental FCS arrangement.

Using an electrophoretic mobility shift assay, dimer exchange between Texas Red-labeled wildtype BsPFK and Alexa488-labeled "charge-tagged" BsPFK K90, 91E was demonstrated in the presence of 4 mM PEP. This ligand-induced loss of subunit affinity was specific for the inhibitor, PEP, as no exchange was observed in the presence of ADP, F6P or in the absence of ligands. In the crystal structures of the phosphate bound, "active conformation" and a phosphoglycolate bound "inhibited conformation" a 7° rotation of the subunits around the active site interface is observed [151,152]. These data suggest that the inhibitor-bound conformation has lower subunit affinity than the uninhibited conformation. This PEP-induced dissociation of the active site interface is confirmed independently by FCS, urea denaturation, FRET and anisotropy. The affinity of the active site interface with PEP bound is 107±17 nM, while the affinity of this interface in the absence of inhibitor is beyond the limits of experimental determination.

The rate constants for PEP-induced dissociation are $k_a = 4.7 \pm 0.6*10^2$ $M^{-1}s^{-1}$ and $k_d = 5.3 \pm 0.9*10^{-5}$ s^{-1}. Interestingly, these data imply that PEP binds more tightly to the PFK dimer than the tetramer. F6P binding stabilizes the ternary complex to dissociation by over 130-fold relative to the PEP-bound form.

In evolutionary context, these results are particularly revealing. *T. thermophilus* PFK undergoes dissociation under conditions of PEP-binding. A double point mutant of BsPFK, W179Y/Y164W similarly undergoes dissociation when PEP is bound to the enzyme. While this mutant was initially presented as a novel phenotype, in light of these data, this mutation can be considered an augmentation of the wildtype phenotype. Many eukaryotic PFK isoforms undergo extensive aggregation under conditions of ligand binding or at high concentrations. Collectively these data hint at the possible role of subunit associations in allosteric inhibition by PEP. To test the hypothesis that subunit interactions play a role in the allosteric inhibition in BsPFK, the subunit affinities of all 4 unique ligand-bound states of the disproportionation equilibrium must be determined. Two of those 4 affinities cannot be obtained with available methodologies. The assumption can be made, however, that the likelihood that F6P stabilization of free enzyme is exactly the opposite of PEP destabilization of the ternary complex is small and consequently an inequality exists in the disproportionation equilibrium. This suggests that subunit interactions do play a significant role in the allosteric inhibition of BsPFK.

REFERENCES

[1] D. Voet, J.G. Voet, Biochemistry: 2nd edition, John Wiley and Sons, New York, 1995.

[2] E.M. Phizicky, S. Fields, Protein-protein interactions: methods for detection and analysis, Microbiol. Rev. 59 (1995) 94 – 123.

[3] S. Jones, J.M. Thornton, Principles of protein-protein interactions, Proc. Natl. Acad. Sci. USA 93 (1996) 13 – 20.

[4] S.A. Teichmann, A.G. Murzin, C. Chothia, Determination of protein function, evolution and interactions by structural genomics, Curr. Opin. Struct. Biol. 11 (2001) 354 – 363.

[5] S. Shaw, R. Geyer, G.M. Alter, Dissociation of mitochondrial malate dehydrogenase into active soluble subunits, Biochim. Biophys. Act. 1478 (2000) 248 – 256.

[6] S.I. Chang, G.G. Hammes, Structure and mechanism of action of a multifunctional enzyme: fatty acid synthase, Acc. Chem. Res. 23 (1990) 363 – 369.

[7] J.K. Angelides, G.G. Hammes, Mechanism of action of the pyruvate dehydrogenase complex from *E. coli*, Proc. Natl. Acad. Sci. USA 75 (1978) 4877 – 4880.

[8] E.R. Kantrowitz, W.N. Lipscomb, *Escherichia coli* aspartate transcarbamoylase: the molecular basis for a concerted allosteric transition, Trends Biochem. Sci. 15 (1990) 53 – 59.

[9] B. Lewin, Genes V, Oxford University Press, New York, 1994.

[10] T. Ushiroyama, T. Fukushima, J.D. Styre, H.O. Spivey, Substrate channeling of NADH in mitochondrial redox processes, in: E.R. Stadtman, P.B. Chock (Eds) Current Topics in Cellular Regulation: Volume 33, Academic Press, New York, 1992, pp. 291 – 307.

[11] H.O. Spivey, J.M. Merz, Metabolic compartmentation, Bioessays. 10 (1989) 127 – 130.

[12] D.K. Srivastava, S.A. Bernhard, Metabolite transfer via enzyme-enzyme complexes, Science 234 (1986) 1081 –1086.

[13] P.A. Srere, Complexes of sequential metabolic enzymes, Ann. Rev. Biochem. 56 (1987) 89 – 124.

[14] E.W. Miles, S. Rhee, D.R. Davies, The molecular basis of substrate channeling, J. Biol. Chem. 274 (1999) 12193 – 12196.

[15] H. Yong, G.A. Thomas, W.L. Peticolas, Metabolite-modulated complex formation between α-glyercerophosphate dehydrogenase and lactate dehydrogenase, Biochemistry 32 (1993) 11124 – 11131.

[16] J. Rudolf, J. Stubbe, Investigation of the mechanism of phosphoribosylamine transfer from glutamine phosphoribosylpyrophosphate amidotransferase to glycinamide ribonucleotide synthetase, Biochemistry 34 (1995) 2241 – 2250.

[17] H.O. Spivey, J. Ovádi, Substrate channeling, Methods. 19 (1999) 306 – 321.

[18] M.K. Geck, J.F. Kirsch, A novel, definitive test for substrate channeling illustrated with the aspartate aminotransferase/malate dehydrogenase system, Biochemistry 38 (1999) 8032 – 8037.

[19] P.H. Liang, K.S. Anderson, Substrate channeling and domain-domain interactions in bifunctional thymidylate synthase – dihydrofolate reductase, Biochemistry 37 (1998) 12195 – 12205.

[20] B. Sümegi, L. Gyócsi, I. Alkonyi, Interaction between the pyruvate dehydrogenase complex and citrate synthase, Biochim. Biophys. Act. 616 (1980) 158 – 166.

[21] Z. Porpaczy, B. Sümegi, I. Alkonyi, Association between the α-ketoglutarate dehydrogenase complex and succinate thiokinase, Biochim. Biophys. Act. 749 (1983) 172 – 179.

[22] S. Beeckman, L. Kanarek, Demonstration of physical interaction between consecutive enzymes of the citric acid cycle and the aspartate-malate shuttle, Eur. J. Biochem. 117 (1981) 527 – 535.

[23] Z. Porpaczy, B. Sümegi, I. Alkonyi, Interaction between NAD-dependent isocitrate dehydrogenase, α-ketoglutarate dehydrogenase complex and NADH:ubiquinone oxidoreductase, J. Biol. Chem. 262 (1987) 9509 – 9514.

[24] B.G. Vértessy, J. Kovács, P. Löw, A. Lehotzky, A. Molnár, F. Orosz, J. Ovádi, Characterization of microtubule – phosphofructokinase complex: specific effects of MgATP and vinblastine, Biochemistry 36 (1997) 2051 – 2062.

[25] B. Raïs, F. Ortega, J. Puigjaner, B. Comin, F. Orosz, J. Ovádi, M. Cascante, Quantitative characterization of homo- and heteroassociations of muscle phosphofructokinase with aldolase, Biochim. Biophys. Act. 1479 (2000) 303 – 314.

[26] J.M Merz, T.A. Webster, J.R. Appleman, E.R. Manley, H.A. Yu, A. Datta, B.J. Ackerson, H.O. Spivey, Polyethylene glycol-induced heteroassociations of malate dehydrogenase and citrate synthase, Arch. Biochem. Biophys. 258 (1987) 132 – 142.

[27] A. Datta, J.M. Merz, H.O. Spivey, Substrate channeling of oxaloacetate in solid-state complexes of malate dehydrogenase and citrate synthase, J. Biol. Chem. 260 (1985) 15008 – 15012.

[28] K. Shatalin, S. Lebreton, M. Rault-Leonardon, C. Vélot, P.A. Srere, Electrostatic channeling of oxaloacetate in a fusion protein of porcine citrate synthase and porcine mitochondrial malate dehydrogenase, Biochemistry 38 (1999) 881 – 889.

[29] I. Morgunov, P.A. Srere, Interaction between citrate synthase and malate dehydrogenase: substrate channeling of oxaloacetate, J. Biol. Chem. 273 (1998) 29540 – 29544.

[30] C. Vélot, P.A. Srere, Reversible transdominant inhibition of a metabolic pathway: *in vivo* evidence of an interaction between two sequential tricarboxylic acid cycle enzymes in yeast, J. Biol. Chem. 275 (2000) 12926 – 12933.

[31] L.I. Ashmarina, A.V. Pshezhetsky, H.O. Spivey, M. Potier, Demonstration of enzyme associations by countermigration electrophoresis in agarose gel, Anal. Biochem. 219 (1994) 349 – 355.

[32] C. Vélot, M.B. Mixon, M. Teige, P.A. Srere, Model of a quinary structure between Krebs TCA cycle enzymes: a model for the metabolon, Biochemistry 36 (1997) 14271 – 14276.

[33] P. Tompa, J. Batke, J. Ovádi, G.R. Wech, P.A. Srere, Quantitation of the interaction between citrate synthase and malate dehydrogenase, J. Biol. Chem. 262 (1987) 6089 – 6092.

[34] C. Vélot, S. Lebreton, I. Morgunov, K.C. Usher, P.A. Srere, Metabolic effects of mislocalized mitochondrial and peroxisomal citrate synthases in yeast *Saccharomyces cerevisiae*, Biochemistry 38 (1999) 16195 – 16204.

[35] B.E. Glatthaar, G.R. Barbarash, B.E. Noyes, L.J. Banaszak, R.A. Bradshaw, The preparation of the cytoplasmic and mitochondrial forms of malate dehydrogenase and aspartate aminotransferase from pig heart by a single procedure, Anal. Biochem. 57 (1974) 432 – 451.

[36] K. Smith, T.K. Sundaram, A facile method for the isolation of porcine heart mitochondrial malate dehydrogenase by affinity elution chromatography on Procion Red HE3B, Biosci. Reports. 3 (1983) 1035 – 1043.

[37] M.S. Weininger, L.J. Banaszak, Mitochondrial malate dehydrogenase. Crystallographic properties of the pig heart enzyme, J. Mol. Biol. 119 (1978) 443 – 449.

[38] J.J. Birktoft, L.J. Banaszak, Refined crystal structure of cytoplasmic malate dehydrogenase at 2.5Å resolution, Biochemistry 28 (1989) 6065

[39] P.A. Mueggler, R.G. Wolfe, Malate dehydrogenase. Kinetic studies of substrate activation of supernatant enzyme by L-malate, Biochemistry 17 (1978) 4615 – 4620.

[40] S.A. Sánchez, T.L. Hazlett, J.E. Brunet, D.M. Jameson, Aggregation states of mitochondrial malate dehydrogenase, Protein Sci. 7 (1998) 2184 – 2189.

[41] D.M. Jameson, V. Thomas, D. Zhou, Time resolved fluorescence studies on NADH bound to mitochondrial malate dehydrogenase, Biochim. Biophys. Act. 994 (1989) 187 – 190.

[42] P.P. Tung, G.M. Alter, Substrate and cofactor binding to fluorescently labeled cytoplasmic malate dehydrogenase, Biochim. Biophys. Act. 1545 (2001) 132 – 145.

[43] J.R. Stern, Oxalacetate transacetase (condensing enzyme), In: P.D. Boyer, H.A. Lardy, H. Myrbok (Eds) The Enzymes: 2nd edition, 1961, pp. 367 – 380.

[44] S. Remington, G. Wiegand, R. Huber, Crystallographic refinement and atomic models of two different forms of citrate synthase at 2.7 and 1.7Å resolution, J. Mol. Biol. 158 (1982) 111 – 152.

[45] S.J. Remington, Structure and mechanism of citrate synthase, Curr. Top. Cell. Regul. 33 (1992) 209 – 229.

[46] W.S.J. Valdar, J.M. Thornton, Protein-protein interfaces: analysis of amino acid conservation in homodimers, Prot. Struct. Funct. Gene. 42 (2001) 108 – 124.

[47] L.Lo Conte, C. Chothia, J. Janin, The atomic structure of protein-protein recognition sites, J. Mol. Biol. 285 (1999) 2177 – 2198.

[48] I.M. Klotz, D.W. Darnall, N.R. Langerman, Quaternary structure of proteins, In: H. Neurath, R.L. Hill (Eds) The Proteins, Academic Press, Inc., New York, 1975, pp. 293 – 411.

[49] L. Patthy, Protein Evolution, Blackwell Science, Ltd., Oxford, 1999, pp. 51 – 74.

[50] T. Dobzhansky, Genetics of natural populations. XIII. Recombination and variability in populations of *Drosophila psudoobscura*, Genetics, 31 (1946) 269 – 290.

[51] J.B. Allen, M.W. Walberg, M.C. Edwards, S.J. Elledge, Finding prospective partners in the library: the two hybrid system and phage display find a match, TIBS. 20 (1995) 511 – 516.

[52] J.C. Hu, M.G. Kornacker, A. Hochschild, *Escherichia coli* one- and two-hybrid systems for the analysis and identification of protein-protein interactions, Methods. 20 (2000) 80 – 94.

[53] H. Okamura, K. Yoshida, H. Morimoto, T. Haneji, Transciption factor NF-Y regulates mdr1 expression through binding to inverted CCAAT sequence in drug-resistant human squamous carcinoma cells, Int. J. Oncol. 25 (2004) 1031 – 1037.

[54] J.R. Lakowicz, Principles of Fluorescence Spectroscopy: 2nd edition, Plenum Press, New York, 1999.

[55] D.M. Jameson, W.H. Sawyer, Fluorescence anisotropy applied to biomolecular interactions, Methods Enzymol. 246 (1995) 283 –300.

[56] G. Weber, Polarization of the fluorescence of macromolecules. I. Theory and experimental method, Biochem. J. 51 (1952) 145 – 155.

[57] G. Weber Rotational Brownian motion and polarization of fluorescence solutions, Adv. Protein Chem. 8 (1953) 415 – 459.

[58] G. Mocz, M.K. Helms, D.M. Jameson, I.R. Gibbons, Probing the nucleotide binding sites of axonemal dynein with the fluorescent nucleotide analog 2'(3')-O-(-N-Methylanthraniloyl)-adenosine 5'-triphosphate, Biochemistry 37 (1998) 9862 – 9868.

[59] P.R. Callis, 1La and 1Lb transitions of tryptophan: applications of theory and experimental observations to fluorescence of proteins, Methods Enzymol. 278 (1997) 113 – 150.

[60] E.J. Gratton, J.R. Alcala, F.G. Pendergast, Protein dynamics: fluorescence lifetime distributions, In D.M. Jameson and G.D. Reinhart (Eds) Fluorescent Biomolecules, Plenum Press, New York, 1989, pp. 17 – 32.

[61] A. Jablonski, On the notation of emission anisotropy, Bull. Acad. Pol. Sci. Ser. A. 8 (1960) 259 – 264.

[62] A. Jablonski, Über den mechanisms des photolumineszenz von farbstoffphophoren, Z. Phys. 94 (1935) 38 – 46.

[63] M. Kasha, Characterization of electronic transitions in complex molecules, Dis. Faraday Soc. 9 (1950) 14 – 19.

[64] G.G. Stokes, On the change of refangibility of light, Phil. Trans. R. Soc. London 142 (1852) 463 – 562.

[65] E.J. Gratton, D.M. Jameson, R.D. Hall, Multifrequency phase and modulation fluorometry, Ann. Rev. Biophys. Bioeng. 13 (1984) 105 – 124.

[66] R.D. Spencer, G. Weber, Measurement of subnanosecond fluorescence lifetimes with a cross correlation phase fluorometer, Ann. N. Y. Acad. Sci. 158 (1969) 361 – 376.

[67] R.D Spencer, G. Weber, Influence of Brownian rotations and energy transfer upon the measurements of fluorescence lifetime, J. Chem. Phys. 52 (1970) 1654 – 1663.

[68] P.R. Callis, Two-photon induced fluorescence, Ann. Rev. Phys. Chem. 48 (1997) 271 – 297.

[69] C. Xu, W.W. Webb, Multiphoton excitation of molecular fluorophore and nonlinear laser microscopy, In: J.R. Lakowicz (Ed) Topics in Fluorescence Spectroscopy, Volume 5: Nonlinear and Two-Photon Induced Fluorescence, Plenum Press, New York, 1997, pp. 471 – 540.

[70] G. Weber, Polarization of the fluorescence of solutions, In: D.M. Hercules (Ed) Fluorescence and Phosphorescence Analysis, John Wiley and Sons, New York, 1966, pp. 217 – 240.

[71] F. Perrin, La fluorescence des solutions. Induction moléculaire. Polarisation et durée d'émission. Photochimie, Ann. Phys. Ser. 10 (1926) 169 – 275.

[72] T. Förster, Intermolecular energy migration and fluorescence, Ann. Phys. 2 (1948) 55 – 75.

[73] G. Weber, M. Shinitzky, Failure of energy transfer between identical aromatic molecules on excitation at the long wave edge of the absorption spectrum, Proc. Natl. Acad. Sci. USA 65 (1970) 823 – 830.

[74] E. Elson, D. Magde, Fluorescence correlation spectroscopy. I. Conceptual basis and theory, Biopolymers. 13 (1974) 1 – 27.

[75] D. Magde, E.L. Elson, W. W. Webb, Fluorescence correlation spectroscopy. II. An experimental realization, Biopolymers. 13 (1974) 29 – 60.

[76] N.L. Thompson, Fluorescence correlation spectroscopy, in: J.R. Lakowicz (Ed) Topics in Fluorescence Spectroscopy, Volume 1: Techniques, Plenum Press, New York, 1991, pp 337 – 378.

[77] D. Bonn, W.K. Kegel, Stokes-Einstein relations and the fluctuation-dissipation theorem in a supercooled colloidal fluid, J. Chem. Phys. 118 (2003) 2005 – 2009.

[78] Y. Chen, J.D. Muller, K.M. Berland, E. Gratton, Fluorescence fluctuation spectroscopy, Methods. 19 (1999) 234 – 252.

[79] K.G. Heinze, A. Koltermann, P. Schwille, Simultaneous two-photon excitation of distinct labels for dual-color fluorescence crosscorrelation analysis, Proc. Nat. Acad. Sci. USA 97 (2000) 10377 – 10382.

[80] P. Schwille, F.J. Meyer-Almes, R. Rigler, Dual color fluorescence cross-correlation spectroscopy for multicomponent diffusional analysis in solution, Biophys. J. 72 (1997) 1878 – 1886.

[81] U. Kettling, A. Koltermann, P. Schwille, M. Eigen, Real-time enzyme kinetics monitored by dual-color fluorescence cross-correlation spectroscopy, Proc. Natl. Acad. Sci. USA 95 (1998) 1416 – 1420.

[82] Y. Chen, J.D. Müller, P.T.C. So, E. Gratton, The photon counting histogram in fluorescence fluctuation spectroscopy, Biophys. J. 77 (1999) 553 – 567.

[83] W.W. Cleland, The kinetics of enzyme-catalyzed reactions with two or more substrates or products. I. Nomenclature and rate equations, Biochim. Biophys. Acta 67 (1963) 104 – 137.

[84] W.W. Cleland, The kinetics of enzyme-catalyzed reactions with two or more substrates or products. II. Inhibition: nomenclature and theory, Biochim. Biophys. Acta 67 (1963) 137 – 187.

[85] B. Silverman, The Organic Chemistry of Enzyme-Catalyzed Reactions, Academic Press, San Diego, 2000, pp. 563 – 596.

[86] G.D. Reinhart, The determination of thermodynamic allosteric parameters of an enzyme undergoing steady-state turnover, Arch. Biochem. Biophys. 224 (1983) 389 – 401.

[87] G.D. Reinhart, Quantitative analysis and interpretation of allosteric behavior, Methods Enzymol. 380 (2004) 187 – 203.

[88] A.V. Hill, The possible effects of the aggregation of the molecules of hemoglobin on its dissociation curves, J. Physiol. 40 (1910) iv – vii.

[89] G. Fermi, M.F. Perutz, B. Shaanan, R. Fourme, The cystal structure of human deoxyhaemoglobin at 1.74Å, J. Mol. Biol. 175 (1984) 159 – 174.

[90] M.F. Perutz, Stereochemistry of cooperative effects in haemoglobin, Nature 228 (1970) 726 – 734.

[91] J. Monod, J. Wyman, J.P. Changeaux, On the nature of allosteric transitions: a plausible model, J. Mol. Biol. 12 (1965) 88 – 118.

[92] D.E. Koshland, G. Nemethy, D. Filmer, Comparison of experimental binding data and theoretical models in proteins containing subunits, Biochemistry 5 (1966) 365 – 385.

[93] G.K. Ackers, M.L. Doyle, D. Myers, M.A. Daugherty, Molecular code for cooperativity in hemoglobin, Science 255 (1992) 54 – 63.

[94] J.L. Johnson, G.D. Reinhart, Failure of a two-state model to describe the influence of phospho(enol)pyruvate on phosphofructokinase from *Escherichia coli*, Biochemistry 36 (1997) 12814 – 12822.

[95] J.L. Kimmel, G.D. Reinhart, Reevaluation of the accepted allosteric mechanism of phosphofructokinase from *Bacillus stearothermophilus*, Proc. Natl. Acad. Sci. USA 97 (2000) 3844 – 3849.

[96] G.D. Reinhart, Allosteric regulation of pig heart fumarase, In D.L.F. Lennon, F.W. Stratman, R.N. Zahlten (Eds) Biochemistry of Metabolic Processes, Elsevier Science, New York, 1983, pp 273 – 284.

[97] B.L. Braxton, L.S. Mullins, F.M. Raushel, G.D. Reinhart, Allosteric effects of carbamoyl phosphate synthetase from *Escherichia coli* are entropy dominated, Biochemistry 35 (1996) 11918 – 11924.

[98] G. Weber, Ligand binding and internal equilibrium in proteins, Biochemistry 11 (1972) 864 – 878.

[99] G. Weber, Energetics of ligands binding to proteins, Adv. Protein Chem. 29 (1975) 1 – 83.

[100] J. Wyman, Linked functions and reciprocal effects in hemoglobin: a second look, Adv. Protein Chem. 19 (1964) 223 – 286.

[101] J. Wyman, Allosteric linkage, J. Am. Chem. Soc. 89 (1967) 2202 – 2218

[102] G.D. Reinhart, Linked-function origins of cooperativity in a symmetrical dimer, Biophys. Chem. 30 (1988) 159 – 172.

[103] J.L. Kimmel, G.D. Reinhart, Isolation of an individual allosteric interaction in tetrameric phosphofructokinase from *Bacillus stearothermophilus*, Biochemistry 40 (2001) 11623 – 11629.

[104] A.W. Fenton, N.M.Parichartttanakul, G.D. Reinhart, Identification of substrate contact residues important for the allosteric regulation of phosphofructokinase from *Escherichia coli*, Biochemistry, 42 (2003) 6453 – 6459.

[105] A.D. Ortigosa, J.L. Kimmel, G.D. Reinhart, Disentangling the web of allosteric communication in a homotetramer: heterotropic inhibition of phosphofructokinase from *Bacillus stearothermophilus*, Biochemistry 43 (2004) 577 – 586.

[106] G.K. Ackers, J.H. Hazzard, Transduction of binding energy into hemoglobin cooperativity, TIBS, 18 (1993) 385 – 390.

[107] A.S. Pham, G.D. Reinhart, MgATP-dependent activation by phosphoenolpyruvate of the E187A mutant of *Escherichia coli* phosphofructokinase, Biochemistry 40 (2001) 4150-4158.

[108] J.L. Johnson, G.D. Reinhart, Failure of a two-state model to describe the influence of phospho(enol)pyruvate on phosphofructokinase from *Escherichia coli*, Biochemistry 42 (1997) 12814 – 12822.

[109] G.D. Reinhart, S.B. Hartleip, M.M. Symcox, Role of coupling entropy in establishing the nature and magnitude of allosteric response, Proc. Natl. Acad. Sci. USA 86 (1989) 4032 – 4036.

[110] B.L. Braxton, V.L. Tlapak-Simmons, G.D. Reinhart, Temperature-induced inversion of allosteric phenomena, J. Biol. Chem. 269 (1994) 47 – 50.

[111] J.L. Johnson, G.D. Reinhart, Effects of high pressure on the allosteric properties of phosphofructokinase from *Escherichia coli*, in: J.L. Markley, D.B. Northrup, C.A. Royer

(Eds.) High-Pressure Effects in Molecular Biophysics and Enzymology, Oxford University Press, New York, 1996, pp. 242 - 255.

[112] J.L. Silva, G. Weber, Pressure stability of proteins, Annu. Rev. Phys. Chem. 44 (1993) 89 - 113.

[113] N. Tanaka, A. Koyasu, I. Kobayashi, S. Kunugi, Pressure-induced change in proteins studied through chemical modifications, Int. J. Biol. Macromol. 18 (1996) 275 - 280.

[114] M.W. Lassalle, H. Yamada, K. Akasaka, The pressure-temperature free energy-landscape of staphylococcal nuclease monitored by ^{1}H NMR, J. Mol. Biol. 298 (2000) 293-302.

[115] E. Bismuto, I. Sirangelo, G. Irace, E. Gratton, Pressure-induced perturbation of apomyoglobin structure: fluorescence studies on native and acidic compact forms, Biochemistry 35 (1996) 1173 - 1178.

[116] T. Hosseini-nia, A.A. Ismail, S. Kubow, Pressure-induced conformational changes of β-lactoglobulin by variable-pressure fourier transform infrared spectroscopy, J. Agric. Food Chem. 47 (1999) 4537 - 4542.

[117] M. Panda, J. Ybarra, P.M. Horowitz, High hydrostatic pressure can probe the effects of functionally related ligands on the quaternary structures of the chaperonins GroEL and GroEs, J. Biol. Chem. 276 (2001) 6253 - 6259.

[118] L. Erijman, R.M. Clegg, Reversible stalling of transcription elongation by high pressure, Biophys. J. 75 (1998) 453 - 462.

[119] A.A. Paladini, Jr., G. Weber, Pressure-induced reversible dissociation of enolase, Biochemistry 20 (1981) 2587 - 2593.

[120] S. Pin, C.A. Royer, E. Gratton, B. Alpert, G. Webber, Subunit interactions in hemoglobin probed by fluorescence and high-pressure techniques, Biochemistry 29 (1990) 9194 - 9202.

[121] V.L. Valente-Mesquita, M.M. Botelho, S.T. Ferreira, Pressure-induced subunit dissociation and unfolding of dimeric β-lactoglobulin, Biophys J. 75 (1998) 471 - 476.

[122] D. Foguel, C.R. Robinson, P.C. de Sousa, Jr., J.L. Silva, A.S. Robinson, Hydrostatic pressure rescues native protein from aggregates, Biotechnol. Bioeng. 63 (1999) 552 - 558.

[123] N. Hillson, J. Nelson Onuchic, A.E. Garcia, Pressure-induced protein-folding/unfolding kinetics, Proc. Natl. Acad. Sci. USA 96 (1999) 14848 - 14853.

[124] C.A. Royer, Revisiting volume changes in pressure-induced protein unfolding, Biochim. Biophys. Acta 1595 (2002) 201 - 209.

[125] G.J.A. Vidugiris, C.A. Royer, Determination of the volume changes for pressure-induced transitions of apomyoglobin between the native, molten-globule and unfolded states, Biophys. J. 75 (1998) 463 - 470.

[126] H. Seeman, R. Winter, C.A. Royer, Volume, expansivity and isothermal compressibility changes associated with temperature and pressure unfolding of staphylococcal nuclease, J. Mol. Biol. 307 (2001) 1091 - 1102.

[127] A. Zipp, W. Kauzmann, Pressure denaturation of metmyoglobin, Biochemistry 12 (1973) 4217 - 4228.

[128] J.N. Webb, J.F. Carpenter, T.W. Randolf, Stability of subtilisin and lysosyme under high hydrostatic pressure, Biotechnol. Prog. 16 (2000) 630 - 636.

[129] G. Panick, R. Malessa, R. Winter, Differences between the pressure- and temperature- induced denaturation and aggregation of β-lactoglobulin A, B, and AB monitored by FT-IR spectroscopy and small-angle X-ray scattering, Biochemistry 38 (1999) 6512 - 6519.

[130] D. Foguel, Carolyn M. Teshke, P.E. Prevelige, Jr., J.L. Silva, Role of entropic interactions in viral capsids: single amino acid substitutions in P22 bacteriophage coat protein resulting in loss of capsid stability, Biochemistry 34 (1995) 1120 - 1126.

[131] J. Jonas, L. Ballard, D. Nash, High-resolution, high-pressure NMR studies of proteins, Biophys. J. 75 (1998) 445 - 452.

[132] M. Lin, R.B. Macgregor, The activation volume of a DNA helix-coil transition, Biochemistry 35 (1996) 11846 - 11851.

[133] R.B. Macgregor, Jr., The interactions of nucleic acids at elevated hydrostatic pressure, Biochim. Biophys. Act. 1595 (2002) 266 - 176.

[134] T.W. Lynch, D. Kosztin, M.A. McLean, K. Schulten, S.G. Sligar, Dissecting the molecular origins of specific protein-nucleic acid recognition: hydrostatic pressure and molecular dynamics, Biophys. J. 82 (2002) 93 - 98.

[135] T.W. Lynch, S.G. Sligar, Experimental and theoretical high pressure strategies for investigating protein-nucleic acid assemblies, Biochim. Biophys. Act. 1595 (2002) 277 - 282.

[136] N. Kalchayanand, P. Dunne, A. Sikes, B. Ray, Viability loss and morphology change of foodborne pathogens following exposure to hydrostatic pressures in the presence and absence of bacteriocins, Int. J. Food Micro. 91 (2004) 91 - 98.

[137] H. Chen, R.D. Joerger, D.H. Kingsley, D.G. Hoover, Pressure inactivation kinetics of phage lambda cI 857, J. Food Prot. 67 (2004) 505 – 511.

[138] J.C. Cheftel, J. Culioli, Effects of high pressure on meat: a review, J. Meat Science 46 (1997) 211.

[139] M. Hayert, J.M. Perrier-Cornet, P. Gervais, A simple method for measuring the pH of acid solutions under high pressure, J. Phys. Chem. 103 (1999) 1785 - 1789.

[140] R.C. Neuman, Jr., W. Kauzmann, A. Zipp, Pressure dependence of weak acid ionization in aqueous buffers, J. Phys. Chem. 77 (1973) 2687 - 2691.

[141] D.P. Bloxham, H.A. Lardy, Phosphofructokinase, in: P. Boyer (Ed) The Enzymes: 3rd Edition, Academic Press, New York, 1973, 239 – 278.

[142] A.M. Fordyce, C.H. Moore, G.G. Pritchard, Phosphofructokinase from *Streptococcus lactis*, Methods Enzymol. 90 (1982) 77 – 82.

[143] E. Hofmann, G. Kopperschloger, Phosphofructokinase from yeast, Methods Enzymol. 90 (1982) 70 – 77.

[144] E. Kolb, P.J. Hudson, J.I. Harris, Phosphofructokinase: complete amino acid sequence of the enzyme from *Bacillus stearothermophilus*, Eur. J. Biochem. 108 (1980) 587 – 597.

[145] A. Parmeggiani, J.H. Luft, D.S. Love, E.G. Krebs, Crystallization and properties of rabbit skeletal muscle phosphofructokinase, J. Biol. Chem. 241 (1966) 4625 – 4637.

[146] R.A. Poorman, A. Randolf, R.G. Kemp, R.L. Heinrikson, Evolution of phosphofructokinase- gene duplication and reaction of new effector sites, Nature 309 (1984) 467 – 469.

[147] B.A. French, S.H. Chang, Nucleotide sequence of the phosphofructokinase gene from *Bacillus stearothermophilus* and comparison with the homologous *Escherichia coli* genes, Gene. 54 (1987) 279 – 283.

[148] W.R. Rypniewski, P.R. Evans, Crystal structure of unliganded phosphofructokinase from *Escherichia coli*, J. Mol. Biol. 207 (1989) 805 – 521.

[149] Y. Shirikihara, P.R. Evans, Crystal structure of the complex of phosphofructokinase from *Escherichia coli* with its reaction products, J. Mol. Biol. 204 (1988) 973 – 994.

[150] P.J. Hudson, H. Hengartner, J.I. Harris, The primary structure of phosphofructokinase from *Bacillus stearothermophilus*, in Protein: Structure, Function and Industrial Applications, FEBS 12th Meeting, Oxford University Press, New York, 1979, pp. 341 – 347.

[151] P.R. Evans, G.W. Farrants, P.J. Hudson, Phosphofructokinase: structure and function, Phil. Trans. R. Soc. London B. 293 (1981) 83 – 62.

[152] T. Shirmer, P.R. Evans, Structural basis of the allosteric behavior of phosphofructokinase, Nature. 343 (1990) 140 – 145.

[153] N.M. Parichartttanakul, Texas A&M University, College Station, Department of Biochemistry and Biophysics, unpublished results, 2004.

[154] D. Deville-Bonne, G. LeBras, W. Teschner, J.R. Garel, Ordered disruption of subunit interfaces during the stepwise reversible dissociation of *Escherichia coli* phosphofructokinase with KSCN, Biochemistry 28 (1989) 1917 – 1922.

[155] G. LeBras, I. Auzat, J.R. Garel, Tetramer-dimer equilibrium of phosphofructokinase and formation of hybrid tetramers, Biochemistry 34 (1995), 13203, 13210.

[156] G.D. Reinhart and H.A. Lardy, Rat liver phosphofructokinase: use of fluorescence polarization to study aggregation at low protein concentration, Biochemistry 19 (1980) 1484 – 1490.

[157] G.D. Reinhart, Influence of polyethylene glycols on the kinetics of rat liver phosphofructokinase, J. Biol. Chem. 255 (1980) 10576 – 10578.

[158] K.H. Ling, F. Marcus, H.A. Lardy, Purification and some properties of rabbit skeletal muscle phosphofructokinase, J. Biol. Chem. 240 (1965) 1893 –1899.

[159] C.J. Coffee, R.P. Aaronson, C. Frieden, Rabbit muscle phosphofructokinase: studies of the subunit molecular weight and structure. Isolation of carboxymethylated cysteinyl peptides and sedimentation equilibrium studies, J. Biol. Chem. 248 (1973) 1381 - 1387.

[160] J. Xu, T. Oshima, M. Yoshida, Tetramer-dimer conversion of phosphofructokinase from *Thermus thermophilus* induced by its allosteric effectors, J. Mol. Biol. 215 (1990) 597 – 606.

[161] M.R. Riley-Lovingshimer, D.R. Ronning, J.C. Sacchettini, G.D. Reinhart, Reversible ligand-induced dissociation of a tryptophan-shift mutant of

phosphofructokinase from *Bacillus stearothermophilus*, Biochemistry 41 (2002) 12967 – 12974.

[162] J.L. Johnson, G.D. Reinhart, MgATP and fructose-6-phosphate interactions with phosphofructokinase from *Escherichia coli*, Biochemistry 31 (1992) 11510 – 11518.

[163] J.L. Johnson, G.D. Reinhart, Influence of MgADP on phosphofructokinase from *Escherichia coli*. Elucidation of coupling interactions with both substrates, Biochemistry 33 (1994) 2635 – 2643.

[163] V.L. Tlapak-Simmons, G.D. Reinhart, Obfuscation of allosteric structure-function relationships by enthalpy-entropy compensation, Biophys. J. 75 (1998) 1010 – 1015.

[164] H. Leonhardt, L. Gordon, R. Livingston, Acid-base equilibria of fluorescein and 2′,7′-dichlorofluorescein in their ground and fluorescent states, J. Phys. Chem. 75 (1971) 245 - 249.

[164] J.L. Johnson, M.D. Lasagna, G.D. Reinhart, Influence of a sulfhydryl cross-link across the allosteric-site interface of *E. coli* phosphofructokinase, Prot. Sci. 10 (2001) 2186 – 2194.

[165] C.C. Overly, K. Lee, E. Berthiame, P.J. Hollenbeck, Quantitative measurement of intraorganelle pH in the endosomal-lysosomal pathway in neurons by using ratiometric imaging with pyranine, Proc. Nat. Acad. Sci. USA 92 (1995) 3156 - 3160.

[166] A. Agostiano, F. Mavelli, F. Milano, L. Giotta, M. Trotta, L. Nagy, P. Maroti, pH-sensitive fluorescent dye as probe for proton uptake in photosynthetic reaction centers, Bioelectrochemistry, 63 (2004) 125 – 128.

[167] E. Kuwana, E.M. Sevick-Muraca, Fluorescence lifetime spectroscopy for pH sensing in scattering media, Anal. Chem., 75 (2003) 4325 – 4329.

[168] A. Masuda, M. Oyamada, T. Nagaoka, N. Tateishi, T. Takamatsu, Regulation of cytosol-nucleus pH gradients by K^+/H^+ exchange mechanism in the nuclear envelope of neonatal rat astrocytes, Brain Res., 807 (1998) 70 – 77.

[169] R.P. Haugland, Handbook of Fluorescent Probes and Research Chemicals: 6th Edition, Molecular Probes Inc., Eugene, OR, 1996.

[170] R.C. Weast, CRC Handbook of Chemistry and Physics: 52nd Edition, The Chemical Rubber Company, Cleveland, OH, 1971, pp D-121.

[171] P. Targowski, L. Davenport, A direct method for the correction of pressure-induced scrambling of polarized fluorescence intensities, Anal. Biochem. 274 (1999) 249 – 263.

[172] D. Blangy, H. Buc, J. Monod, Kinetics of the allosteric interactions of phosphofructokinase from *Escherichia coli*, J. Mol. Biol. 31 (1968) 13 – 35.

[173] A.D. Ortigosa, Texas A&M University, College Station, Department of Biochemistry and Biophysics, unpublished results, 2004.

[174] P.R. Evans, P.J. Hudson, Structure and control of phosphofructokinase from *Bacillus stearothermophilus*, Nature. 279 (1979) 500 – 504.

[175] H. Brismar, O. Trepte, B. Ulhafke, Spectra and fluorescence lifetimes of lissamine rhodamine, tetramethylrhodamine isothiocyanate, texas red and cyanine 3.18 fluorophores: influences of some environmental factors recorded with a scanning confocal microscopy, J. Hist. Cytochem. 43 (1995) 699 – 707.

[176] W.L. Marshall, E.U. Franck, Ion product of water substance, 0-1000C, 1-10000bars: new international formulation and its background, J. Phys. Chem. Ref. Data 10 (1981) 295 - 301.

[177] M. Foquet, J. Korlach, W.R. Zipfel, W.W. Webb, H.G. Craighead, Focal volume confinement by submicrometer-sized fluidic channels, Anal. Chem. 76 (2004) 1618 – 1626.

[178] J. Sambrook, E.F. Fritsch, T. Maniatis, Molecular Cloning: A Laboratory Manual Second Edition, Cold Spring Harbor Laboratory Press, Plainview, NY, 1989, pp B.21.

[179] C.N. Pace, F. Vajdos, L. Fee, G. Grimsley, T. Gray, How to measure and predict the molar absorption coefficient of a protein, Prot. Sci. 4 (1995) 2411 – 2423.

VITA

Robert Jason Quinlan
RR#3, 117 Fredrick Street
Bracebridge, Ontario
P1L 1X1, Canada

Education

1999 - 2004 Texas A&M University, College Station, TX
Ph.D. in Biochemistry

1994 - 1998 Laurentian University, Sudbury, Ont., Canada
B.Sc. (Hons.) in Biochemistry

Professional experience

2000 - 2004 Texas A&M University College Station, TX
Teaching Assistant - Lecture

1997 - 1998 Laurentian University Sudbury, Ont., Canada
Undergraduate Teaching Assistant

- Organic Chemistry Lab

1997 - 1998 Laurentian University Sudbury, Ont., Canada
Undergraduate Lab Assistant

- NMR Facility – Laurentian University

Awards received

1997 – CIC (Canadian Institute of Chemists) silver medal. Highest standing in the penultimate year of the undergraduate Biochemistry program at Laurentian University.

1998 – SOUCC (Southwestern Ontario University Undergraduate Chemistry Competition) 3rd place, physical chemistry.

2004 - Robert E. Welch Fellowship

2004 – Texas A&M Biochemistry Research Competition, 2nd place.

2004 – Texas A&M Student Research Week Research Competition, 1st place, biological sciences – graduate level.